ONE MILLIMETER CONTINUUM OBSERVATIONS OF QUASARS

Thesis by
David James Ennis

In Partial Fulfillment of the Requirements
for the Degree of
Doctor of Philosophy

California Institute of Technology
Pasadena, California

1982
(Submitted on November 30, 1981)

ACKNOWLEDGEMENTS

This thesis would not have been possible without the support, friendship, and guidance I have received for many years from many people. Foremost among these are my fellow graduate students and coworkers: John (JJ) Nugent, Kristen Sellgren, Eric Tollestrup, Graham Berriman, Eric Grossman, Steve Pravdo, Pat Niell, John Nousek, and Gordon Forrester. For helping to make the observing sessions bearable, as well as fruitful, and for his friendship I owe a large debt of gratitude to Tom Roellig.

I have had the fortunate experience of having two men- Mike Werner and Gerry Neugebauer- act as advisors during my research. I am grateful to them for giving me the opportunity to do the independent research culminating in the present work. In addition to Mike and the Chief, I would like to thank Tom Soifer and Roger Blandford for useful scientific discussions and critical reading of the thesis.

To all the people who have taught me experimental technique and given me technical assistance I am most grateful. Specifically, I would especially like to thank Vagn Stephensen and Mel Kriegel for an education in machining and Jim Smith for training in bolometer construction.

On a more personal note, I would like to acknowledge the support and love of my parents and brothers. For all that they have given me throughout the years, I cannot thank Mom, Dad, Mike or Paul enough. I would also like to give heartfelt thanks to Chris Ennis for the help, love, and caring she has provided for me.

Special thanks to Bee and Slim, I couldn't have done it without you guys.

ABSTRACT

Forty-one extragalactic objects including radio quiet quasars, radio loud quasars, and blazars (BL Lac objects and OVV quasars) have been observed at a wavelength of one millimeter. The measured 1mm flux densities agree with direct extensions of the radio continua of blazars and radio loud quasars. Furthermore, for the blazars, the 1mm flux density is correlated with an extrapolation of the power law infrared continuum. This result is supportive of a model in which the radio through optical continuum of blazars is beamed synchrotron radiation from a relativistic jet.

No radio quiet quasar was detected at a wavelength of 1mm to a limiting flux density of 1 Jy. The steep inverted radio continua characteristic of synchrotron self-absorption and free-free absorption models for radio quiet quasars are incompatible with the 1mm flux density upper limits. The "quiet" radio continuum from a relativistic jet oriented away from the observer's line of sight is consistent with the 1mm observations. A Comptonization model for quasar infrared emission, in which low frequency photons are upscattered by a thermal plasma will be in accord with the 1mm and infrared data provided the frequencies of the soft photons are in the range 10^{12} to 10^{13} Hz.

Repeated measurements have established that the 1mm flux densities of 3C273, BL Lac, 3C84, OJ 287, and 3C345 are variable on the time scale of a few months. Emission outbursts of blazars occur simultaneously and have similar amplitude at wavelengths of 1mm and 2cm. This result cannot be accounted for in the canonical expanding source model of radio variability; injection-type models, in which emission variability is governed by a change in the number of radiating electrons are preferred.

Three of the quasars undetected at a wavelength of 1mm have high redshift and anomalously low $L\alpha/H\alpha$ emission line ratios. The 1mm flux density upper limits are used to constrain the temperature of a hypothetical dust shell with optical depth sufficient to account for the emission line ratio discrepancy.

The development of the composite germanium bolometer and lead light cone used for the 1mm quasar observations is described in the Appendix.

TABLE OF CONTENTS

INTRODUCTION

The one millimeter wavelength continuum radiation from astronomical sources is produced primarily by two distinct radiation processes. In Galactic molecular clouds (e.g., Westbrook *et al.* 1976) and normal galaxies (Roellig 1980) the observed 1mm flux is attributed to thermal emission from cold dust. On the other hand, the 1mm emission from compact radio sources (Elias *et al.* 1978) is attributed to non-thermal electron synchrotron radiation. Thus, a wavelength of one millimeter can be viewed as either a far-infrared wavelength or as a short radio wavelength depending upon the radiation mechanism which obtains. The one millimeter observations presented in this thesis represent a combination of these two viewpoints.

This thesis consists primarily of three papers each of which deals with the emission from quasars at a wavelength of one millimeter. In Paper I, one millimeter observations of a sample of radio loud quasars, radio quiet quasars, and blazars (BL Lac objects and OVV quasars) are presented. These observations can be used to establish the relationship between the 1mm, radio, and infrared radiation observed from these three classes of extragalactic objects. For this sample of objects, the 1mm observations act as a probe for the presence of physical processes which could effect the radio synchrotron radiation at high frequencies. At a wavelength as short as 1mm, a spectral break in the observed power law radio continuum of radio loud quasars and blazars could be caused by synchrotron radiation losses, emission from compact components, optical depth effects, or a high energy cutoff in the relativistic electron energy distribution. If the free-free absorption or synchrotron self-absorption mechanisms is responsible for the weak radio emission observed from radio quiet quasars, considerable emission should be present at a wavelength of 1mm because of the steep inverted radio continua characteristic of these processes.

In Paper II the question of the time variability of the 1mm emission from several of the objects from the sample of Paper I is addressed. If traditional expanding synchrotron source models of the radio variability of quasars obtain, a given emission outburst will appear first and have large amplitude at short radio wavelengths such as 1mm. The observations of Paper II compliment the results of Paper I since the effect of a given physical process on the 1mm wavelength emission of a synchrotron source would appear both in the observed energy distribution and in the nature of the 1mm flux density variability.

In Paper III one millimeter observations of high redshift quasars are presented. In contrast with Papers I and II, these observations are viewed purely as a probe for possible thermal emission from dust grains. Reddening by dust has been proposed as an explanation for the observed discrepancy between the measured $L\alpha/H\alpha$ emission line ratio and the predictions of standard recombination theory. Part of the power absorbed from the quasar ultraviolet continuum by the hypothetical dust would be thermally reradiated at an observed wavelength of 1mm.

In the Appendix, a description of the detection system used for the 1mm observations is presented. The sensitivity levels needed for the present observations were realized through an optimization program aimed at developing a high responsivity composite bolometer and high transmission light cone optics.

REFERENCES

Elias, J.H., *et al.* 1978, *Ap. J.*, **220**, 25.

Roellig, T.L. 1980, Ph. D. Thesis, Cornell University

Westbrook, W.E. 1976, *Ap. J.*, **209**, 94.

PAPER I: ONE MILLIMETER CONTINUUM OBSERVATIONS OF QUASARS

ABSTRACT

Broadband one millimeter continuum observations of 37 active extragalactic objects are presented. The sources observed included radio loud quasars, radio quiet quasars, and blazars (BL Lac objects and OVV quasars). The 1mm flux density of radio loud quasars and blazars agrees well with a direct extension of the observed radio continuum. In addition, the blazars exhibit a correlation between the observed 1mm flux density and an extrapolation of the power-law infrared continuum to a wavelength of 1mm. No radio quiet quasar was detected regardless of its infrared properties; three sigma upper limits of 1 Jy for the 1mm flux density were obtained.

The 1mm results are discussed within the context of several models of the radio and infrared continuum emission of compact extragalactic objects. The observed correlation of the 1mm flux density of blazars with both the radio and infrared emission is a natural consequence of attributing the entire radio through optical blazar continuum to synchrotron radiation from a relativistic jet viewed nearly along its axis. The weak radio continuum produced by a relativistic jet oriented perpendicular to the observer is consistent with the observed limit to the 1mm-6cm spectral index of radio quiet quasars; other models in which synchrotron self absorption or free-free absorption suppress the emission of radio quiet quasars are characterized by steep radio energy distributions incompatible with the 1mm observations. It is shown that a Comptonization model in which the infrared continuum of quasars is produced by the upscattering of soft photons into the infrared by a thermal plasma will be in accord with the 1mm and infrared data if these photons have frequencies in the range 10^{12} to 10^{13} Hz.

I. INTRODUCTION

At radio, infrared, and optical wavelengths the continuum emission from quasars is relatively well determined. Due to sensitivity limitations, the millimeter through far-infrared region of the electromagnetic spectrum is essentially unexplored. Only one quasar- 3C345- has been detected at far-infrared wavelengths (Harvey *et al.* 1981); flux density upper limits exist for 3C273 (Hildebrand *et al.* 1977). Elias *et al.* (1978) have measured the one millimeter flux densities of the two radio loud quasars 3C273 and 3C279; these authors show that the observed 1mm flux density is in good agreement with a direct extrapolation of the measured radio continuum. Neugebauer *et al.* (1979) point out that, in addition, the 1mm flux densities of 3C273 and 3C279 fall on smooth extensions of the observed infrared power law continua. One millimeter flux density limits of radio quiet quasars have been reported by Rowan-Robinson *et al.* (1975) although the results are not particularly sensitive (two sigma upper limits of ~30 Jy.).

Unfortunately, the conclusions that can be reached from these one millimeter results are limited due to the small number of detected quasars. It is important to establish, through one millimeter observations of a large sample of both radio quiet and radio loud quasars, the relationship between the one millimeter, infrared, and radio continuum emission. In particular, it can be ascertained if it is characteristic of the radio and/or infrared continua observed from quasars to extend to a wavelength of one millimeter.

In order to properly test the proposed radiative mechanisms responsible for quasar emission, observational data covering as much of the electromagnetic spectrum as possible, are required. In a previous paper (Ennis *et al.* 1981) one millimeter continuum observations were used as a probe for the thermal emission from dust which might be reddening the emission lines observed from high

redshift quasars. In radio loud quasars the radio continuum is traditionally attributed to electron synchrotron radiation (e.g., O'Dell 1979). At a frequency as high as 300 GHz (λ= 1 mm) it is possible that the observed synchrotron spectrum could have a turnover due to optical depth effects, a high energy cutoff in the electron energy distribution, or the effects of electron energy loss mechanisms. For radio quiet quasars it has been proposed that the radio emission is suppressed via the synchrotron self-absorption or free-free absorption processes (Strittmatter *et al.* 1981). One millimeter observations of radio quiet quasars are particularly sensitive in this regard since both these mechanisms produce steep inverted radio continua: a quasar "quiet" at a wavelength of 6cm would emit considerable power at 1mm if these processes obtained.

In this paper one millimeter wavelength observations of a large sample of quasars are presented. The purpose of this project is twofold: (1) to establish the observational relationship between the 1mm emission from quasars and the emission at other wavelengths, and (2) to use the results of the 1mm observations to discriminate between the physical processes which could be producing the radio and infrared radiation of quasars. In total, 28 quasars- both radio loud and radio quiet- have been observed at 1mm. In addition, because of their observational similarity to certain quasars, 9 BL Lac objects have also been observed. In section II the observational procedure and data reduction process are described. Section III includes a description of the quasar sample chosen for the one millimeter observations as well as a summary of the observational properties of this sample at other wavelengths. In section IV the results of the observations are presented. A discussion of these results is given in section V. The major conclusions of this paper are summarized in section VI.

II. OBSERVATIONS

The one millimeter wavelength observations presented in this paper were made between November 1977 and December 1980 at the prime focus of the 5 meter Hale telescope on Palomar Mountain. Two broadband incoherent detection systems were used for the observations. For observations between November 1977 and April 1979 and between November 1980 and December 1980 the detector employed was a liquid ^{4}He cooled composite germanium bolometer (Hauser and Notarys 1975) operating at a temperature of ~2 K. The wavelength response of this detection system was between 600 μm and 1.5 mm; the long wavelength cutoff was due to diffraction at the primary of the 5 meter Hale telescope and a decrease in the bolometer sensitivity. The short wavelength cuton is a function of the atmospheric conditions prevailing during a specific observing session; the short wavelength limit is determined by the line of sight water vapor content of the atmosphere (Elias *et al.* 1978) and a cooled fluorogold filter (Muehlner and Weiss 1973). The 1mm measurements were made with a 55 arcsecond diameter diaphragm. A lead-molded Winston light cone was employed as field optics (Winston 1970; Harper *et al.* 1976). Between December 1979 and April 1980 a liquid ^{3}He cooled composite germanium bolometer (Roellig 1980) operating at a temperature of 0.3 K was used for the observations. In this system an antireflection coated KRS 5 filter (Wolfe 1965) cooled to 4.2 K establishes a short wavelength cuton of 750 μm and a fused silica lens was used as field optics. With both systems the 1mm photometry was performed with a f/3.3 "reimaging primary" photometer (Elias *et al.* 1978) in which a wobbling tertiary mirror allowed dual beam chopping at a frequency of 10 Hz and a beam separation up to 4 arc-minutes. Telescope acquisition of the desired source was accomplished by offsetting from bright positional standard stars.

The planets were used to provide flux density calibration at wavelength of 1mm. The measured 1mm brightness temperatures of Jupiter and Saturn

reported in Werner *et al.* (1978) were used; these temperature values are based on the thermal model of Mars of Kieffer *et al.* (1973). For some observing sessions NGC 7027 was used as a secondary calibrator; its 1mm flux density was measured to be 7.0±0.8 Jy (Roellig *et al.* 1981). The energy distribution of the planets in the bandpass of our system can be described by the Rayleigh-Jeans law which has spectral index α ($F_\nu \propto \nu^\alpha$) equal to 2. On the other hand, α is closer to 0 for many of the quasars observed (see Table 1). Due to the wide bandwidth of the observing system this spectral index difference must be taken into account in the flux density calibration at a nominal wavelength of 1mm. The atmospheric modeling and reduction process necessary to accomplish this are described in Elias *et al.* (1978). For the results presented below it was assumed that α = 0 for all the objects observed. The change in the 1mm flux density if a different spectral index is assumed depends upon the amount of water vapor present in the atmosphere; if fluorogold is used as a filter, there is only a 6% decrease in the 1mm flux density as α is changed from 0 to 1 when the atmospheric column density of water vapor is 2.3 percipitable millimeters. A water vapor column density of this value represents good conditions on Palomar Mountain for 1mm wavelength observations.

III. DESCRIPTION OF THE SAMPLE

The 37 objects chosen for observation are listed in Table 1. In general, the objects have not been systematically chosen; the resulting total sample is incomplete and eclectic. In spite of this limitation, this sample represents a significant increase in the total number of quasars observed at 1mm; in addition, radio loud quasars, radio quiet quasars, and BL Lac objects are all well represented.

Sixteen quasars were chosen for the 1mm observations solely on the basis of their having a 10μm flux density greater than 32 mJy; these quasars shall be referred to as the infrared sample. The infrared sample was taken from the list of Neugebauer *et al.* (1979) who have made infrared measurements of 36 quasars with visual magnitudes less than 17. Ten of these quasars are radio loud although no quasar was either included or excluded from the infrared sample on the basis of its radio emission. One object in the infrared sample is III Zw 2 (0007+10) which, although classified as a quasar (Green 1976), has also been identified as a compact galaxy (Zwickey 1967) and a Type 1 Seyfert galaxy (see,e.g.,Weedman 1977). In December 1977 III Zw 2 underwent an emission outburst in the radio reaching a 6cm flux density of 300mJy (Schnopper *et al.* 1978). Since that time its radio flux density has remained high (Aller *et al.* 1981). For present purposes III Zw 2 will be classified as a radio loud quasar.

In total 8 radio quiet quasars have been observed at a wavelength of one millimeter- five from the infrared sample and 3 additional quasars. Four of the radio quiet quasars observed have been detected at radio wavelengths (Condon *etal.* 1981; Fanti *et al.* 1977); they exhibit 6cm flux densities between 2 and 200 mJy.

Nine radio loud quasars and 9 BL Lac objects were chosen for 1mm observations on the basis of their radio emission. These are bright, flat spectrum radio sources taken primarily from the work of Owen *et al.* (1978) and Owen *et al.* (1981). Due to sensitivity and time limitations, this sample of radio loud quasars is in no sense complete and arbitrarily compiled.

Also shown in Table 1 are the relevant data characterizing the observed emission from each object in the present sample at radio, infrared and optical wavelengths. The data in Table 1 were collected from the literature and can be used as an aid in discriminating between models of quasar continuum emission.

The value of the 6cm flux density measured from a quasar will depend on the beam size used for the observations if the quasar exhibits radio structure. In order to make a valid comparison with the 1mm observations it is necessary to tabulate the radio flux which would be measured with a 55 arcsecond beam. For a majority of the radio loud quasars beam size is not a consideration since they have been shown to be extremely compact (see, e.g., Seielstad *et al.* 1979). Five of the quasars observed- 3C95, PKS1004+13, Ton 202, 3C351, and PKS2135-14- have a "triple" radio structure consisting of two lobes on either side of a weak central component associated with the optical position of the quasar (Miley and Hartsuijker 1978). For these quasars the lobe separation is large enough (typically 2 arcminutes) that the desired 6cm flux density is that of the central component.

Many of the compact radio loud quasars as well as the BL Lac objects observed are known to be variable at radio wavelengths (Altschuler and Wardle 1975; Aller *et al.* 1981). Effort was made to tabulate 6cm flux densities measurements coincident with the 1mm observations whenever possible. Particularly useful in this regard was a program of simultaneous 1mm and radio wavelength observations of compact extragalactic radio sources discussed in Jones *et al.* (1981); the 1mm data of that study are included in this paper. Throughout this paper measurements will be considered "simultaneous" if they occurred within a month of each other. Six centimeter measurements simultaneous with the 1mm measurements are marked with a (S) in Table 1.

The radio spectral index tabulated, α_R, was calculated using flux densities at 4.885 GHz and 14.8 GHz. Some of the quasars in the sample exhibit radio continua which cannot be characterized by a single power law over the entire range of observed frequencies; in particular, there is often a steepening at a frequency of 90 GHz (Kellermann and Pauliny-Toth 1981). Those quasars exhibiting this

effect are labeled with a (C) in column 7; (St) indicates that the radio continuum is straight out to 90 GHz. The possible physical significance of the 90 GHz steepening is discussed in section Vc.

Several of the above comments can also be applied to the infrared properties tabulated. The infrared emission from some quasars and BL Lac objects has been shown to be time variable (Neugebauer *et al.* 1979). For this reason, 2μm flux density measurements simultaneous with the 1mm observations have been tabulated whenever possible. As shown by Neugebauer *et al.* (1979), the infrared continua of many quasars can only roughly be described as power law; a "bump" in the continuum at 3.5μm is frequently observed. For this reason, flux densities at 10, 2.2, 1.6, and 1.2μm have been used to determine the power law component of the infrared emission; the data at these wavelengths are well fitted by a power law of spectral index α_{IR}. Those quasars having an infrared energy distribution which shows excess 3.5μm emission are labeled (B) in column 12; those which do not are marked (St) for straight.

Five of the radio loud quasars listed in Table 1 have observed continuum properties significantly different from the other quasars; these quasars are OA 129, PKS 0736+01, 3C279, 3C345, and 3C454.3. These quasars have high optical and radio polarization which exhibit significant variability; their infrared continua also extend smoothly through optical wavelengths. In addition, the observed radio and infrared continua of these quasars are quite straight being well described by power laws; in general, the spectral breaks at 90 GHz and 3.5μm discussed above are not observed. These quasars have large amplitude radio and optical flux variability occurring on a short timescale (Altschuler and Wardle 1977; McGimsey *et al.* 1975). Repeated infrared observations of 3C279, 3C345, and 3C454.3 have established large flux variations at these wavelengths

as well (Neugebauer 1981). All of these properties are characteristic of the emission observed from BL Lac objects (see Stein 1978 and Table 1). For this reason in what follows these 5 quasars and the BL Lac objects observed will be grouped together into one class termed blazars (Angel and Stockman 1980).

IV. RESULTS

The one millimeter flux densities for all the objects observed are presented in Table 2 along with the date of the observation. A 1mm flux density measurement is considered a detection if it is greater than three times the statistical uncertainty. The calibration uncertainty in the 1mm flux density is typically 20%. In Table 2 the uncertainty associated with a given measurement is the quadrature addition of the statistical and calibration uncertainties. All upper limits are three times the statistical uncertainty.

Fourteen blazars and 7 radio loud quasars have been detected. The measured 1mm flux densities range from 0.8 Jy to 10.2 Jy. No radio quiet quasar was detected at a wavelength of 1mm. The upper limit to the 1mm flux density from radio quiet quasars is typically 1 Jy. Some of the radio loud quasars observed were also undetected.

Weather permitting, the 1mm flux density of 3C273, 3C279, OJ 287, and BL Lac has been monitored over the last several years. In addition, III Zw 2 and 3C345 have been measured at a wavelength of 1mm on more than one occasion. Except for 3C279, all of these objects show formal evidence for variability at a wavelength of one millimeter. The details and implications of the 1mm variability are discussed in Ennis *et al.* (1981).

Five of the objects listed in Table 2 - OA 129, PKS 0735+18, PKS 0736+01, 3C273, and 3C454.3 - have been observed at a wavelength of 1mm by Kreysa *et al.* (1980). In general, the present measurements are consistent with their

observations although, with the exception of 3C273, their data do not satisfy the detection criteria of this paper.

The observed values of the 1mm flux densities can be compared with extrapolations of the measured infrared and radio continua to a wavelength of one millimeter. In calculating the radio extrapolated 1mm flux density, a power law through the two data points "closest" in frequency to 300 GHz was used; because of the high frequency curvature in some quasar radio continua (see section III) an accurate extrapolation of the radio continuum was possible only if the 90 GHz flux density had been measured. The infrared extrapolated 1mm flux density was calculated using the spectral index and flux density shown in Table 1.

In Figure 1 the observed 1mm flux density is plotted against the 1mm flux density obtained from an extrapolation of the radio continuum. The data for the blazars observed are shown in Figure 1a; the results for the radio loud quasars observed are shown in Figure 1b. The solid lines shown in Figures 1 and 2 (below) pass through the origin and have slope one; they thus represent the loci of points for which the observed 1mm flux density exactly equals the extrapolation of the radio continuum. Particular weight should be given to the open symbols in Figures 1 and 2 since they correspond to simultaneous 1mm and radio or infrared measurements.

In general, the 1mm flux density observed from both blazars and radio loud quasars agrees with an extrapolation of the radio continuum of these objects. On average, the present data are consistent with the hypothesis that the quasar radio continuum can be directly extended to a wavelength as short as one millimeter; there is no evidence for a spectral steepening at 300 GHz. Note that both non-simultaneous and simultaneous measurements fall on the solid line shown.

In Figure 2 the observed 1mm flux density is shown versus the 1mm flux density obtained from an extrapolation of the infrared continuum. Data for the blazars, radio quiet quasars, and radio loud quasars, are plotted in Figures 2a,2b,2c respectively. For all three classes of object the observed 1mm emission is less than that predicted from an extrapolation of the infrared continuum, although the appearances of these three figures are quite different. For the blazars the observed 1mm flux density appears to be directly related to the extrapolated 1mm flux density; the data are well fit by the dashed line shown which has slope one but is offset from the origin. It should be pointed out that both the data from simultaneous as well as non-simultaneous observations are consistent with the dashed line. Unlike the blazars observed, no radio quiet quasar was detected regardless of its infrared properties. As illustrated in Figure 2b, the 1mm flux density of each radio quiet quasar observed in below $\sim$ 1 Jy independent of the flux density obtained from an extrapolation of the infrared continuum of the quasar. For some of the radio quiet quasars the difference between the observed and extrapolated 1mm flux densities can be larger than two orders of magnitude. Of the seven radio loud quasars detected at 1mm, accurate infrared extrapolations could be made only for 3C273, III Zw 2, and 4C31.63. As can be seen if Figure 2c, the data points corresponding to these three radio loud quasars do not fall on the line shown in Figure 2a to be a good fit to the blazar data. Like the radio quiet quasars the undetected radio loud quasars (primarily the extended radio loud quasars) all have 1mm flux densities less than $\sim$ 1 Jy irrespective of observed infrared characteristics.

A useful parameter in discriminating between theoretical models of radio quiet quasars is the radio spectral index, α_{RQ} measured between 5 and 300 GHz. In Table 3 the radio and 1mm flux densities for the radio quiet quasars detected at centimeter wavelengths are shown. Also shown is the limit to α_{RQ} derived

from these two observations. Typically, α_{RQ} must be less than one.

V. DISCUSSION

A fundamental question concerning quasar continuum emission is what radiation mechanisms are producing it. In particular, the relationship (if any) between the physical processes responsible for the radiation observed at infrared and radio wavelengths is unclear. The purpose of this section will be to discuss in what way the present one millimeter observations constrain the various proposed mechanisms. The philosophy throughout the present discussion will be to discriminate between emission models primarily on a comparison between observed and theoretical energy distributions. A satisfactory emission model must produce a continuum consistent with observed fluxes at all wavelengths, particularly one millimeter. In addition, we require that any valid model produce the observed properties shown in Table 1.

a) Blazars

In Figure 3, the observed energy distributions of several of the sample blazars are presented. Among the three classes of objects observed, the blazars are unique in having 1mm fluxes which are directly related to *both* the infrared and radio continuum emission (see Figures 1a and 2a). The simplest physical explanation for this result is that a single radiation mechanism is producing the radio through optical emission shown in Figure 3. Other evidence supporting this viewpoint is the that the large flux outbursts observed from blazars appear at radio and optical wavelengths (Kinman *et al.* 1974; Reike *et al.* 1976;Puschell *et al.* 1979). In addition, the radio and optical linear polarization of OJ 287 have been found to have identical angles of polarization. (Condon 1978 and references therein). As has been discussed (see,e.g., O'Dell 1978a), a natural choice for the process responsible for the radio through optical emission of blazars is

synchrotron radiation. Synchrotron radiation can produce the high radio and optical polarizations observed for blazars (Wardle 1978; Moore 1981); other optical polarization mechanisms such as dust or electron scattering typically produce polarization of only a few percent (Angel 1969).

i) Optically thin synchrotron radiation: homogeneous source

In the traditional model of a synchrotron source (see, e.g., Kellermann 1964; Marscher 1977a) it is assumed that the magnetic field and relativistic electrons are distributed homogeneously, and that the electrons exhibit a power law distribution of energies ($N(E) \propto E^{-\gamma}$) up to a high energy cutoff E_2. The optically thin synchrotron continuum produced is the well-known power law with spectral index $(1-\gamma)/2$ for frequencies below ν_2 (the critical frequency of electrons with energy E_2) ands falls exponentially at frequencies above ν_2 (Moffet 1975). In Figure 4 the observed energy distribution of the blazar OJ 287 is shown along with the optically thin synchrotron radiation from a homogeneous source with $\gamma = 1$ and $\nu_2 = 10^{14}$; these values of γ and ν_2 were chosen in order that the model continuum be consistent with a flat radio spectrum extending to a wavelength of 1mm. The infrared continuum produced by the optically thin synchrotron model shown is in disagreement with the observations; the model infrared emission is too intense and has too steep a spectral index. Variability can not account for the infrared discrepancy since the radio, one millimeter, and infrared data were all obtained simultaneously in 1978 Nov/Dec (Jones *et al.* 1981; Puschell and Stein 1980).

ii) Synchrotron radiation from an inhomogeneous source: relativistic jet

In more sophisticated models the synchrotron source is inhomogeneous, i.e., the magnetic field, B, and relativistic electron density, $N(E)$, are functions of r the radial distance from the source center. Blandford and Königl (1979) have considered a specific inhomogeneous model for blazar emission in which

the synchrotron source has a anisotropic conical geometry and is undergoing bulk relativistic motion. The relativistic velocities and jet-like geometry are required to account for the radio structure and superluminal expansion exhibited by compact radio sources (Cohen *et al.* 1979).

The synchrotron continuum produced by a relativistic jet is in good agreement with the blazar energy distributions shown in Figure 3. Königl (1981) has shown that the continuum emission observed from a relativistic jet can roughly be described as a broken power law with spectral index change at an observed turnover frequency ν_m. Specifically, if the relativistic jet has $B \propto r^{-1}$ and $N(E) \propto E^{-\gamma}$ r^{-2} the synchrotron emission will have a flat spectral index at frequencies less than ν_m, and have spectral index $1-\gamma$ at frequencies above ν_m. As indicated by the data shown in Figures 1a and 3, blazar radio continua remain flat to a wavelength as short as 1mm; this indicates that $\nu_m > 300$GHz, i.e., the break in the synchrotron continuum must occur in the far infrared (see below). Physically, the change from a flat radio continuum to a steep infrared continuum reflects the transition from partially optically thick to optically thin synchrotron radiation from the jet; such a transition is characteristic of inhomogeneous synchrotron sources. (Condon and Dressel 1971; de Bruyn 1976). The particular assumption $B \propto r^{-1}$ corresponds to equipartition of the magnetic and particle energy densities; similarly, $N(E) \propto r^{-2}$ reflects the assumption of electron number conservation along the jet.

The correlation shown in Figure 2a between the observed 1mm flux density and the extrapolation of the infrared continuum has a simple interpretation within the framework of the relativistic jet model. In the model of Königl (1981) described above the difference between the observed and extrapolated 1mm flux densities for a given blazar will depend only upon γ and ν_m. The dashed line shown in Figure 2a corresponds to $\nu_m = 2.4 \times 10^{12}$Hz($125\mu$m) and $\gamma = 2.3$. The fact

that the data for the observed blazars cluster around this line indicates that the continua of these blazars all have similar observed turnover frequencies (see also Figure 3).

In order for the blazar continua to all exhibit comparable turnover frequencies it is required that the relativistic jets responsible for the observed emission have similar velocities and magnetic field strengths. The observed turnover frequency is related to the physical parameters of the jet through the equation below which follows from the formulae in Königl (1981):

$$\nu_m = 2.4\times10^9 C_\gamma \frac{\Gamma\beta}{\varphi^{1/5}} \frac{z^{2/5}}{(1+z)^{6/5}} \frac{D(\vartheta)^{2/5}}{\sin\vartheta^{1/5}} \frac{F_m^{1/5}}{B_1^{7/5}} \quad \text{Hz} \qquad (1)$$

In this equation, which obtains regardless of the choice of γ, C_γ is a constant close to unity, Γ is the Lorentz factor of the relativistic motion, β is the velocity of the jet in units of c, φ is the semiangle of the conical jet ($\sim$ 0.1), $D(\vartheta)$ ($=1/[\Gamma(1-\beta\cos\vartheta)]$) is the relativistic Doppler factor, ϑ is the angle between the jet axis and the line of sight, F_m is the flux density in Jy at ν_m (which for a flat radio continuum equals the observed 1mm flux density), and B_1 is the magnetic field in Gauss at a radius of one parsec. As can be seen in equation (1), the observed turnover frequency is weakly dependent on all of these quantities except for Γ and B_1. For blazars it is argued that ϑ is small, typically $\sin\vartheta\sim1/\Gamma$ and $D(\vartheta)\sim\Gamma$; with this assumption ν_m is proportional to $\Gamma^{6/5}B_1^{-7/5}$. Using the value for ν_m obtained from Figure 2a, and taking Γ=9, the nine blazars with known redshifts must have magnetic field strengths in the narrow range between 1×10^{-1} and 2×10^{-1} Gauss.

b) Radio Quiet Quasars

One category of physical model for radio quiet quasars maintains that, like blazars, the observed radio through optical emission is direct synchrotron radiation from a single source. The radio emission from radio quiet quasars is

suppressed by an absorption process affecting the synchrotron radiation (Strittmatter *et al.* 1981; Condon *et al.* 1981). The two radio suppression processes considered here are synchrotron self absorption (see, e.g., Ginzburg and Syrovatskii 1965) and free-free absorption (see, e.g., Moffet 1975).

i) Synchrotron self absorption

In the standard, homogeneous synchrotron source model, synchrotron self absorption produces a continuum with α_{RQ} = 2.5 for frequencies below a turnover frequency ν_s determined by the source angular size and magnetic field; above ν_s the synchrotron radiation is optically thin (see, e.g. Tucker 1975). This value of α_{RQ} is inconsistent with the present 1mm observations (Table 3). The radio through infrared energy distribution of the radio quiet quasar PG 1351+64 is presented in Figure 5. In this figure, the continuum produced by a self-absorbed homogeneous synchrotron source with $\nu_s = 1.6\times10^{11}$ and $\gamma = 3.8$ is also shown; these values and the flux density normalization were chosen so that curve would fit the infrared and 6 cm data. The observed 1mm flux density upper limit is a factor of ~80 below the prediction of this model.

A self-absorbed synchrotron continuum can exhibit an optically thick spectral index less than 2.5 if the radiating source is inhomogeneous (Marscher 1977b). As an illustrative example, the continuum produced by a self-absorbed inhomogeneous synchrotron source with $B(r)\propto r^{-2}$, $N(E,r)\propto E^{-\gamma}r^{-2}$ and $\nu_s = 2.4\times10^{12}$ is shown in Figure 5. This curve is in agreement with all the observations including the 1mm upper limit.

Using a homogeneous synchrotron source model, Condon *et al.* (1981) have determined the angular sizes of the radio quiet quasars they detected. As can be seen in Figure 5, the inhomogeneous synchrotron spectrum exhibits a higher ν_s and a lower turnover flux density (F_s) than the homogeneous synchrotron continuum. This is a result of the fact that the inhomogeneous source must be

more compact than the homogeneous source. For both models, the angular radius, Θ, is proportional to $F_s^{\frac{1}{2}} \nu_s^{-\frac{5}{4}}$. Using the numerical parameters appropriate for PG 1351+64, we find that $\Theta_{inhomo} \approx \frac{1}{10}\Theta_{homo}$. In this calculation it was assumed that the inhomogeneous and homogeneous sources have identical geometry and magnetic field strength.

ii) Free-free absorption

An alternate mechanism proposed to account for the weak radio flux observed from radio quiet quasars is free-free absorption of synchrotron radiation by a thermal plasma cloud external to the synchrotron source (Strittmatter *et al.* 1981; Condon *et al.* 1981). In this model, as in the synchrotron self absorbed models discussed above, the infrared continuum is optically thin radiation from the putative synchrotron source. As illustrated by the curve in Figure 5, free-free absorption will produce a extremely sharp turnover in a synchrotron spectrum since $\tau_{free-free} \propto \nu^{-2.1}$ (Williams 1963). The turnover frequency ,ν_t, is determined by the emission measure (EM) and electron temperature (T_e) of the plasma cloud ($\nu_t \propto EM^{\frac{1}{2.1}} T_e^{-\frac{3}{4.1}}$). In order to pass through the 6 cm point, it has been assumed that $\nu_t = 1.7 \times 10^{10}$Hz for the curve shown in Figure 5. The present 1mm observations are clearly inconsistent with the continuum produced by this model.

An additional difficulty with the free-free absorption model arises when one considers possible candidates for the necessary plasma cloud. Condon *et al.* (1981) have considered the possibility that the free-free absorption could occur in the clouds thought to produce the broad emission lines observed in quasar spectra. Kwan and Krolik (1981) have constructed the most detailed and successful model, to date, of a broad line emission cloud. Their numerical values for electron density, electron temperature, and cloud thickness yield a turnover

frequency of $\sim 10^{12}$Hz. A free-free absorbed synchrotron model with this value of ν_t could not produce a high enough 6cm flux density. Furthermore, as pointed out by Condon *et al.* (1981), if the broad emission line clouds were responsible for the free-free absorption their covering factor would have to be unity; observations of high redshift quasars are consistent with a much smaller value (Oke 1974; Baldwin *et al.* 1976).

The radio quiet quasar models considered above have as an implicit assumption that, like blazars, the observed infrared/optical energy distribution is an optically thin synchrotron continuum. For blazars this suggestion is supported by the high optical polarization and straight infrared continua observed since both are characteristic of optically thin synchrotron emission. On the other hand, the optical polarization of radio quiet quasars is quite small and their infrared continua are not straight (Table 1). Moore (1981) argues that such a low optical polarization is inconsistent with a synchrotron model for the optical emission even if the synchrotron radiation is diluted by emission from an unpolarized source.

iii) Two component model of radio quiet quasars

A second, more attractive, category of radio quiet quasar models contends that the "quiet" radio emission is due to a synchrotron source but that the infrared radiation is produced in a distinctly separate component. The 1mm observations will be in agreement with a two component model for radio quiet quasars provided that the following general constraints are satisfied. The weak synchrotron source must produce a radio continuum with small enough α_{RQ}; considering the strictest limit presented in Table 3 ($\alpha_{RQ}<0.4$), an, essentially, flat radio energy distribution is required. The power law continuum produced by the infrared radiation mechanism cannot extend directly to a wavelength of 1mm; a change in the spectral index must occur in order to be consistent with

the results shown in Figure 2b. It is shown below that one specific model in accord with these criteria maintains that the weak synchrotron source is a relativisitic jet whose axis is oriented away from the observer's line of sight (Scheur and Readhead 1979; Marscher 1980) and that the infrared emission is due to inverse Compton scattering of soft photons by a non-relativistic thermal plasma (Katz 1976). Other possible models cannot be ruled out on the basis of the 1mm data alone. For example, the weak, flat-spectrum synchrotron emission could be produced by a isotropic (albeit inhomogenous) source not undergoing bulk relativistic motion.

iv) Radio emission: Orientation of a relativistic jet

As discussed above, a relativistic jet model provides a successful explanation for the observed energy distributions of blazars. For these objects, it is argued that the angle between the jet axis and the observers line of sight, ϑ, is small. If the orientation of the jet is changed such that ϑ is increased, the observed radio flux density rapidly decreases ($F_m(\vartheta) \propto D(\vartheta)^{\frac{3\gamma+7}{\gamma+4}} \sin\vartheta^{\frac{\gamma-1}{\gamma+4}}$; Königl 1981) creating a radio quiet quasar. Also shown in Figure 5, for comparative purposes, is the schematic radio continuum produced by a relativistic jet with physical parameters (magnetic field and electron density distributions) typical of blazars but with $\vartheta = 82°$. The model of Königl (1981) was used in calculating this curve and Γ was taken to be 9, a value in agreement with VLBI observations of superluminal expansion (Pearson *et al.* 1981). Both the observed 6cm and 1mm flux densities are consistent with this specific model continuum. As expected, the high-frequency optically thin synchrotron emission produced by the jet is too weak to account for the observed infrared radiation; a separate radiation mechanism for the infrared is required.

Two of the radio quiet quasars in Table 3- NAB 0024+22 and Ton 256- have been detected at two nearby radio frequencies (see Sramek and Weedman

(1978) for the additional radio measurements). Using the two measurements, the radio spectral index for NAB 0024+22 is -0.2±0.3 and for Ton 256 is 0.3±0.8. Although the uncertainty in these values is large and the frequency baseline is small (≈ 2 GHz) they are in accord with a flat spectrum relativistic jet model of radio quiet quasars.

Possible objections to the simple relativistic beaming model presented in Scheur and Readhead (1979) are raised by radio observations of samples of optically selected quasars. Both the high fraction of bright optically selected quasars detected as radio sources (Condon *et al.* 1981; Smith and Wright 1980) as well as the distribution of quasar radio fluxes (Stritmatter *et al.* 1981) appear to be in conflict with the predictions of this model; the number of objects, though, in these statistical samples is quite small. It has been pointed out (Smith and Wright 1980; Kellermann and Pauliny-Toth 1981) that the objections raised by these observations can be mollified by more sophisticated relativistic jet models involving, for example, a range of Γ.

v) Infrared emission: Comptonization model

One mechanism proposed to account for the infrared emission of quasars is the upscattering of a source of soft photons of frequency ν_0 into the infrared via inverse Compton scattering by non-relativistic electrons in a thermal plasma cloud. In analytical treatments of Comptonization in a cloud having large electron scattering optical depth (τ) (Katz 1976; Shapiro *et al.* 1976; Sunyaev and Titarchuk 1980; Payne 1980) it has been shown that for $\nu>\nu_0$ the emergent steady-state continuum is a power law with spectral index determined by τ and T, the electron temperature. Using Monte Carlo techniques, Pozdnyakov *et al.* (1979) have demonstrated that a power law continuum is also produced in the case where the Comptonizing cloud has $\tau\leq 3$. It is thus apparent that the Comptonization mechanism can account for the observed power law spectral form of

the infrared data; in addition, an appealing feature of electron scattering models having spherical symmetry is that they readily produce the low observed optical polarizations of radio quiet quasars (Moore 1981).

In Figure 6, a Comptonization model continuum with $\nu_0=10^{12}$ is compared with the observed energy distribution of the radio quiet quasar PG 1358+04. As the curve shown illustrates, a Comptonization model can be consistent with both the 1mm observations as well as the infrared data since the continuum produced will exhibit the turnover (at ν_0) required by the present data (Figure 2b). In fact, the upper limit to the 1mm flux density provides a lower limit to the allowed values of ν_0. The actual value of this lower limit is model dependent, being determined by the form of the energy distribution of the seed photons. For the curve in Figure 6, it was assumed that the soft photon source had a blackbody spectrum (Pozdnyakov *et al.* 1979) peaking at $\nu_0=10^{12}$; if the soft photon source is monochromatic (Sunyaev and Titarchuk 1980) the Comptonization continuum has spectral index $3-\alpha_{IR}$ (instead of 2) at $\nu<\nu_0$ and the lower limit to ν_0 obtained is 5×10^{11}. An upper limit to ν_0 of $\sim2\times10^{13}$ can be derived from the observational fact that the infrared power law continuum extends to a wavelength of 10μm (see dashed curve in Figure 6).

The measured value of the infrared spectral index can be used to constrain the electron temperature and Thompson optical depth of the Comptonizing plasma. In Figure 7 each curve is the locus of values of T and τ which correspond to a given α_{IR}; in constructing these curves the formulae of Payne (1980) were used for $\tau\geq3$ and the results of Pozdnyakov (1979) were used for $\tau<3$. The dashed box shown in Figure 7 is the calculated range of temperatures and optical depths available to the hot intercloud medium proposed to be present in quasars in order to confine the dense compact clouds responsible for the broad emission lines (Mathews 1974; McKee and Tarter 1975). Krolik *et al.*

(1981) have calculated the temperature of the hot intercloud medium by requiring it to be in thermal balance (it is heated primarily by the UV and X-ray quasar continuum); they find values in the range 10^8 to 10^9K depending on which specific heating processes obtain. In addition, they point out that the hot intercloud medium must have $0.2<\tau\leq 1.5$ in order not to significantly weaken and distort the emission lines (see Shields and McKee 1981). As can be seen in Figure 7, inverse Compton scattering in the hot intercloud medium could produce infrared power law emission with spectral index consistent with observed values (Table 1). It is also apparent from Figure 7, though, that a cooler, more optically thick Comptonizing plasma cannot be ruled out solely on the basis of the observed infrared energy distribution.

Additional constraints on the physical parameters of the thermal plasma are imposed by two self-consistency requirements of the Comptonization model. A power law Comptonization continuum such as that shown in Figure 6 will be produced under conditions in which stimulated Compton scattering is not significant (see, e.g., Katz 1976); it is thus required that the radiation brightness temperature, T_B , not exceed the electron temperature over the frequency range of interest (Chapline and Stevens 1973; Sunayev 1971; Zeldovich and Levich 1968; Petschek, Colgate, and Colvin 1976). The condition $T_B / T<1$ is satisfied if ν_o is greater than a critical frequency ν_c given by

$$\nu_c = 1.3\times 10^9 \frac{z}{(1+z)^{3/2}} F_c^{1/2} \frac{n_e}{T^{1/2}\tau} \quad \text{Hz} \qquad (2)$$

where F_c is the flux density in mJy at ν_c and n_e is the electron density in cm^{-3}. In deriving equation (2) it has been assumed that $q_0 = 1$ and $H_0 = 50\mathrm{kms}^{-1}\mathrm{Mpc}^{-1}$. Using equation (2) and the observed parameters of PG 1358+04 it is found that the range of values for ν_0 consistent with the infrared and 1mm data (see above) correspond to electron densities of the Comptonizing plasma between 5×10^5 and

$10^8 cm^{-3}$ for $T \sim 10^9$. For electron densities in this range the thermal plasma would be effectively optically thick to free-free absorption at frequencies below $\sim 5 \times 10^8$Hz for typical values of the electron temperature The model thus satisfies the second self-consistency requirement: at the wavelengths under consideration the photons will interact with the plasma primarily through Compton scattering and are not destroyed by free-free absorption. The range of electron densities derived here agree well with calculated densities of the hot intercloud medium. By requiring the hot intercloud medium to be in stable equilibrium with the emission line clouds Krolik *et al.* (1981) obtain electron densities between 10^5 and $10^7 cm^{-3}$ if the broad line clouds have $10^9 < n_e < 10^{10} cm^{-3}$ (Kwan and Krolik 1981). As a final consistency check it should be pointed out (see, also Krolik *et al.* 1981) that a plasma with temperature and density in the ranges discussed here would not produce X-ray bremsstrahlung emission in excess of measured values (Zamorani *et al.* 1980; Ku *et al.* 1980).

c) Radio Loud Quasars

The radio loud quasars observed fall mainly into two categories based on their radio structure. Nine of the radio loud quasars observed are similar to blazars in having an intense 6cm flux density, exhibiting a flat radio spectrum, and being compact at centimeter wavelengths ($\Theta < 1$ arcsecond). These nine quasars will be termed compact radio loud quasars. As discussed in section III, 5 of the radio loud quasars observed show a "triple" radio structure with central components showing weak 6cm emission. These objects are historically classified as radio loud because the large beam sizes of the early radio surveys measured the extended emission. These five quasars shall be referred to as extended radio loud quasars.

i) Infrared emission

Both the compact and extended radio loud quasars have infrared and optical properties more similar to radio quiet quasars than blazars. (Table 1). These include low optical polarization, 3.5 μm infrared excess, and small optical variability. This would suggest that, unlike blazars, the infrared continuum observed from radio loud quasars is most likely not dominated by relativistically beamed synchrotron radiation. It is conceivable, then, that like radio quiet quasars, the infrared/optical emission from radio loud quasars can be primarily attributed to Comptonization in a thermal plasma.

ii) Compact Radio Loud Quasars: Radio emission

It has long been known (Kellermann 1966) that the flat radio spectrum exhibited by compact radio loud quasars can result from the superposition of the synchrotron radiation from a number of homogeneous components of different angular sizes. In the framework of a multicomponent synchrotron model, the fact the high frequency radio continua of compact radio loud quasars do not, in general, turn up at a wavelength of 1mm (Figure 1b) indicates that small components whose emission would peak near 1mm are not required. Cook and Spangler (1980) have fit the radio continua of a large sample of extragalactic radio sources by a model having multiple synchrotron components. They find such a model unattractive since the frequencies of maximum emission of the components must be distributed in a highly regular and artificial manner, a fact referred to as the "cosmic conspiracy" (Cotton *et al.* 1980).

Up to this point, each synchrotron model considered has assumed that the radiating electrons have a power law distribution of energies. An alternate electron energy distribution which can produce a broad flat synchrotron spectrum is a relativistic Maxwellian distribution (Jones and Hardee 1979; Spangler 1980). In Figure 8, the observed flux densities of the radio loud quasar 4C39.25 are compared with the synchrotron continuum produced by electrons with a

relativistic Maxwellian distribution of temperature 140 $m_e c^2$; Spangler (1980) has shown that this model continuum provides a good fit to the radio data. The Maxwellian synchrotron continuum used by Spangler (1980) has been extended to a wavelength of 1mm using the volume emissivity calculated in Jones and Hardee (1979). As can be seen in Figure 8, the Maxwellian continuum is steeply falling at millimeter wavelengths and is thus inconsistent with the present measurement. The physical basis for this discrepancy is that the due to the exponential fall off of a Maxwellian distribution at high energies, there is not a large enough number of electrons which emit primarily at a wavelength of 1mm to account for the observed flux density.

It has been shown above that a relativistic jet model can reproduce the observed radio energy distributions of both blazars and radio quiet quasars. The observed radio emission from compact radio loud quasars can also be attributed to synchrotron radiation from a relativistic jet; the axis of the jet has an angle with the line of sight intermediate to the angles appropriate for blazars and radio quiet quasars (Blandford and Königl 1979; Marscher 1980). A larger value of ϑ will cause both $D(\vartheta)$ and $1/\sin\vartheta$ to decrease which, as can by seen by equation (1), will result in a lower turnover frequency. The fact that a majority of compact radio loud quasars have radio continua which show a steepening at 90 GHz while blazars do not (Table 1; Condon 1978) is attributed to a lower turnover frequency of the jet synchrotron continuum (Königl 1981).

As illustrated by the data in Figure 1b, the 30 to 90 GHz radio continua of compact radio loud quasars can be extended smoothly to a wavelength of 1mm; there is no evidence for a further steepening of the radio continuum. In general, a break in an optically thin synchrotron continuum will occur due to the fact that electrons will lose energy by emitting synchrotron radiation (Kellermann 1966; Kardashev 1962). For a relativistic jet, the frequency of this spectral

break, ν_b, can determined by requiring that the jet reach a radius r_u (it maximum extent) in a synchrotron cooling time (Blandford and Königl 1979); the result is

$$\nu_b = 6.9\times10^7 \frac{D(\vartheta)\Gamma^2\beta^2}{B_1^3(1+z)} r_u \qquad (3)$$

The present data indicate that ν_b>300GHz which, for typical values of the physical parameters of the jet (see above), implies that r_u must be greater than a parsec.

iii) Extended Radio Loud Quasars: Radio emission

As discussed in section III, the present 1mm observations of extended radio loud quasars actually are upper limits to the 1mm flux density from the central components associated with the quasar itself. Like the radio quiet quasars observed, none of the central components were detected at a wavelength of 1mm regardless of their infrared characteristics (compare Figures 2b and 2c). In addition, the central components have the low 6cm flux densities characteristic of radio quiet quasars. From this circumstantial evidence, it can be argued that the radio emission from the central components of extended radio loud quasars is produced by the same mechanism responsible for the radio emission of radio quiet quasars. It has been shown above that a reasonable choice for this mechanism is synchrotron radiation from a relativistic jet whose axis lies near the plane of the sky. A relativistic jet model for the central components of extended radio loud quasars is appealing since it is generally believed that energy is transported to the lobes via collimated jets (Blandford and Rees 1974). The absence of extended radio structure associated with radio quiet quasars could reflect a more tenuous external region surrounding these quasars than that present in double-lobed radio loud quasars (Owen *et al.* 1978).

d) Summary

The 1mm observations are consistent with, and supportive of, an overall picture in which the observed nature of an object, i.e., whether it is a blazar, radio-loud quasar, or radio quiet quasar depends on the orientation of a relativistic jet with respect to the line of sight (Blandford and Königl 1978; Scheur and Readhead 1979). In this scenario, each of these objects are composed primarily of two components: (1) a jet of synchrotron radiating electrons undergoing bulk relativistic motion, and (2) a Comptonizing thermal plasma. In blazars, the jet axis is pointed toward the observer causing its synchrotron radiation to dominate the shape and polarization of the observed continuum at radio through optical wavelengths. In radio quiet quasars the relativistic jet lies in the plane of the sky and is responsible for the weak radio emission. The infrared continuum of radio quiet quasars is produced in the thermal plasma by the Comptonization of soft photons. In radio loud quasars the angle of the jet axis is between zero and ninety degrees. In this case the observed infrared emission is most likely due, primarily, to the Comptonization process; the jet alone produces the radio emission. There are difficulties with this simple scenario. As pointed out by Moore (1981) if jet orientation is primarily responsible for object type, blazars should have larger optical luminosities than radio loud and radio quiet quasars but on average do not. Also, an additional radiation component is needed in the infrared to produce the excess 3.5μm emission.

VI. CONCLUSIONS

In this paper we have presented one millimeter wavelength observations of a sample of 37 extragalactic objects including blazars, radio loud quasars, and radio quiet quasars. The major observational results are:

1. No radio quiet quasar was detected at wavelength of 1mm; three sigma upper limits to the 1mm flux density are ~ 1 Jy.
2. For blazars and radio loud quasars the observed radio continuum can, on average, be directly extrapolated to a wavelength of 1mm.
3. The 1mm flux density of blazars exhibits a correlation with an extrapolation of the infrared continuum.

An interpretation of these results leads to the following conclusions concerning the radiative processes responsible for the continuum emission of active extragalactic objects:

1. A model in which the radio through optical continuum observed from blazars is attributed to synchrotron radiation from a relativistic jet whose axis makes a small angle with the line of sight naturally accounts for the observed correlation of the 1mm emission with both the radio and infrared continua. The 1mm and infrared data suggest that the jets associated with blazars observed have similar velocities, magnetic field distributions, and electron energy distributions.
2. Radio quiet quasar models invoking synchrotron self absorption or free-free absorption to suppress the radio emission of these objects produce steep energy distributions incompatible with the 1mm observations. A model in which the weak radio emission from radio quiet quasars is due to a relativistic jet oriented perpendicular to the observer's line of sight can produce the flat radio continuum required by the 1mm observations.
3. A model in which the infrared continua of radio loud and radio quiet quasars is produced by the Comptonization of soft photons having frequencies in the range 10^{12} to 10^{13} Hz is consistent with both the 1mm observations and the infrared data. The hot medium in which the quasar emission line clouds are believed to be imbeded in is a possible candidate for the required thermal

plasma.

4. The radio continua of the radio loud quasars observed do not show the effect of synchrotron radiation losses at wavelengths as short as one millimeter. In addition, the 1mm measurements of radio loud quasars preclude the existence of synchrotron radiation from small components which would emit primarily at this wavelength. Finally, the 1mm data for radio loud quasars are inconsistent with a relativistic Maxwellian energy distribution of synchrotron radiating electrons.

TABLE 1

OBSERVED CONTINUUM PROPERTIES OF QUASARS AND BL LAC OBJECTS

				Radio			
(1)	(2)	(3)	(4)	(5)	(6)	(7)	(8)
Object	Coord.	Redshift z[a]	Type[b]	$\log F_\nu^{6cm}$ (mJy)[c]	Ref.	α_R[d]	Ref.
III Zw 2	0007+10	0.089	L	3.28(S)	1	-0.3	1
NAB	0024+22	1.118	Q	2.30	7	-0.2	8
PG	0026+12	0.142	Q	0.26	7		
PKS	0106+01	2.107	L	3.58	2	-0.1(C)	2
3C48	0134+32	0.367	L	3.73	3	-0.9(St)	4
AO	0235+16		BL	3.32(S)	6	-0.1(St)	6
4C47.08	0300+47		BL	3.29(S)	6	-0.2(C)	6
3C95	0349-14	0.614	L(ex)	1.30	5		
OA129	0420-01	0.915	BL	3.47(S)	6	0.4(St)	6
OI 158	0735+18		BL	3.27	2	0.0(St)	2
PKS	0736+01	0.191	BL	3.35	2	0.0(St)	2
OJ 287	0851+20	(0.306)	BL	3.49(S)	6	0.4(St)	6
PG	0906+48	0.118	Q	<-0.22	7		
4C39.25	0923+39	0.699	L	3.87	2	0.0(C)	2
PG	1001+05	0.161	Q	<-0.22	7		
PKS	1004+13	0.240	L(ex)	0.95	5		
PKS	1055+01	0.890	L	3.44	2	0.0(St)	2
W Com	1219+28		BL	3.29	2	0.0(St)	2
Mrk 205	1219+76	0.070	O				
3C273	1226+02	0.158	L	4.52(S)	6	-0.1(C)	6
3C279	1253-05	0.538	BL	4.20	9	-0.4(St)	10
PKS	1308+32	(0.996)	BL	3.37(S)	6	0.1(St)	6
PG	1351+64	0.088	Q	1.51	7		
PG	1358+04	0.427	Q	<0.70	13		
Ton 202	1425+26	0.366	L(ex)	1.78	5	-0.1	5
PKS	1510-08	0.361	L	3.46(S)	6	0.4(C)	6
LB9743	1525+23	0.253	L	2.11	7	-0.7	8
Ton 256	1612+26	0.131	Q	1.26	14	0.3	8
SW 77	1623+26	2.540	Q	<0.95	15		
3C345	1641+39	0.595	BL	3.84(S)	6	0.1(St)	6
Mrk 501	1652+39	(0.034)	BL	3.10	16	-0.3(St)	16
3C351	1704+60	0.371	L(ex)	1.26	5		
OT 081	1749+09		BL	3.32(S)	1	0.2(St)	1
PKS	2135-14	0.200	L(ex)	1.99	5		
BL Lac	2200+42	(0.070)	BL	3.45(S)	1	0.3(St)	1
4C31.63	2201+31	0.297	L	3.34	9	0.1(C)	10
3C454.3	2251+16	0.859	BL	3.90(S)	1	-0.2(C)	1

[a] Values shown are from Hewitt and Burbridge (1980).
Redshift estimates for the BL Lac objects are taken from references 11 and 12
[b] Type designation is BL= blazar, Q= radio quiet quasar,
L= radio loud quasar, L(ex)= radio loud quasar with extended emission,
O= optically selected quasar; See text for type definitions.
[c] Flux density shown is in a 55 arsecond beam. (S) denotes
simultaneous radio and 1mm observations.
[d] Typically, flux densities at 5 and 15 GHz were used to
calculate α_R. (C) denotes radio continua which exhibit a spectral
steepening at 90 GHz; (St) indicates that the radio continuum is straight.

TABLE 1
(continued)

		Infrared	Optical				
(9)	(10) 3.7 cm Polarization	(11)	(12)	(13)	(14)	(15)	(16) Optical Polarization
Coord.	(%)	Ref.	$\log F_\nu^{1.6\mu}$ (mJy)	α_{IR}^{e}	Ref.	α_{opt}^{f}	(%)[f]
0007+10	1.0	1	1.05(S)	-1.1(B)	21	-0.7	0.3
0024+22							0.6
0026+12			0.81	-1.0(B)	20	-1.0	0.3
0106+12	1.6	18				-1.1	2.5
0134+22	5.2	18	0.41	-1.5(B)	20	-1.3	1.5
0235+16	3.8	17	1.03	-1.3(St)	6	-4.0	6-25
0300+47	11.5	17	0.67	-1.3	23		12-24
0349-14			0.10	-1.8(B)	20	-0.5	1.4
0420-01	4.0	1					10-20
0735+18	4.7	17	1.33	-1.0(St)	22	-1.3	3-31
0736+01	4.8	18	0.65		22	-1.1	1-6
0851+20	16.6	17	1.09(S)	-1.3(St)	21	-1.4	1-32
0906+48			0.49	-1.3(B)	20	-0.9	1.1
0923+39	0.5	18					0.7
1001+05			0.89	-1.1	20	-0.5	0.5
1004+13			0.58	-1.2	20	-0.3	1.0
1055+01	5.5	18					
1219+28	5.8	17	0.82	-1.3(St)	21	-2.3	2-10
1219+76			1.01	-0.9(St)	20	-0.9	0.4
1226+02	2.4	19	1.63(S)	-1.2(B)	21	-0.2	0.3
1253-05			0.57(S)	-1.6(St)	21	-1.5	4-12
1308+32			1.37	-1.2(St)	22	-1.6	2-17
1351+64			0.85	-1.6	20	-0.4	0.7
1358+04			0.22	-1.5(B)	20	-0.3	0.5
1425+26			0.26		20	-0.7	2.0
1510-08	3.0	1	0.36		20	-0.9	1.8
1525+23			0.09		21		0.7
1612+26			0.68	-1.2(B)	20	-0.8	0.2
1623+26			-0.35		21		
1641+39	2.5	18	0.95(S)	-1.6(St)	21	-1.2	3-17
1652+39			1.72		23	-2.5	2-14
1704+60			0.57	-1.3	20	-0.6	0.3
1749+09	7.2	17				-2.2	3-9
2135-14			0.63	-1.1(B)	20	-0.6	0.4
2200+42	6.4	17	1.79(S)	-1.4(St)	21	-1.6	2-23
2201+31			0.79	-1.3(B)	20	-0.3	0.2
2251+16	3.6	18	0.27	-1.2	21	-1.3	1-4

[e] The infrared spectral index was calculated using flux densities at 10, 2.2, 1.6, and 1.2 μm. (B) denotes that emission in excess of the power law is observed at 3.5 μm (see text); (St) indicates straight infrared continua well fit by a power law.
[f] Values taken from Moore (1981).

References for Table 1

1. Aller, Aller, and Hodge (1981)
2. Owen *et al.* (1980)
3. Pauliny-Toth and Kellermann (1968)
4. Kellermann and Pauliny-Toth (1971)
5. Miley and Hartsuijker (1978)
6. Jones *et al.* (1981)
7. Condon *et al.* (1981)
8. Sramek and Weedman (1980)
9. Kuhr *et al.* (1980)
10. Geldzahler and Witzel (1979)
11. Miller *et al.* (1978)
12. Smith (1978)
13. Shaffer and Green (1978)
14. Fanti *et al.* (1977)
15. Sramek and Weedman (1978)
16. Owen *et al.* (1978)
17. Wardle (1978)
18. Altschuler and Wardle (1977)
19. Rudnick *et al.* (1978)
20. Neugebauer *et al.* (1979)
21. Neugebauer (1981)
22. O'Dell *et al.* (1978b)
23. Puschell and Stein (1980)

TABLE 2

ONE MILLIMETER OBSERVATIONS OF QUASARS AND BL LAC OBJECTS

Object	Coordinates	Type	Date of Observation	1mm Flux Density[a] (Jy)
III Zw 2	0007+10	L	06 Dec 79	0.8±0.2[b]
NAB	0024+22	Q	07 Dec 79	<1.1
PG	0026+12	Q	04 Dec 79	<1.0
PKS	0106+01	L	06 Dec 79	2.4±0.5
3C48	0134+32	L	17 Feb 79	<0.7
AO	0235+16	BL	16 Feb 79	1.7±0.3
4C47.08	0300+47	BL	18 Feb 79	1.0±0.3
3C95	0349-14	L(ex)	06 Dec 79	<0.9
OA 129	0420-01	BL	12 Jan 79	2.6±0.8
OI 158	0735+18	BL	06 Dec 79	1.2±0.3
PKS	0736+01	BL	06 Dec 79	1.0±0.3
OJ 287	0851+20	BL	09 Nov 78	4.9±1.0[b]
PG	0906+48	Q	12 Jan 79	<0.8
4C39.25	0923+39	L	08 Dec 79	2.0±0.4
PG	1001+05	Q	09 Nov 78	<1.3
PKS	1004+13	L(ex)	13 Jan 79	<0.8
PKS	1055+01	L	06 Dec 79	1.7±0.3
W Com	1219+28	BL	04 Apr 80	2.9±0.6
Mrk 205	1219+76	O	15 Oct 78	<0.9
3C273	1226+02	L	25 Nov 77	10.2±2.1[b]
3C279	1253-05	BL	11 Jan 79	4.6±1.2[b]
PKS	1308+32	BL	20 Dec 78	2.1±0.4
PG	1351+64	Q	06 Dec 79	<0.9
PG	1358+04	Q	13 Jan 79	<0.9
Ton 202	1425+26	L(ex)	24 Dec 80	<0.9
PKS	1510-08	L	15 Mar 79	2.7±0.9
LB 9743	1525+23	L	30 Mar 80	<0.9
Ton 256	1612+26	Q	13 Jan 79	<0.9
SW 77	1623+26	Q	15 Mar 79	<2.7
3C345	1641+39	BL	29 Mar 80	7.7±1.5[b]
Mrk 501	1652+39	BL	31 Mar 80	0.8±0.2
3C351	1704+60	L(ex)	16 Feb 79	<1.0
OT 081	1749+09	BL	04 Apr 80	2.6±0.5
PKS	2135-14	L(ex)	05 Dec 79	<0.8
BL Lac	2200+42	BL	08 Dec 79	5.1±1.2[b]
4C31.63	2201+31	L	08 Dec 79	1.7±0.3
3C454.3	2251+16	BL	04 Dec 79	4.6±0.9

[a] The upper limits are three times the statistical uncertainty.
For each measurement the value of the 1mm flux density is at least three times the statistical uncertainty; the uncertainty shown is the larger of the statistical or calibration (20%) uncertainties.

[b] Source shown to have time variable 1mm flux density.
See Ennis *et al.* 1981.

TABLE 3

ONE MILLIMETER OBSERVATIONS OF RADIO QUIET QUASARS

Object	Coordinates	1mm Flux Density (Jy)	Radio Flux Density[a] (mJy)	Radio-1mm Spectral Index α_{RQ}
NAB	0024+22	<1.1	200±10	<0.4
PG	0026+12	<1.0	1.8±0.3	<1.5
PG	1351+64	<0.9	32.0±1.4	<0.8
Ton 256	1612+36	<0.9	18±3.3	<0.7

[a] For all quasars except Ton 256, the value shown is the 4.885 GHz flux density taken from Condon *et al.* (1981). For Ton 256 the 1.415 GHz flux density from Fanti *et al.* (1977) was used.

REFERENCES

Aller, M.F., Aller, H.D., and Hodge, P.E. 1981, preprint.

Altschuler, D.R., and Wardle, J.F.C. 1975, *Nature*, **255**, 306.

Altschuler, D.R., and Wardle, J.F.C. 1977, *M. N. R. A. S.*, **179**, 153.

Angel, J.R.P. 1969, *Ap. J.*, **158**, 219.

Angel, J.R.P., and Stockman, H.S. 1980, *Ann. Rev. Astr. Ap.*, **18**, 321.

Baldwin, J.A., Smith, H.E., Burbridge, E.M., Hazard. C., Mudoch, H.S., and Jauncy, D.L. 1976, *Ap. J. (Letters)*, **206**, L83.

Blandford, R.D., and Königl, A. 1979, *Ap. J.*, **232**, 34.

Blandford, R.D., and Rees, M.J. 1974, *M. N. R. A. S.*, **169**, 395.

Chapline, G., and Stevens, J. 1973, *Ap. J.*, **184**, 1041.

Cohen, M.H., Pearson, T.J., Readhead, A.C.S., Seielstad, G.A., Simon, R.S., and Walker, R.C. 1979, *Ap. J.*, **231**, 293.

Condon, J.J. 1978 in *Pittsburgh Conference on BL Lac Objects*, ed. A.M. Wolfe (Pittsburgh: University of Pittsburgh Press), p. 21.

Condon, J.J., and Dressel, L.L. 1973, *Astro. Lett.*, **15**, 203.

Condon, J.J., O'Dell, S.L., Puschell, J.J., and Stein, W.A. 1981, *Ap. J.*, **246**, 624.

Cook, D.B., and Spangler, S.R. 1980, *Ap. J.*, **240**, 751.

Cotton, W.D., Wittels, J.J., Shapiro, I.I., Marcaide, J., Owen, F.N., Spangler, S.R., Rius, A., Angulo, C., Clark, T.A., and Knight, C.A. 1980, *Ap. J. (Letters)*, **238**, L123.

de Bruyn, A.G. 1976, *Astr. Ap.*, **52**, 439.

Elias, J.H., Ennis, D.J., Gezari, D.Y., Hauser, M.G., Houck, J.R., Lo K.Y., Matthews, K., Nadeau, D., Neugebauer, G., Werner, M.W., and Westbrook, W.E. 1978, *Ap. J.*, **220**, 25.

Ennis, D.J., Soifer, B.T., Neugebauer, G., Werner, M. 1981, *Astro. Lett.*, **22**, 143.

Ennis, D.J., and Werner, M.W. 1981, preprint.

Fanti, C., Fanti, R., Lari, C., Padrielli, L., van der Laan, H., de Ruiter, H. 1977, *Astr. Ap.*, **61**, 487.

Geldzahler, B.J., and Witzel, A. 1979, preprint.

Ginzburg, V.L., and Syrovatskii, S.I. 1965, *Ann. Rev. Astr. Ap.*, **3**, 297.

Green, R.F. 1976, *Pub. A. S. P.*, **88**, 665.

Harper, D.A., Hildebrand, R.H., Stiening, R., and Winston, R. 1976, *Appl. Opt.*, **15**, 53.

Harvey, P.M., Wilking, B.A., and Joy, M., 1981, preprint.

Hauser, M.G., and Notarys, H.A. 1975, *Bull. AAS*, **7**, 409.

Hewitt, A. and Burbridge, G. 1980, *Ap. J. Suppl.*, **43**, 57.

Hildebrand, R.H., Whitcomb, S.E., Winston, R., Stiening, R.F., Harper, D.A., and Moseley, S.H. 1977, *Ap. J.*, **216**, 698.

Jones, T.W., and Hardee, P.E. 1979, *Ap. J.*, **228**, 268.

Jones, T.W., Rudnick, L., Owen, F.N., Puschell, J.J., Ennis, D.J., and Werner, M.W. 1981, *Ap. J.*, **243**, 97.

Kardashev, N.S. 1962, *Soviet Astronomy-AJ*, **6**, 317.

Katz, J.I. 1976, *Ap. J.*, **206**, 910.

Kellermann, K.I. 1964, *Ap. J.*, **140**, 969.

Kellermann, K.I. 1966, *Ap. J.*, **146**, 621.

Kellermann, K.I., and Pauliny-Toth, I.I.K. 1971, *Astro. Lett.*, **8**, 153.

Kellermann, K.I., and Pauliny-Toth, I.I.K. 1981, *Ann. Rev. Astr. Ap.*, **19**, 373.

Kieffer, H.H., Chase, S.C., Miner, E., Munch, G., and Neugebauer, G. 1973, *J. Geophys. Res.*, **78**, 4291.

Kinman, T.D., Wardle, J.F.C., Conklin, E.K., Andrew, B.H., Harvey, G.A., MacLeod, J.M., and Medd, W.J. 1974, *A. J.*, **79**, 349.

Königl, A. 1981, *Ap. J.*, **243**, 700.

Kreysa, E., Pauliny-Toth, I.I.K., Schultz, G.V., Sherwood, W.A., and Witzel, A. 1980, *Ap. J. (Letters)*, **240**, L17.

Krolik, J.H., McKee, C.F., and Tarter, C.B. 1981, preprint.

Ku, W.H.-M., Helfand, D.J., and Lucy, L.B. 1980, *Nature*, **288**, 323.

Kuhr, H. 1980, in preparation.

Kwan, J. and Krolik, J.H. 1981, preprint.

Marscher, A.P. 1977a, *A. J.*, **82**, 781.

Marscher, A.P. 1977b, *Ap. J.*, **216**, 244.

Marscher, A.P. 1980, *Ap. J.*, **235**, 386.

Mathews, W.G. 1974, *Ap. J.*, **189**, 23.

McGimsey, B.Q., Smith, A.G., Scott, R.L., Leacock, R.S., Edwards, P.L., Hackney, R.L., and Hackney, K.R. 1975, *A. J.*, **80**, 895.

McKee, C.F., and Tarter, C.B. 1975, *Ap. J.*, **202**, 306.

Miley, G.K., and Hartsuijker, A.P. 1978, *Astr. Ap. Suppl.*, **34**, 129.

Miller, J.S., French, H.B., and Hawley, S.A. 1978 in *Pittsburgh Conference on BL Lac Objects*, ed. A.M. Wolfe (Pittsburgh: University of Pittsburgh Press), p. 176.

Moffet, A.T. 1975 in *Galaxies and the Universe*, ed. A. Sandage, M. Sandage, and J. Kristian (Chicago: University of Chicago Press), p. 211.

Moore, R.L. 1981, Ph.D. Thesis, University of Arizona

Muehlner, D. and Weiss, R. 1973, *Phys. Rev. D*, **7**, 326.

Neugebauer, G., Oke, J.B., Becklin, E.E., and Matthews, K. 1979, *Ap. J.*, **230**, 79.

Neugebauer, G. 1981, unpublished data.

O'Dell, S.L. 1978a in *Pittsburgh Conference on BL Lac Objects*, ed. A.M. Wolfe (Pittsburgh: University of Pittsburgh Press), p. 312.

O'Dell, S.L., Puschell, J.J., Stein, W.A., Owen, F., Porcas, R.W., Mufson, S., Moffett, T.J., and Ulrich, M.-H. 1978b, *Ap. J.*, **224**, 22.

O'Dell, S.L. 1979, in *Active Galactic Nucleii*, ed. C. Hazard and S. Mitton (Cambridge: Cambridge University Press), p. 95.

Oke, J.B. 1974, *Ap. J. (Letters)*, **189**, L47.

Owen, F.N., Porcas, R.W., Mufson, S.L., and Moffett, T.J. 1978, *A. J.*, **83**, 685.

Owen, F.N., Porcas, R.W., and Neff, S.G. 1978, *A. J.*, **83**, 1009.

Owen, F.N., Spangler, S.R., and Cotton, W.D. 1980, *A. J.*, **85**, 351.

Pauliny-Toth, I.I.K., and Kellermann, K.I. 1968, *A. J.*, **73**, 953.

Payne, D.G. 1980, *Ap. J.*, **237**, 951.

Pearson, T.J., Unwin, S.C., Cohen, M.H., Linfield, R.P., Readhead, A.C.S., Seielstad, G.A., and Simon, R.S. 1981, preprint.

Petschek, A.G., Colgate, S.A., and Colvin, J.D. 1976, *Ap. J.*, **209**, 356.

Pozdnyakov, L.A., Sobol, I.M., and Sunyaev, R.A. 1979, *Sov. Astron. Lett.*, **5**, 149.

Puschell, J.J., and Stein, W.A. 1980, *Ap. J.*, **237**, 331.

Puschell, J.J., Stein, W.A., Jones, T.W., Warner, J.W., Owen, F., Rudnick, L., Aller, H., and Hodge, P. 1979, *Ap. J. (Letters)*, **227**, L11.

Rieke, G.H., Grasdalen, G.L., Kinman, T.D., Hintzen, P., Wills, B.J., and Wills, D. 1976, *Nature*, **260**, 754.

Roellig, T.L. 1980, Ph.D. Thesis, Cornell University

Roellig, T.L., Houck, J.R., Ennis, D.J., Elliot, K.H. 1981, preprint.

Rowan-Robinson, M., Clegg, P.E., and Ade, P.A.R. 1975, *M. N. R. A. S.*, **172**, 603.

Rudnick, L., Owen, F.N., Jones, T.W., Puschell, J.J., and Stein, W.A. 1978, *Ap. J. (Letters)*, **225**, L5.

Scheuer, P.A.G., and Readhead, A.C.S. 1979, *Nature*, **277**, 182.

Schnopper, H.W., Delvaille, J.P., Epstein, A., Cash, W., Charles, P., Bowyer, S., Hjellming, R.M., Owen, F.N., and Cotton, W.D. 1978, *Ap. J. (Letters)*, **222**, L91.

Seielstad, G.A., Cohen, M.H., Linfield, R.P., Moffet, A.T., Romney, J.D., Schilizzi, R.T., and Shaffer, D.B. 1979, *Ap. J.*, **229**, 53.

Shaffer, D.B., and Green, R.F. 1978, *Pub. A. S. P.*, **90**, 22.

Shapiro, S.L., Lightman, A.P., and Eardley, D.M. 1976, *Ap. J.*, **204**, 187.

Shields, G.A., and McKee, C.F. 1981, *Ap. J. (Letters)*, **246**, L57.

Smith, H.E. 1978 in *Pittsburgh Conference on BL Lac Objects*, ed. A.M. Wolfe (Pittsburgh: University of Pittsburgh Press), p. 211.

Smith, M.G., and Wright, A.E. 1980, *M. N. R. A. S.*, **191**, 871.

Spangler, S.S. 1980, *Astro. Lett.*, **20**, 123.

Sramek, R.A., and Weedman, D.W. 1978, *Ap. J.*, **221**, 468.

Sramek, R.A., and Weedman, D.W. 1980, *Ap. J.*, **238**, 435.

Stein, W.A. 1978, in *Pittsburgh Conference on BL Lac Objects*, ed. A.M. Wolfe (Pittsburgh: University of Pittsburgh Press), p. 1.

Strittmatter, P.A., Hill, P., Pauliny-Toth, I.I.K., Steppe, H., and Witzel, A. 1981, preprint.

Sunyaev, R.A. 1970, *Astro. Lett.*, **7**, 19.

Sunyaev, R.A., and Titarchuk, L.G. 1980, *Astr. Ap.*, **86**, 121.

Tucker, W.H. 1975, *Radiation Processes in Astrophysics*, (Cambridge: MIT Press)

Wardle, J.F.C. 1978 in *Pittsburgh Conference on BL Lac Objects*, ed. A.M. Wolfe (Pittsburgh: University of Pittsburgh Press), p. 39.

Weedman, D.W. 1977, *Ann. Rev. Astr. Ap.*, **15**, 69.

Werner, M.W., Neugebauer, G., Houck, J.R., and Hauser, M.G. 1978, *Icarus*, **35**, 289.

Williams, P.J.S. 1963, *Nature*, **200**, 56.

Winston, R. 1970, *J. Opt. Soc. Am.*, **60**, 245.

Wolfe, W.L. 1965 in *Handbook of Military Infrared Technology*, ed. W.L. Wolfe (Washington, D.C.: U.S. Government Printing Office), p. 50.

Zamorani, G., Henry, J.P., Maccacaro, T., Tananbaum, T., Soltan, A., Avni, Y., Liebert, J., Stocke, J., Strittmatter, P.A., Weymann, R.J., Smith, M.G., and Condon, J.J. 1980, *Ap. J.*, in press

Zeldovich, Ya.B., and Levich, E.V. 1969, *Soviet Phys.- JETP*, **28**, 1287.

Zwicky, F. 1967, *Adv. Astr. Ap.*, **5**, 267.

FIGURE CAPTIONS

Figure 1- a) The observed 1mm flux density of blazars versus the 1mm flux density obtained from an extrapolation of the high frequency radio continuum. The open circles correspond to simultaneous radio and 1mm measurements. The solid line shown has slope one and passes through the origin. The radio data used for the extrapolation are taken from the references listed in Table 1.

b) The same as a) except that the data plotted is for the radio loud quasars measured at 1mm.

Figure 2- a) The observed 1mm flux density of blazars versus the 1mm flux density obtained from an extrapolation of the infrared continuum. The open circles correspond to simultaneous infrared and 1mm measurements. The lines shown have slope one; the dashed line has intercept -1.22 and the solid line passes through the origin, as in Figure 1. The infrared extrapolated 1mm flux density is calculated using the flux density and spectral index listed in Table 1.

b) The same as a) except that the data plotted are for the radio quiet quasars observed at 1mm.

c) The same as a) except that the data plotted are for the radio loud quasars observed at 1mm. The crosses are the data points for the radio loud quasars with extended radio emission (see text).

Figure 3- The observed radio through infrared energy distributions of the blazars observed at 1mm. The 1mm data (at $\log\nu$=11.5) are from this paper; The radio and infrared data shown are taken from the references of Table 1.

Figure 4- The observed energy distribution of the blazar OJ 287; the radio, infrared, and 1mm data were taken concurrently in Nov/Dec 1978. The radio observations are from Jones *et al.* (1981); the infrared measurements were reported in Puschell and Stein (1980). The curve shown is the expected continuum from a canonical optically thin synchrotron source with a high energy cutoff in its electron energy distribution. The parameters of the model synchrotron source (see text) were chosen to provide a good fit to the radio and 1mm observations.

Figure 5- The observed energy distribution of PG 1351+64 compared with the continuum emission produced by several theoretical models of radio quiet quasars. The upper limit to the 1mm flux density is from this paper. The 5 GHz flux density is taken from Condon *et al.* (1981); the infrared data are from Neugebauer *et al.* (1979). The curve labelled free-free is the continuum produced by a canonical synchrotron source whose emission is affected by free-free absorption in an external plasma. The curve labelled homogeneous (inhomogeneous) synchrotron is the continuum which would be observed from a self-absorbed synchrotron source with homogeneously (inhomogeneously) distributed physical parameters. The details of these models are found in the text; continuum normalization and model parameters were chosen so that the model emission would be consistent with both the infrared data and the measured 6cm flux density. For comparison, the synchrotron emission from a relativistic jet with physical parameters

typical of blazars but viewed at angle of 82° is also shown.

Figure 6- The observed energy distribution of the radio quiet quasar PG 1358+04. The upper limit to the 1mm flux density is from the present work; the infrared data were taken from Neugebauer *et al.* (1979). The curve shown is the emergent continuum produced by the Comptonization model discussed in the text, in which the infrared quasar emission is due to the upscattering of photons with frequency ν_0 by a plasma of thermal electrons. For the solid curve $\nu_0 \sim 10^{12}$; for the dashed line $\nu_0 \sim 10^{13}$.

Figure 7- Electron temperature, T, versus electron scattering optical depth, τ of the model Comptonizing plasma. Each curve is the locus of values of T and τ which correspond to the labelled value of the infrared spectral index α_{IR}. These curves were constructed using the results of Payne (1980) and Pozdnyakov, *et al.* (1979). The dashed box is the calculated range of temperatures and optical depths available to the hot inter-cloud medium; see text.

Figure 8- A comparison between the observed radio continuum of the radio loud quasar 4C39.25 and theoretical synchrotron continuum produced by a relativistic Maxwellian distribution of electrons. All the radio data except for the present 1mm flux density (the point lying above the curve), were taken from Owen *et al.* (1980). The curve shown is the from the model of Spangler (1980) which has the following parameters: electron temperature- 140 $m_e c^2$, ν_T, the synchrotron characteristic frequency for electrons of this energy - 4.8 GHz, and τ_1, the source optical depth at ν_T- 0.50.

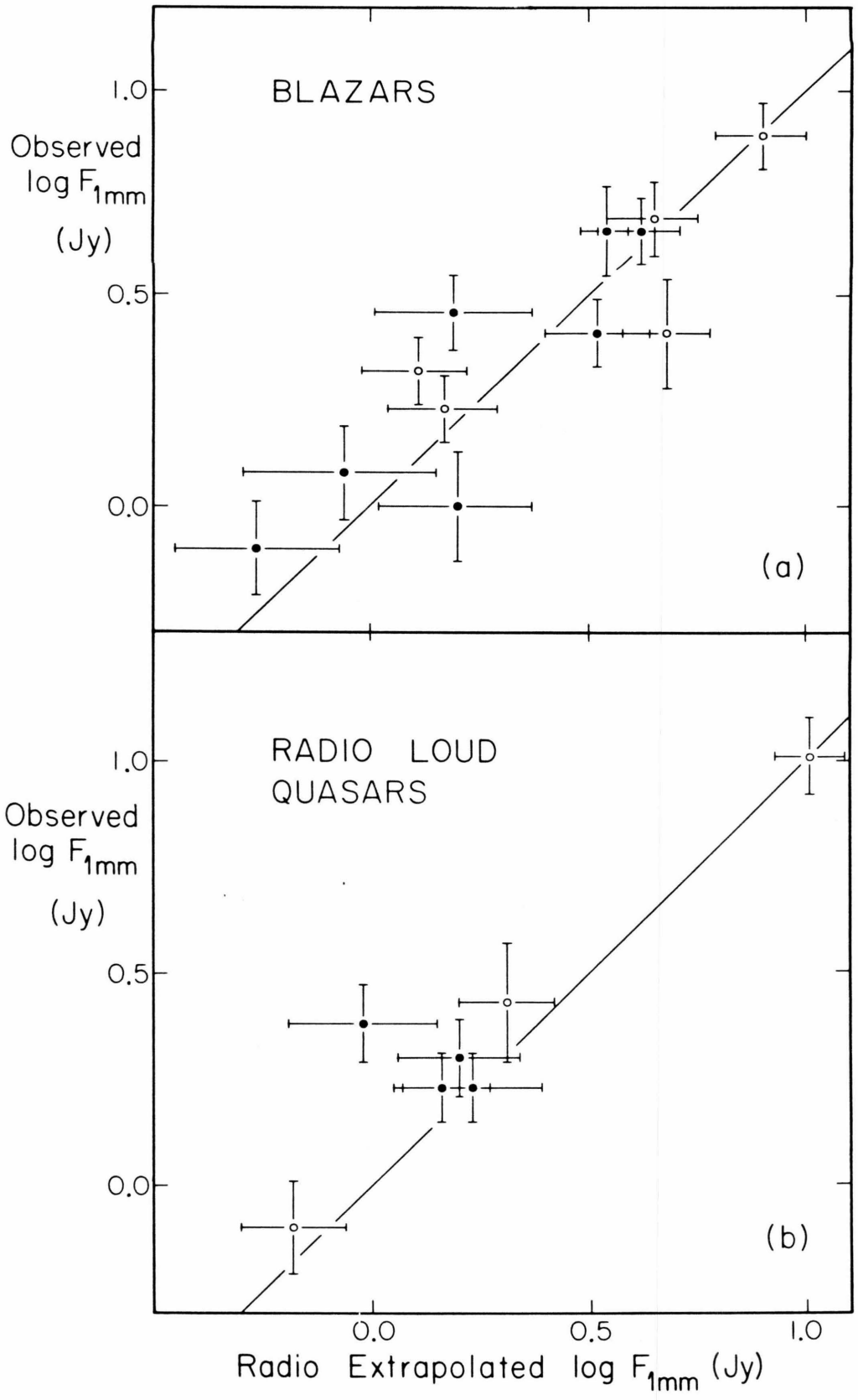
BLAZARS
Observed log F_{1mm} (Jy)
1.0
0.5
0.0
(a)
RADIO LOUD QUASARS
Observed log F_{1mm} (Jy)
1.0
0.5
0.0
(b)
0.0
0.5
1.0
Radio Extrapolated log F_{1mm} (Jy)

Figure 1

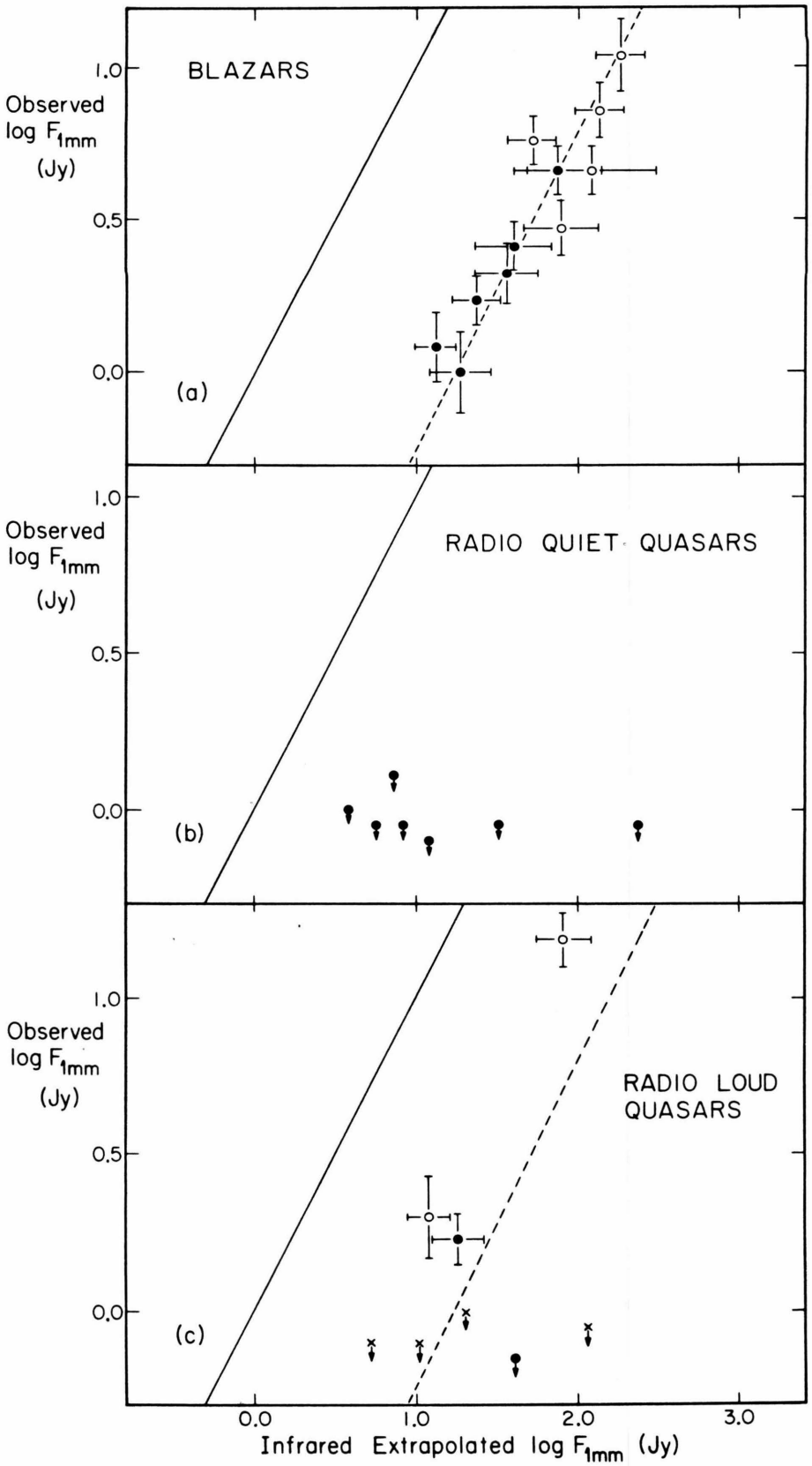
BLAZARS
(a)
RADIO QUIET QUASARS
(b)
RADIO LOUD QUASARS
(c)
Observed log F_{1mm} (Jy)
1.0
0.5
0.0
0.0
1.0
2.0
3.0
Infrared Extrapolated log F_{1mm} (Jy)

Figure 2

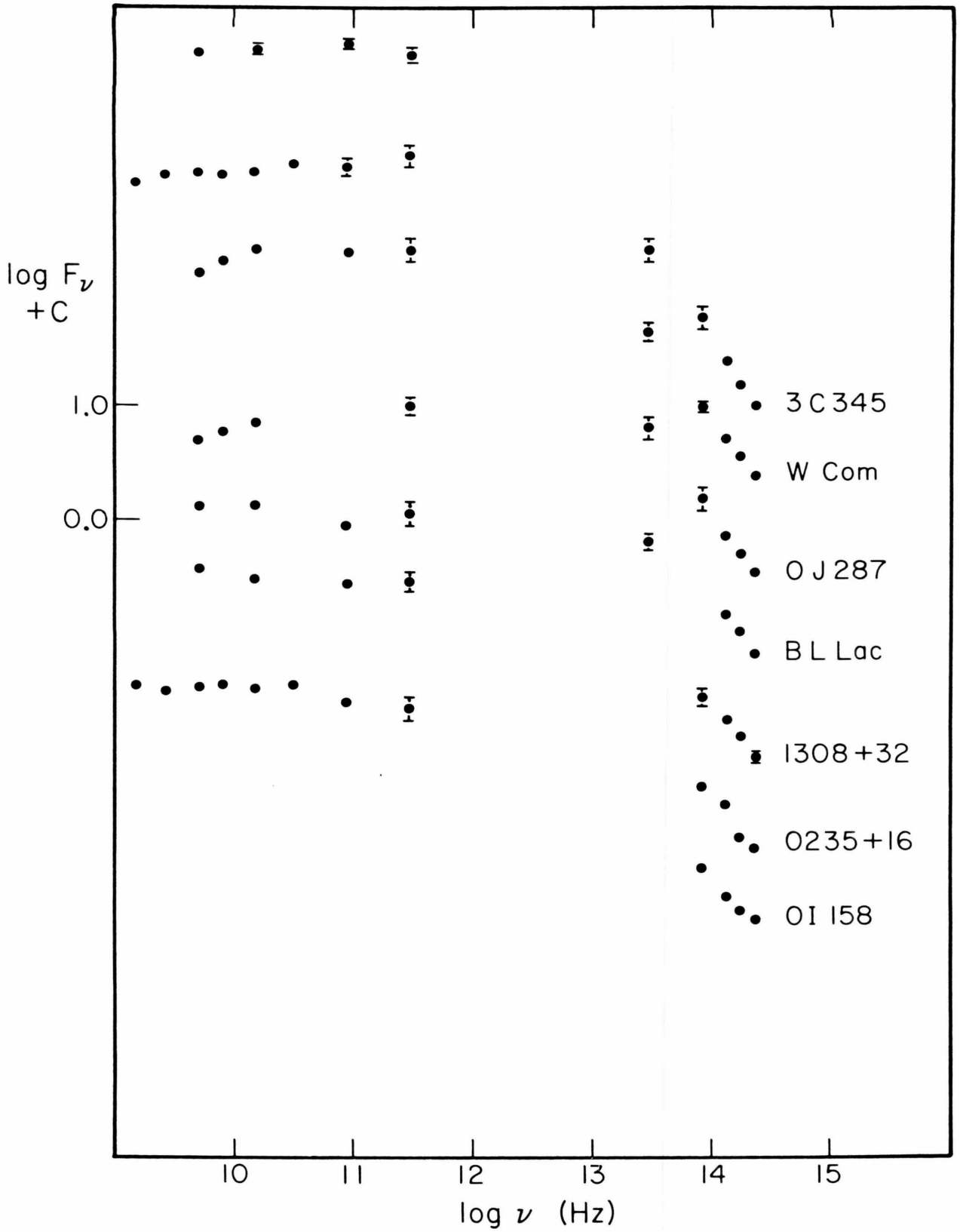
log F_ν
+C
1.0
0.0
10
11
12
13
14
15
log ν (Hz)
3C345
W Com
OJ287
BL Lac
1308+32
0235+16
OI 158

Figure 3

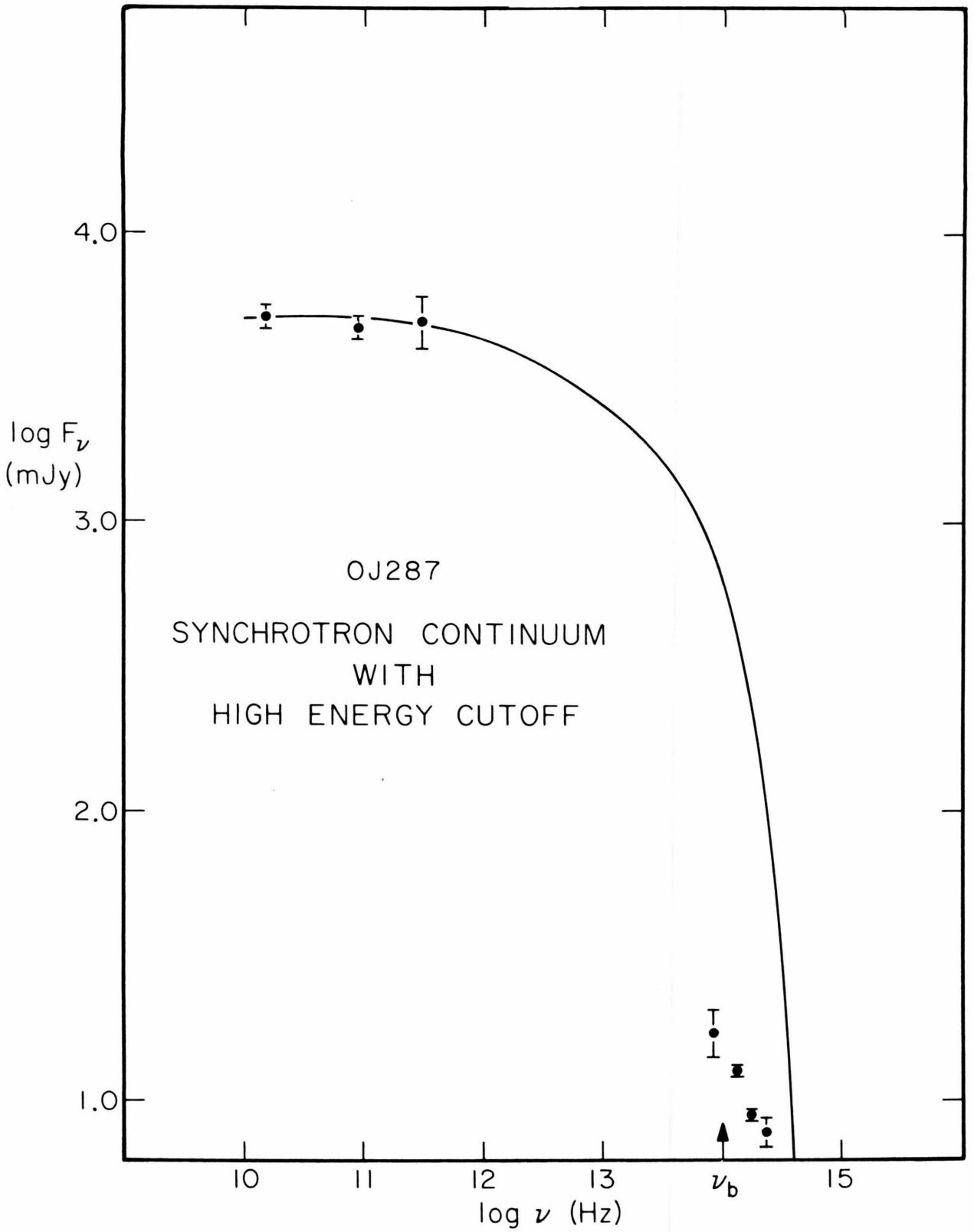
4.0
3.0
2.0
1.0
log F_ν
(mJy)
OJ287
SYNCHROTRON CONTINUUM
WITH
HIGH ENERGY CUTOFF
10
11
12
13
ν_b
15
log ν (Hz)

Figure 4

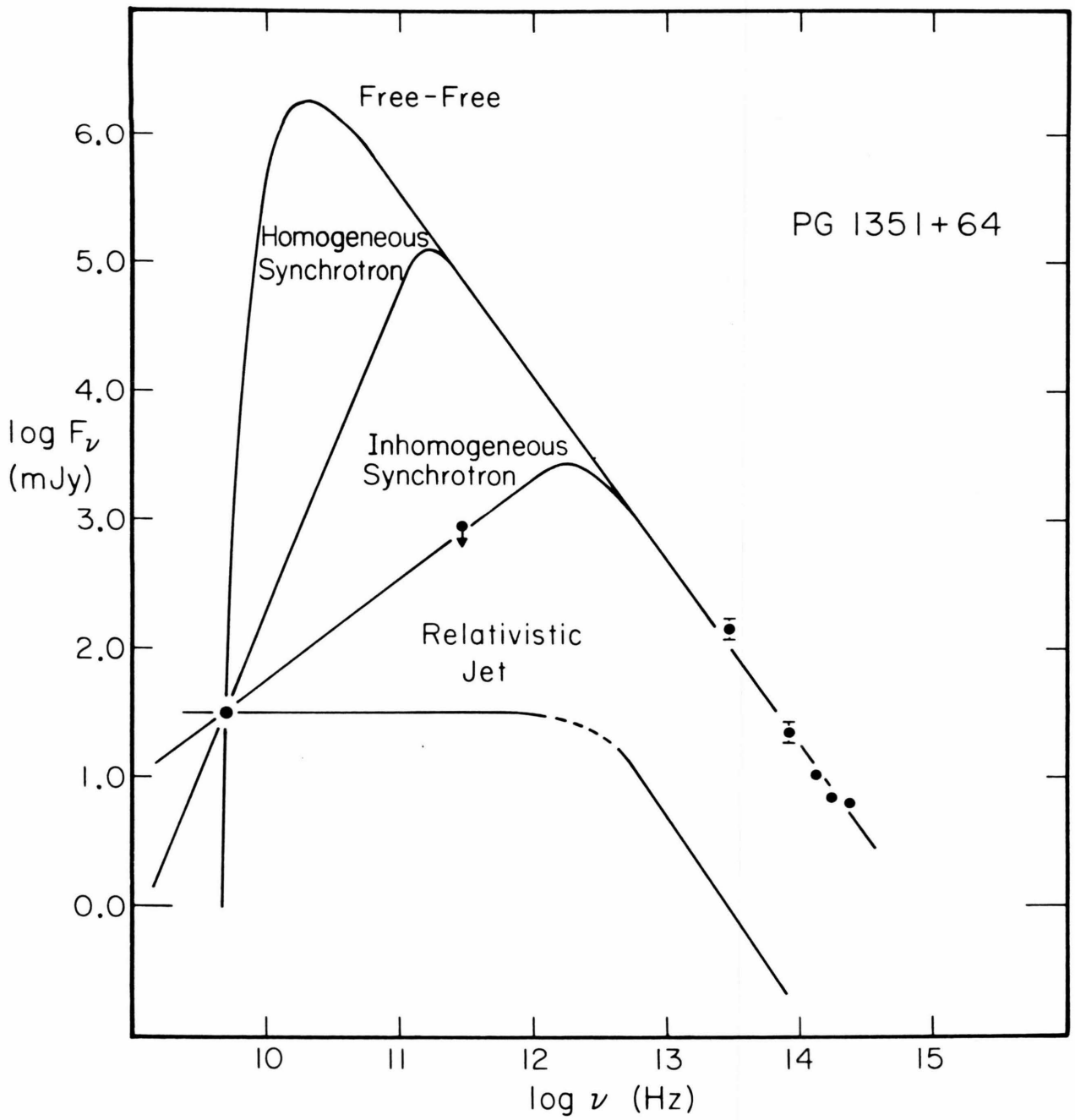
Free-Free
Homogeneous
Synchrotron
Inhomogeneous
Synchrotron
Relativistic
Jet
PG 1351+64
6.0
5.0
4.0
3.0
2.0
1.0
0.0
log F_ν
(mJy)
10
11
12
13
14
15
log ν (Hz)

Figure 5

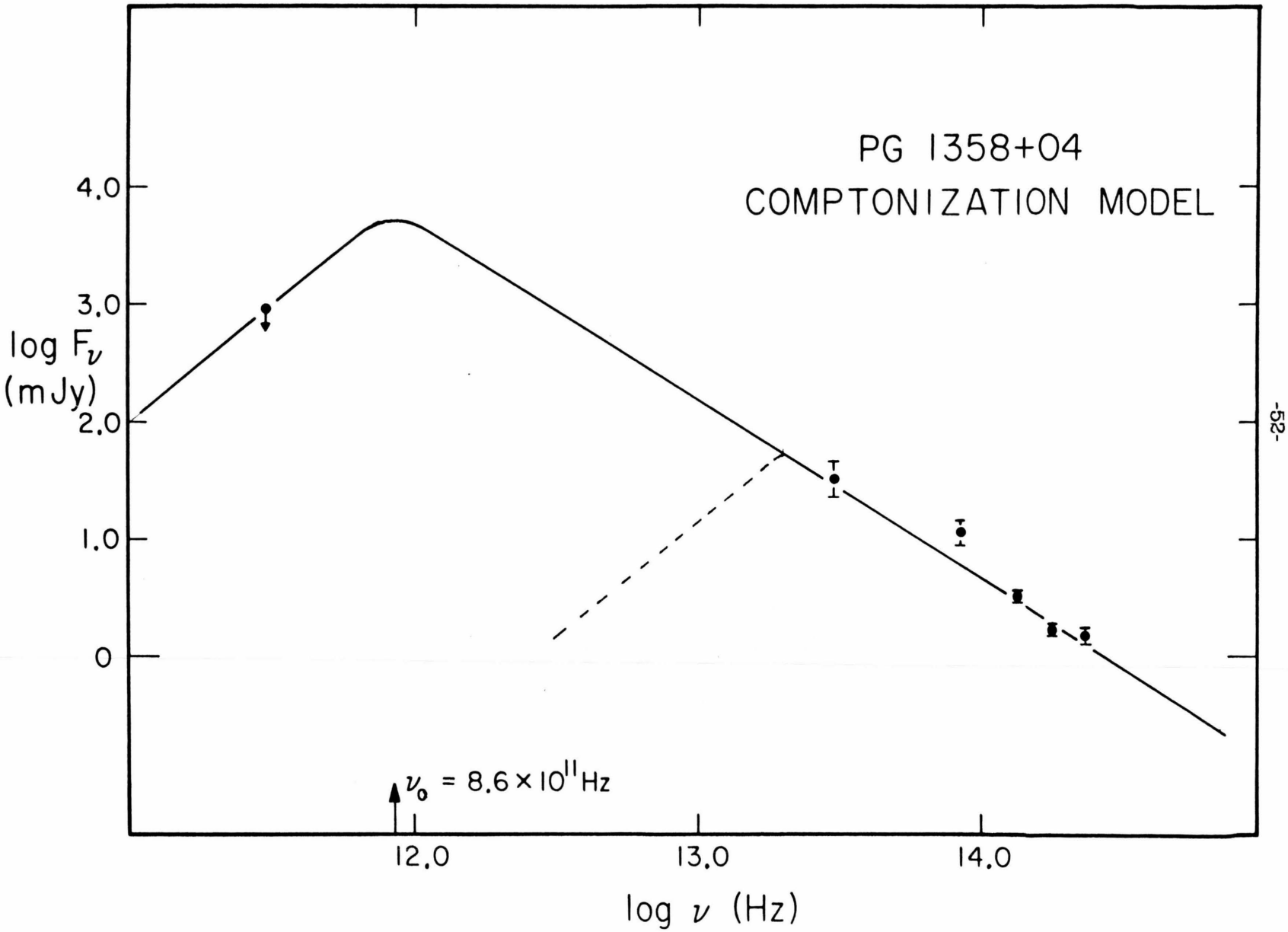
PG 1358+04
COMPTONIZATION MODEL
4.0
3.0
2.0
1.0
0
log F_ν
(mJy)
$\nu_0 = 8.6 \times 10^{11}$ Hz
12.0
13.0
14.0
log ν (Hz)

Figure 6

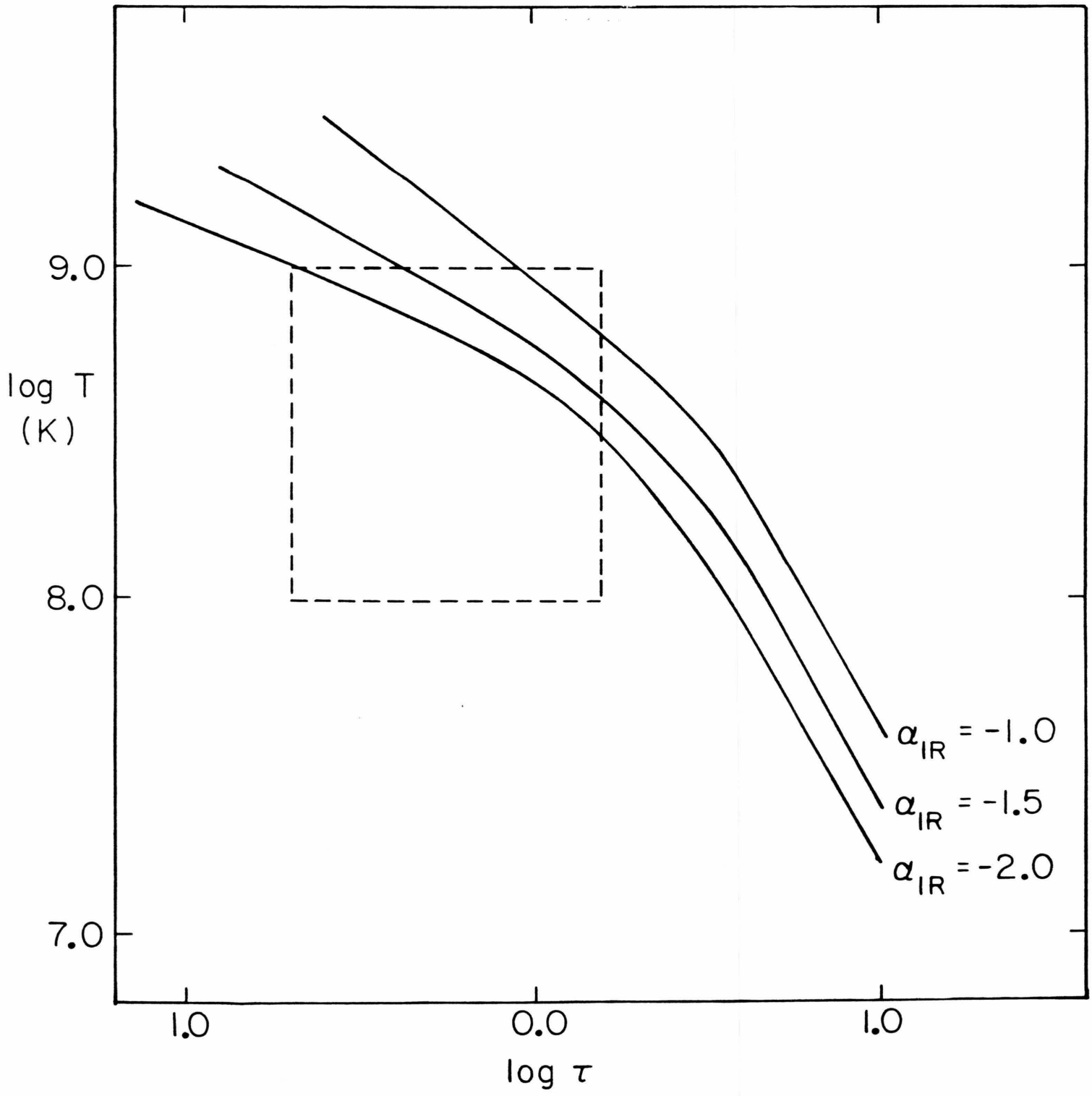

Figure 7

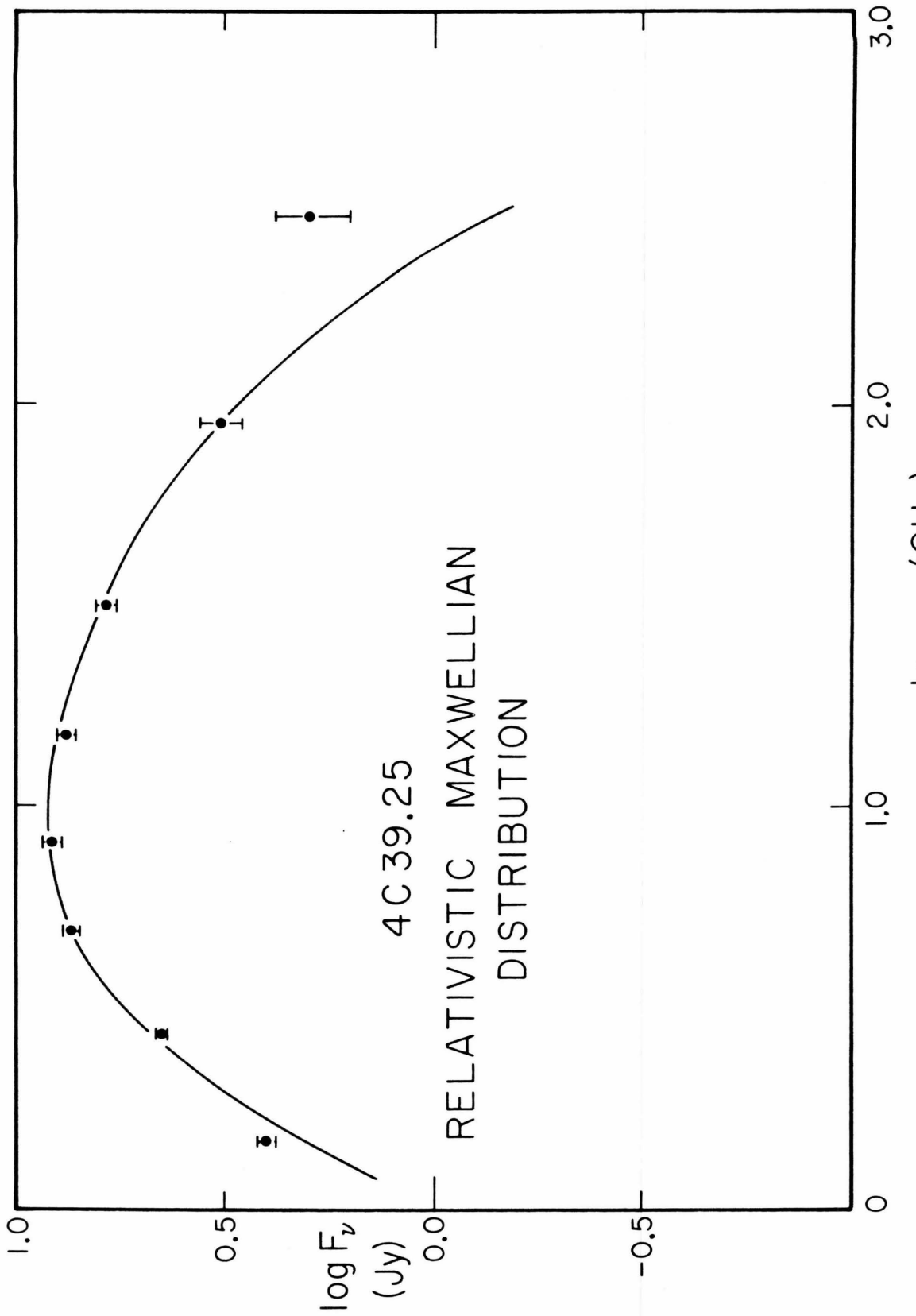
4C 39.25
RELATIVISTIC MAXWELLIAN
DISTRIBUTION
log F_ν (Jy)
log ν (GHz)
1.0
0.5
0.0
-0.5
0
1.0
2.0
3.0

Figure 8

PAPER II: VARIABILITY OF COMPACT RADIO SOURCES AT A WAVELENGTH OF ONE MILLIMETER

ABSTRACT

Broadband one millimeter continuum observations of 3C273, 3C279, BL Lac, 3C84, OJ287, and 3C345 made between March 1977 and January 1981 are reported. With the possible exception of 3C279, all of the objects exhibited evidence for variability in the 1mm flux density on the time scale of a few months. Flux variations at wavelengths of 1mm and 2cm are well correlated for the blazars (BL Lac objects and OVV quasars) observed; emission outbursts occur simultaneously and have similar amplitude at the two wavelengths. In contrast, an outburst in the flux from the Seyfert Galaxy 3C84 was observed at a wavelength of 1mm in early 1980 but has not appeared at 2cm as of one year later. The observed relationship between blazar emission variability at 1mm and 2cm is inconsistent with the canonical expanding source model of radio variability or any of its modifications. Instead, models in which the number of synchrotron radiating electrons is time variable (due to particle injection or acceleration behind a relativistic shock) are required.

I. INTRODUCTION

Many compact radio sources have been shown to have variable emission at centimeter wavelengths (e.g., Altschuler and Wardle 1977; Kesteven *et al.* 1977; Andrew *et al.* 1978). The variability often takes the form an outburst lasting several months to a year; outbursts typically occur every few years (Kellermann and Pauliny-Toth 1968). High radio frequency observations of the variability of radio sources are, in general, scarce, although outbursts of 3C273 and AO 0235+16 have been observed at 90 GHz (Schorn *et al.* 1968; Ledden *et al.* 1976; see, also Hobbs and Dent 1977). In a previous publication (Elias *et al.* 1978) the initial results of a program to monitor the one millimeter (300 GHz) flux density from BL Lac, 3C273, 3C279, and 3C84 have been reported. As reported in Elias *et al.* 1978, during the time span of these observations- June 1974 to January 1977- the 1mm flux density showed formal evidence for variability in all sources except 3C279, although no distinct outbursts in the 1mm emission were observed.

The appearance of a given outburst at various radio wavelengths often shows a distinctive pattern; an outburst will reach its maximum earlier and have a larger amplitude at the shortest radio wavelength (Kellermann and Pauliny-Toth 1968; Van der Laan 1970). This observational fact provides one motivation for monitoring variable radio sources at a wavelength of 1mm; an emission outburst could be detected first and be quite intense at a wavelength of one millimeter. A further motivation for observations of variable radio sources at 1mm is that at this short a wavelength the synchrotron radiation from high energy electrons is being observed. Such energetic electrons can lose a significant amount of energy via synchrotron losses, a mechanism traditionally not taken into account in theoretical models of radio variability (see, e.g., Van der Laan 1966). One millimeter observations of variable radio sources can thus act as a probe for

which energy loss processes are dominant during emission outbursts.

In this paper the monitoring of the 1mm flux density from BL Lac, 3C273, 3C279, 3C84, OJ 287 and 3C345 between March 1977 and January 1981 is reported. For BL Lac, 3C273, 3C279, and 3C84 these observations extend those presented in Elias *et al.* (1978) to a longer time base. Improvements in detector sensitivity have allowed the inclusion of the fainter objects OJ 287 and 3C345 in the monitoring program. This monitoring program constitutes a search for variability in the 1mm flux density from the objects observed on a time scale of several months. The observing procedure is described in Section II; the results of the program are presented in section III. In section IV, the observed nature of the 1mm variability is discussed within the context of present models of radio source variability.

II. OBSERVATIONS

All the new observations at a wavelength of one millimeter presented in this paper were made at the prime focus of the five meter Hale telescope between March 1977 and January 1981. A detailed description of the incoherent detectors used, the spectral filtering, the observational procedure, and the data reduction process has been presented in previous publications (Elias *et al.* 1978; Ennis and Werner 1981; Ennis *et al.* 1981). Briefly, two systems were employed each containing a composite germanium bolometer as detector; in one the bolometer was cooled with liquid ^{4}He (Hauser and Notarys 1975) in the other liquid ^{3}He was the cryogen (Roellig 1980). Each system had a broad spectral response with an effective wavelength of 1mm and $\Delta\lambda/\lambda \sim 1$. The 1mm measurements were made with a 55 arcsecond diameter aperture.

Absolute 1mm flux density calibration is based on the measured brightness temperatures of the planets (Werner *et al.* 1978). NGC 7027 was used as a secondary calibrator; it has a 1mm flux density of 7.0 Jy (Roellig *et al.* 1981). Due to

weather limitations 1mm observations of a given source were typically made every several months; the most complete time coverage was for the quasar 3C273 (see Figure 1a). During the summer months observations at a wavelength of 1mm were, in general, not possible due to the high water vapor content of the atmosphere resulting in low atmospheric transparency.

III. RESULTS

The objects for which the 1mm flux density has been monitored are listed in Table 1. These sources were chosen for observation because they are relatively bright extragalactic sources of 1mm radiation and because they have shown large emission variability at centimeter wavelengths (see, e.g., Altschuler and Wardle 1977). Because of their similar observed continuum properties, the optically violent variable quasars 3C279 and 3C345 (McGimsey *et al.* 1975) are often grouped with the the BL Lac objects OJ 287 and BL Lac into one class termed blazars (Angel and Stockman 1981; Ennis and Werner 1981). 3C84 has been classified a Type 1 Seyfert Galaxy (see, e.g., Weedman 1977) and 3C273 is a radio loud quasar.

The one millimeter flux density and corresponding date of observation for the objects in the monitoring program are also shown in Table 1. If a flux density shown in Table 1 is an average of measurements made over a number of days, a range of dates is shown. The uncertainty associated with a given 1mm flux density measurement is a quadrature sum of the statistical and calibration uncertainties. The calibration uncertainty is due primarily to the dispersion in the sensitivity determinations given by the individual planet measurements (Elias *et al.* 1978). A measurement of the 1mm flux density is considered a detection if it is at least three times the statistical uncertainty. All upper limits are three times the combined uncertainties. A spectral index α ($F_\nu \propto \nu^\alpha$) of zero was assumed for all six objects in determining the 1mm flux density (Ennis and

Werner 1981 and references therein).

In Figure 1 the 1mm flux density is plotted versus the date of observation for the objects observed. Included in Figure 1 are the earlier data from Elias *et al.* (1978). From the appearance of these light curves, it can be seen that with the possible exception of 3C279, all of these sources exhibit time variability of the 1mm flux density. Statistical analysis confirms the impression of Figure 1. In Table 2 values of the reduced χ^2 are given for the fit of the observations to a line with constant 1mm flux density equal to the weighted mean. The data for none of the objects are well fit by a constant flux density line; the most significant deviation is for 3C84 and the least significant is for 3C279. For comparison, an analysis of the 1mm measurements of planets made over the time span shown in Figure 1 gives a reduced χ^2 of ~ 0.4. In this analysis, the variation in the 1mm flux density of a planet due to changes in its angular size with time, was taken into account; the resulting value of χ^2 is, thus, that expected from a source of constant flux density.

During the time period of the present observations there were several well sampled instances of large amplitude 1mm flux density changes occurring on the time scale of several months to a year (Figure 1). A notable example is the early 1980 emission outburst of 3C84 in which the 1mm flux density rose from a quiescent level of 24±2 Jy to a maximum of 64±6 Jy measured in April 1980. Over a period of 8 months (October to May 1978) the 1mm flux density of OJ 287 decreased by a factor of two from a peak value of 5±1 Jy.

The 1mm observations shown in Table 1 can be compared with measurements made at longer radio wavelengths. As part of ongoing monitoring program, Aller *et al.* (1981) have made 2cm flux density measurements of the objects in Table 1 on a weekly basis over the time period of the present 1mm observations. In Figure 2, the 2cm and 1mm light curves have been

superimposed upon each other. For the blazars OJ287, BL Lac, 3C345, and 3C279, the flux density variability at wavelengths of 1mm and 2cm are well correlated; changes in the emission at the two wavelengths occurs simultaneously and are of the same magnitude. For example, in early 1979, both the 1mm and 2cm flux densities of OJ 287 decreased by a factor of ~ 2 on the same time scale. Similarly, the increase in the 1mm emission from BL Lac in early 1980 corresponds to an observed 2cm outburst. Simultaneous radio emission variability at nearby wavelengths has, on occasion, been observed (Locke *et al.* 1969) but not over such a large range in radio wavelengths as in the present data.

In contrast to what is observed for blazars, the 1mm and 2cm flux densities of 3C84 and 3C273 do not show simultaneous variability (Figure 2). This is most clearly demonstrated by the early 1980 outburst of 3C84 which was observed at a wavelength of 1mm but was not present at 2cm; the 2cm flux density showed no sign of a significant increase through November 1980. During the time period of the present observations the 1mm flux density from 3C273 has gradually risen while the 2cm flux density fell and then levelled off.

IV. DISCUSSION

In this section the observed 1mm emission variability and its relationship to the variability of the 2cm flux density are compared to theoretical models of variable radio sources. Any acceptable model must be able to reproduce the major result of the last section, namely, that for the blazars observed the 1mm and 2cm flux densities vary simultaneously and have similar amplitude outbursts.

a) Models of Blazar Emission Variability

It is convenient to characterize the variability of a source by two model dependent parameters. These quantities, which are readily compared with observations (see Altschuler and Wardle 1977), are the ratio of the strengths of

an outburst at two different observing wavelengths, R, and the ratio of the times of the peak of an outburst at the same two wavelengths, termed x. In our case, $R=\Delta F_{1mm}/\Delta F_{2cm}$ where $\Delta F_{1mm}=F_{1mm}^{max}-F_{1mm}^{min}$ and F_{1mm} is the observed 1mm flux density. Also, $x=(t_{2cm}-t_0)/(t_{1mm}-t_0)$ where t_{1mm} is the time at which the 1mm flux density is at a maximum and t_0 is the time at which the outburst began. For the blazars in the present sample, the observed simultaneity of the 1mm and 2cm flux density variations imply that $x\sim1$. As demonstrated most convincingly by the late 1978 moderate outburst of OJ 287 (Figure 2a), the amplitude of variations observed at 1mm and 2cm are comparable indicating that $R\sim1$.

i) Canonical Model

In what has become known as the canonical model for radio source variability (Shklovsky 1960; Van der Lann 1966; Pauliny-Toth and Kellermann 1966) an emission outburst is attributed to a cloud of electrons emitting synchrotron radiation and expanding uniformly with constant velocity; the expansion causes the optical depth to synchrotron radiation through the cloud to decrease with time. The observed flux density from the cloud will increase during the time at which the cloud is optically thick at the observation wavelength and decreases as the cloud becomes optically thin. Due to the frequency dependence of the synchrotron absorption opacity the following expressions obtain for the canonical model (Pauliny-Toth and Kellermann 1966):

$$R = \left(\frac{\lambda_2}{\lambda_1}\right)^{\frac{7\gamma+3}{4\gamma+6}} \qquad x = \left(\frac{\lambda_2}{\lambda_1}\right)^{\frac{\gamma+4}{4\gamma+6}} \tag{1}$$

where γ is the spectral index of the assumed power law distribution of electron energies ($N(E)\propto E^{-\gamma}$) and λ_i is an observing wavelength. The values for R and x shown in the first row of Table 3 are obtained from equation (1); for this

calculation the observation wavelengths considered in this paper ($\frac{\lambda_2}{\lambda_1}$=20) were used, and a typical value for γ of 2 was assumed. It is seen that if this model obtains the amplitude of a given outburst would be 40 times stronger and and the time delay of peak emission would be 4 times shorter at a wavelength of 1mm than at a wavelength of 2cm. As indicated above, for the blazars observed, x and R are typically 1. Thus the observed variability of the sample blazars is inconsistent with the canonical model.

The canonical model contains a number of simplifying physical assumptions in order to facilitate the mathematical analysis. Among these assumptions are:

1) The expansion is spherically symmetric.

2) The expansion is homogeneous and has constant velocity.

3) Electrons lose energy solely through the adiabatic expansion.

In Table 3, the values for R and x obtained in other models in which each of these assumptions are relaxed in turn are presented. For example, a variation of the canonical model characterized by an expansion along one axis instead of in three dimensions (Vitello and Pacini 1977; Vitello and Pacini 1978) gives the values for R and x shown in row 2 of Table 3; For the one-dimensional model the disparity between the observed and theoretical outburst amplitude ratio is lessened, but the discrepancy between the time delay ratios is exacerbated.

Assumption 2) above reflects the fact that the dynamics of the cloud expansion are not taken into account in the canonical model. In the literature, two dynamical treatments of the temporal evolution of the emission from a expanding synchrotron source have appeared. Vitello and Pacini (1977) have considered a direct extension of the canonical model which includes implicitly the hydrodynamics of the free expansion of a synchrotron radiating plasma into a vacuum (Vitello and Salvati 1976). Basically, their numerical calculations give

results for R and x close to the values of the canonical model.

In an alternate dynamical model for radio flux variability, a ultrarelativistic blast wave caused by the release of a large amount of energy propagates through a magnetized plasma (Blandford and Mckee 1976,1978; Jones and Tobin 1978). In a shell-like structure behind the shock front, part of the blast energy goes into accelerating the ambient electrons and amplifying the magnetic field of the plasma thus producing the observed synchrotron radiation. As in the canonical model, the flux density produced by the shocked medium would increase and then decrease as the optical depth through the shell changed. In row 3 of Table 3 the values for R and x are shown for one of the cases considered by Blandford and McKee (1978) in which the energy release is impulsive and the external medium has constant density.

Since the energy loss rate for electrons of energy E in a radio source undergoing adiabatic expansion goes as E/t while the loss rate due to synchrotron radiation (assuming a frozen-in magnetic field) is proportional to E^2/t^4, assumption 3) of the canonical model can be violated for high energy electrons at times close to the onset of the expansion (see, e.g., Kardashev 1962). In order to reproduce the observed wavelength dependence the radio outbursts of Cyg X-3, Marscher and Brown (1975) have developed an extension of the canonical model in which the electron energy loss mechanism is adiabatic expansion for electrons with energy less than a critical energy E_b and synchrotron radiation for electrons with energy greater than E_b. An analytical treatment of the model of Marscher and Brown (1975) gives the following expressions:

$$R = \left[\frac{\lambda_2}{\lambda_1}\right]^{\frac{7\gamma-10}{4\gamma+2}} \qquad x = \left[\frac{\lambda_2}{\lambda_1}\right]^{\frac{\gamma+5}{4\gamma+2}} \tag{2}$$

The numerical results obtained from equation (2) with γ=2 and the wavelength

ratio considered here are shown in row 4 of Table 3. The higher synchrotron energy loss rate implies that the population of relativistic electrons responsible for the observed 1mm emission is lower than in the canonical model; this thus accounts for for the lower value of R.

In summary, it is apparent from the model results presented in Table 3 that even if the canonical model is modified to incorporate more physically reasonable assumptions, it does not successfully account for the observed values of R and x for the blazars in the present program.

ii) Injection Model of Blazar Emission Variability

In contrast to the canonical model (in which the number of electrons is assumed constant) it has been argued that an increase in the observed radio emission from a synchrotron source is due simply to the injection of new relativistic electrons into the radiating volume (Locke *et al.* 1969; Simon 1969; Peterson and Dent 1973; Aller *et al.* 1979). Peterson and Dent (1973) have developed a detailed model in which electrons are injected at a given rate into a magnetized plasma expanding uniformly from an initial non-zero radius r_0. The appealing feature of their model is that an outburst will be observed simultaneously at two frequencies for which the synchrotron source is at all times optically thin; the onset, extent, and time profile of an outburst is determined by the functional form of the time-dependent injection rate and the mechanism for electron energy loss obtaining. In addition, if the injected electrons are characterized by an energy distribution with $\gamma \sim 1$, the observed amplitude of an outburst will be similar at the two frequencies. It is thus seen that an injection model can qualitatively reproduce the observed nature of the 1mm and 2cm flux variation of the sample blazars.

The injection-expansion model of Peterson and Dent (1973) assumes that all electrons lose energy solely through adiabatic expansion. A modified version of

the injection model of Peterson and Dent in which electrons lose energy through the combined effects of adiabatic expansion and their own synchrotron radiation has been considered here. It is found that both the profile of an outburst, i.e, the the shape of the flux density versus time curve, and the amplitude of the outburst will differ for observing frequencies above or below a break frequency ν_b; for frequencies below ν_b, adiabatic lossed dominate while for frequencies above ν_b synchrotron losses dominate. The identical nature of the observed 1mm and 2cm blazar variability would thus indicate that the electrons responsible for the 1mm radiation are not significantly affected by synchrotron losses; in the framework of this model the observations require $\nu_b > 300$ GHz. For the case of constant injection rate (see, also, Kardashev 1962), the break frequency is given by

$$\nu_b(r) = \frac{18.2}{H_0^3 (r_0/v)^2} \left[\frac{r}{r_0}\right]^4 \quad \text{GHz} \qquad (3)$$

where r and v are the radius and velocity of the cloud respectively, H_0 is the magnetic field, in Gauss, in the cloud when the expansion begins, and r_0/v is measured in years. Peterson and Dent (1973) have found that the quantity r_0/v is on the order of the time it takes a given outburst to reach maximum which is, typically, 0.5 yr. From equation (3) it can be shown that the inequality $\nu_b(r_0) > 300$ GHz is satisfied if $H_0 < 0.6$ Gauss. These calculations illustrate the general point that injected electrons with sufficient energy to produce one millimeter wavelength radiation will not be severly affected by synchrotron losses if the source magnetic field has a small enough value. It should be noted that, in addition, the continuum energy distributions of the sample blazars do not show the spectral steepening required if synchrotron losses are significant at a wavelength of 1mm (Ennis and Werner 1981).

As in the canonical model, Peterson and Dent (1973) assume the expansion to have constant velocity. Marscher (1978) has developed a modification of the blast wave variability model (Blandford and McKee 1978) which conceptually is similar to the simple injection model considered above but which incorporates fully consistent expansion dynamics; he has successfully applied this model to the 1975 radio outburst observed from the blazar AO 0235+16. In the signal-screen model of Marscher (1978) a thin shell of magnetized plasma (the "screen") is located at a radius r_0 from a central origin from which an ultrarelativistic blast wave propagates (the "signal"). The analogous process to the injection of synchrotron radiating electrons is the electron acceleration and magnetic field amplification which occurs behind the shock front as it passes through the shell. As before, the observed similarity of the 1mm and 2cm flux variations argues against synchrotron losses dominating at a frequency of 1mm since in Marscher's model the time dependence of the outburst decay is dependent upon the electron energy loss mechanism.

One requirement of a model of variable emission from a source is that it be a physically reasonable extension of the radiation mechanism believed responsible for the quiescent, steady-state emission from the source. Among others, Ennis and Werner (1981) have argued that the radio continuum energy distribution of blazars is produced by a jet of synchrotron radiating plasma undergoing bulk relativistic motion and making a small angle with the line of sight. The blast wave emission variability models of Blandford and McKee (1978) and Marscher (1978) are readily consistent with a relativistic jet model since instabilities in the jet flow can generate the requisite shocks (Rees 1978) and density enhancements within the jet can be produced (Blandford and Rees 1978; Blandford and Königl 1979).

iii) Relation to Infrared Blazar Variability

In a previous paper (Ennis and Werner 1981) it was shown that the 1mm flux densities of blazars are correlated with both the radio and infrared power law continua. As noted above, an interpretation of this result is that the entire radio through optical energy distribution of blazars is due to beamed synchrotron radiation from a relativistic jet. If such a model obtains a correspondence between blazar emission variability at 1mm and in the infrared could be expected. In fact, a comparison of the 1mm observations with 2μm measurements made over the same time period (Neugebauer; unpublished data) indicates that blazar flux changes observed at 1mm also appear in the infrared. In particular, the 2μ flux density of BL Lac exhibited an outburst in the summer of 1980 which was also seen at 1mm and 2cm (Figure 2c).

b) The 1mm emission variability of 3C84 and 3C273

As shown in the figures, the 1mm variability of 3C84 and 3C273 has a different character than the 1mm variability observed from blazars; this difference is most clearly illustrated by the early 1980 outburst of 3C84 seen at a wavelength of 1mm but not appearing at 2cm. From Figure 1c it is possible to make the following crude estimates for this outburst: t_0= Nov 1979, t_{1mm} = Apr 1980, and t_{2cm} > Nov 1980. Using these values and equation (1) it is found that $x \gtrsim 2$; no estimate of R is possible from the present data. This lower limit to x suggests that the canonical model discussed above (or its modifications, see Table 3) could provide a viable explanation for the 1mm variability of 3C84.

Differences between the observed properties of the radio loud quasar 3C273 and those of blazars are not confined to the nature (and interpretation) of the 1mm emission variability. As discussed in Ennis and Werner (1981), the radio continua of radio loud quasars typically exhibit a high frequency curvature not apparent in the radio energy distributions of blazars; in addition, the infrared continua of blazars are quite smooth showing no evidence for the "bump" at 3.5

μm often seen in the infrared energy distributions of radio loud quasars (Neugebauer *et al.* 1979).

V. CONCLUSIONS

In this paper the results of monitoring the 1mm flux density from 3C273, 3C279, BL Lac, 3C84, OJ287, and 3C345 between March 1977 and January 1981 are presented. The following results were found:

1. With the possible exception of 3C279, all of the objects showed evidence for variability of the 1mm flux density during the observation period.
2. For the blazars in the sample, the flux density variations at wavelengths of 1mm and 2cm occurred simultaneously and had similar amplitudes.
3. An outburst in the 1mm flux density of 3C84 was observed in early 1980 and has not appeared at 2cm as of one year later.

From analysis of these results the following conclusions concerning the 1mm emission variability of the sample blazars are possible:

1. The canonical expanding source model of radio variability fails to reproduce the observed relationship between the 1mm and 2cm flux variability.
2. Models in which the effective number of synchrotron radiating electrons in the variable source changes with time- either by electron injection or electron acceleration behind a relativistic shock- can account for observational result 2).

TABLE 1

ONE MILLIMETER OBSERVATIONS OF VARIABLE RADIO SOURCES

Object	Date of Observation	1mm Flux Density (Jy)	Object	Date of Observation	1mm Flux Density (Jy)
3C273	24-25 Nov 77	11±2	3C345	23 Apr 78	5±1
	23 Apr 78	13±4		15 Dec 78	9±2
	20 May 78	12±2		10 Apr 79	7±2
	15 Dec 78	17±2		29 Mar 80	8±1
	11-13 Jan 79	13±1		24 Nov 80	11±3
	10-12 Apr 79	17±2			
	03-06 Dec 79	27±2	BL Lac	23 Apr 78	< 6
	02 Apr 80	19±3		09 Nov 78	< 3
	22-28 Nov 80	20±2		03 Jan 79	< 3
OJ 287	17 Oct 78	5±1		04-08 Dec 79	3.7±0.5
	09 Nov 78	5±1		02 Apr 80	8±1
	10-11 Jan 79	3.0±0.5		22 Nov 80	6±1
	14 Mar 79	3±1			
	10 Apr 79	< 3	3C84	16-17 Mar 78	35±4
	05 May 79	2.2±0.4		11-13 Jan 79	24±2
	06 Dec 79	4.3±0.5		06-08 Dec 79	45±5
	28 Mar 80	3.3±0.5		28 Mar 80-03 Apr 80	64±6
	24 Nov 80	4±1		22-24 Nov 80	41±4
				22-24 Dec 80	46±5
3C279	24-25 Nov 77	4±1		19-20 Jan 81	34±3
	11 Jan 79	4±1			
	12 Apr 79	7±1			
	06 Dec 79	5±1			
	02 Apr 80	4±1			
	23 Nov 80	5±1			

TABLE 2

CHI-SQUARED ANALYSIS

Object	χ^2_ν
3C273	5.1
3C279	1.1
3C84	45
BL Lac	5.3
OJ 287	2.8
3C345	1.5

TABLE 3

VARIABLE RADIO SOURCE MODELS

Model[a]	R^b	x^b
Canonical Expanding Source	40	3.7
One-Dimensional Expansion (Vitello and Pacini 1978)	2.1	940
Blast Wave (Blandford and McKee 1978)	6.7	96
Synchrotron Losses (Marscher and Brown 1975)	3.4	8.4

[a] For details of the models see the references cited in the text.

[b] Value shown assumes γ=2. The observed values are

$x \sim 1$ and R

REFERENCES

Aller, H.D., and Ledden, J.E. 1979, *Ap. J. (Letters)*, **227**, L117.

Aller, M.F., Aller, H.D., and Hodge, P.E. 1981, preprint.

Altschuler, D.R., and Wardle, J.F.C. 1975, *Nature*, **255**, 306.

Andrew, B.H., MacLeod, J.M., Harvey, G.A., and Medd, W.J. 1978, *A. J.*, **83**, 863.

Angel, J.R.P., and Stockman, H.S. 1980, *Ann. Rev. Astr. Ap.*, **18**, 321.

Blandford, R.D., and Königl, A. 1979, *Ap. Letters*, **20**, 15.

Blandford, R.D., and McKee, C.F. 1976, *Phys. Fluids*, **19**, 1130.

Blandford, R.D., and McKee, C.F. 1978, *M. N. R. A. S.*, **180**, 343.

Blandford, R.D., and Rees, M.J. 1978, in *Pittsburgh Conference on BL Lac Objects*, ed. A.M. Wolfe (Pittsburgh: University of Pittsburgh Press), p. 328.

Elias, J.H., Ennis, D.J., Gezari, D.Y., Hauser, M.G., Houck, J.R., Lo K.Y., Matthews, K., Nadeau, D., Neugebauer, G., Werner, M.W., and Westbrook, W.E. 1978, *Ap. J.*, **220**, 25.

Ennis, D.J., Soifer, B.T., Neugebauer, G., Werner, M. 1981, *Astro. Lett.*, **22**, 143.

Ennis, D.J., and Werner, M.W. 1981, preprint.

Hauser, M.G., and Notarys, H.A. 1975, *Bull. AAS*, **7**, 409.

Hobbs, R.W., and Dent, W.A. 1977, *A. J.*, **82**, 257.

Jones, T.W., and Tobin, W. 1977, *Ap. J.*, **215**, 474.

Kardashev, N.S. 1962, *Soviet Astronomy- AJ*, **6**, 317.

Kellermann, K.I, and Pauliny-Toth, I.I.K. 1968, *Ann. Rev. Astron. Astrophys.*, **6**, 417.

Kesteven, M.J.L., Bridle, A.H., and Brandie, G.W. 1977, *A. J.*, **82**, 541.

Ledden, J.E., Aller, H.D., and Dent, W.A. 1976, *Nature*, **260**, 752.

Locke, J.L., Andrew, B.H., and Medd, W.J. 1969, *Ap. J. (Letters)*, **157**, L81.

Marscher, A.P. 1978, *Ap. J.*, **224**, 816.

Marscher, A.P., and Brown, R.L. 1975, *Ap. J.*, **200**, 719.

McGimsey, B.Q., Smith, A.G., Scott, R.L., Leacock, R.S., Edwards, P.L., Hackney, R.L., and Hackney, K.R. 1975, *A. J.*, **80**, 895.

Neugebauer, G., Oke, J.B., Becklin, E.E., and Matthews, K. 1979, *Ap. J.*, **230**, 79.

Pauliny-Toth, I.I.K., and Kellermann, K.I. 1966, *Ap. J.*, **146**, 634.

Peterson, F.W., and Dent, W.A. 1973, *Ap. J.*, **186**, 421.

Rees, M.J. 1978, *M. N. R. A. S.*, **184**, 61.

Roellig, T.L. 1980, Ph.D. Thesis, Cornell University

Roellig, T.L., Houck, J.R., Ennis, D.J., Elliot, K.H. 1981, preprint.

Schorn, R.A., Epstein, E.E., Oliver, J.P., Soter, S.L., and Wilson, W.J. 1968, *Ap. J. (Letters)*, **151**, L27.

Shklovsky, I.S. 1965, *Astr. Zh.*, **42**, 30.

Simon, M. 1969, *Ap. J.*, **158**, 865.

Van der Laan, H. 1966, *Nature*, **211**, 1131.

Van der Laan, H. 1970 in *Nuclei of Galaxies*, ed. D.J.K. O'Connell (New York: American Elsevier Publishing Co.), p. 245

Vitello, P. and Pacini, F. 1977, *Ap. J.*, **215**, 452.

Vitello, P. and Pacini, F. 1978, *Ap. J.*, **220**, 756.

Vitello, P. and Salvati, M. 1976, *Phys. Fluids*, **19**, 1523.

Weedman, D.W. 1977, *Ann. Rev. Astr. Ap.*, **15**, 69.

Werner, M.W., Neugebauer, G., Houck, J.R., and Hauser, M.G. 1978, *Icarus*, **35**, 289.

FIGURE CAPTIONS

Figure 1- One millimeter flux density light curves of 3C273 (a), 3C279 (b), 3C84 (c), BL Lac (d), OJ 287 (e), and 3C345 (f). The data after March 1977 are from the present work. The data before March 1977 are taken from Elias *et al.* (1978).

Figure 2- In this figure 2 cm flux density light curves (solid circles) are compared to 1mm flux density light curves (open circles). The data shown are for the objects OJ 287 (a), 3C345 (b), BL Lac (c), 3C84 (d), and 3C273 (e). The 2 cm data are from Aller *et al.* (1981); the 1mm data are from the present work.

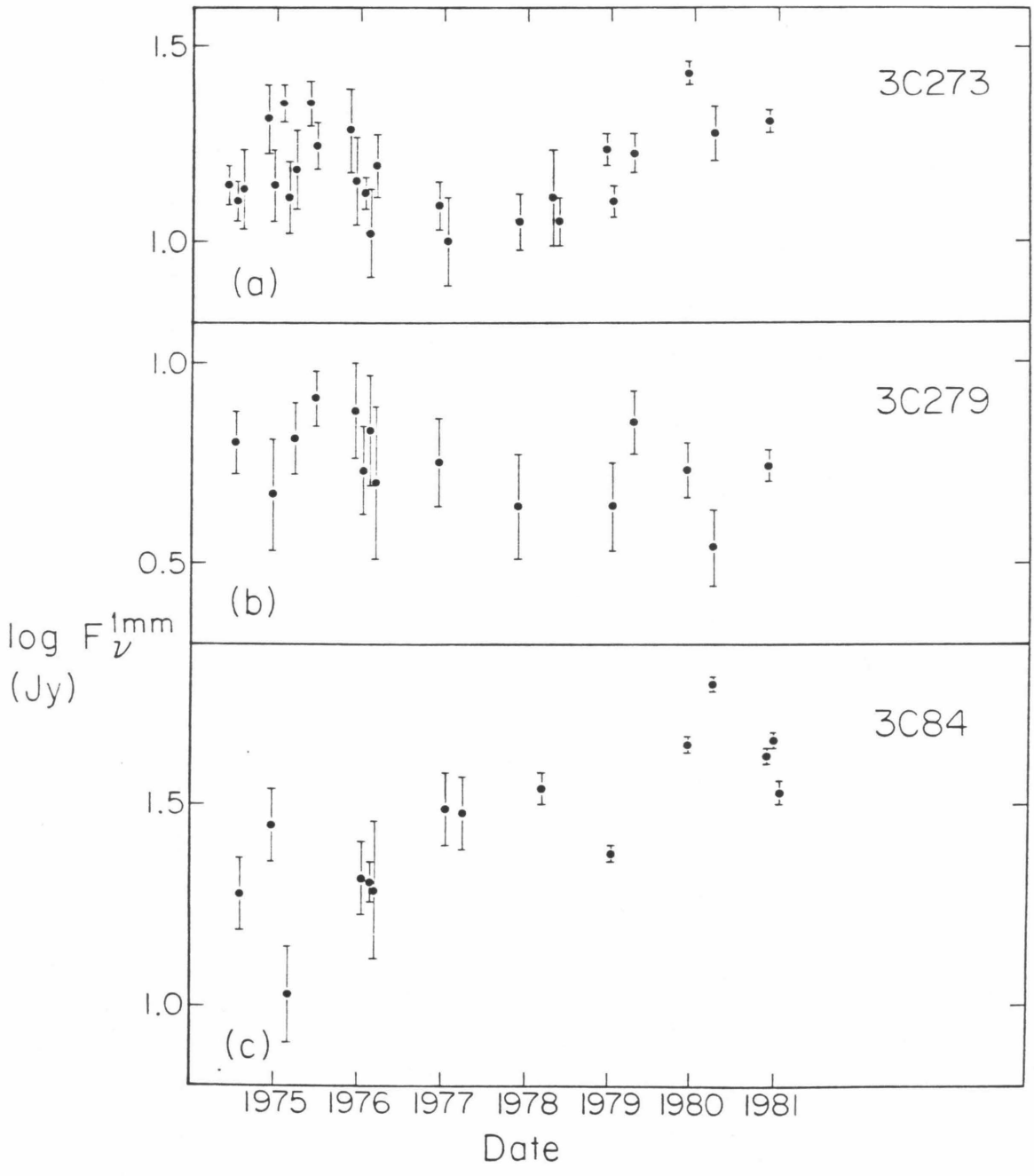
3C273
3C279
3C84
(a)
(b)
(c)
1.5
1.0
1.0
0.5
1.5
1.0
log F_ν^{1mm}
(Jy)
1975 1976 1977 1978 1979 1980 1981
Date

Figure 1

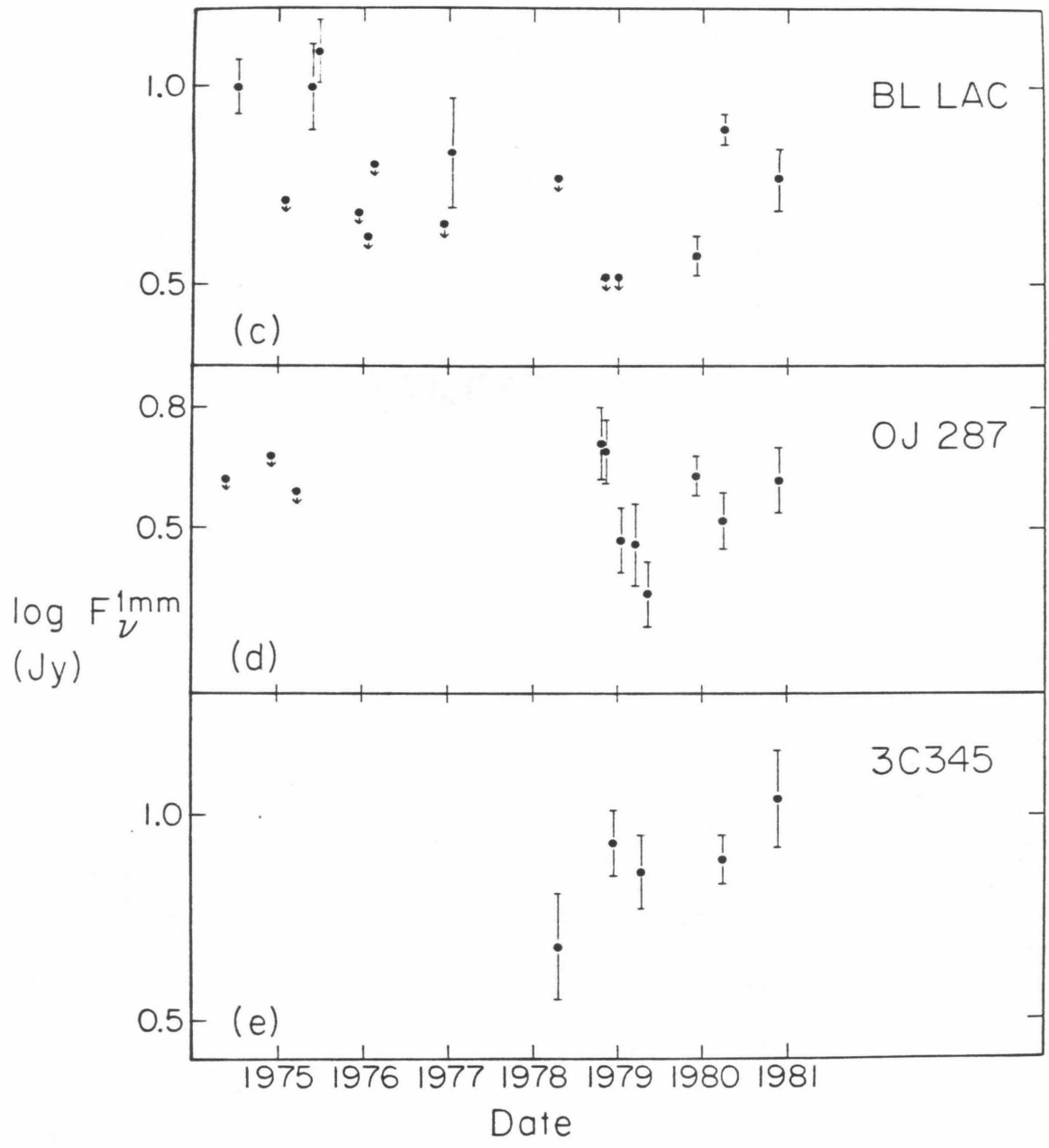

Figure 1 (cont.)

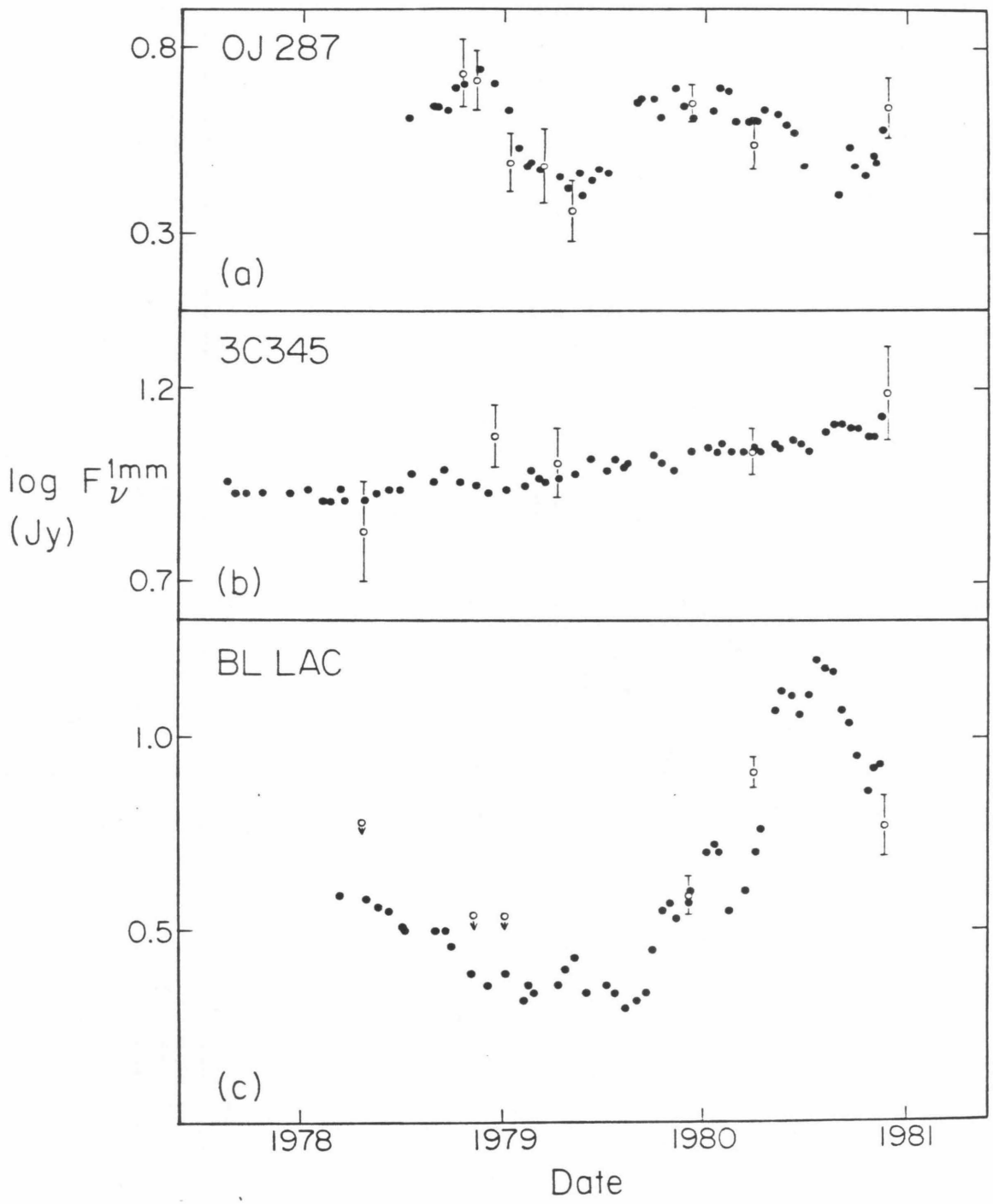
0.8
0.3
OJ 287
(a)
1.2
0.7
3C345
(b)
log F_ν^{1mm}
(Jy)
1.0
0.5
BL LAC
(c)
1978
1979
1980
1981
Date

Figure 2

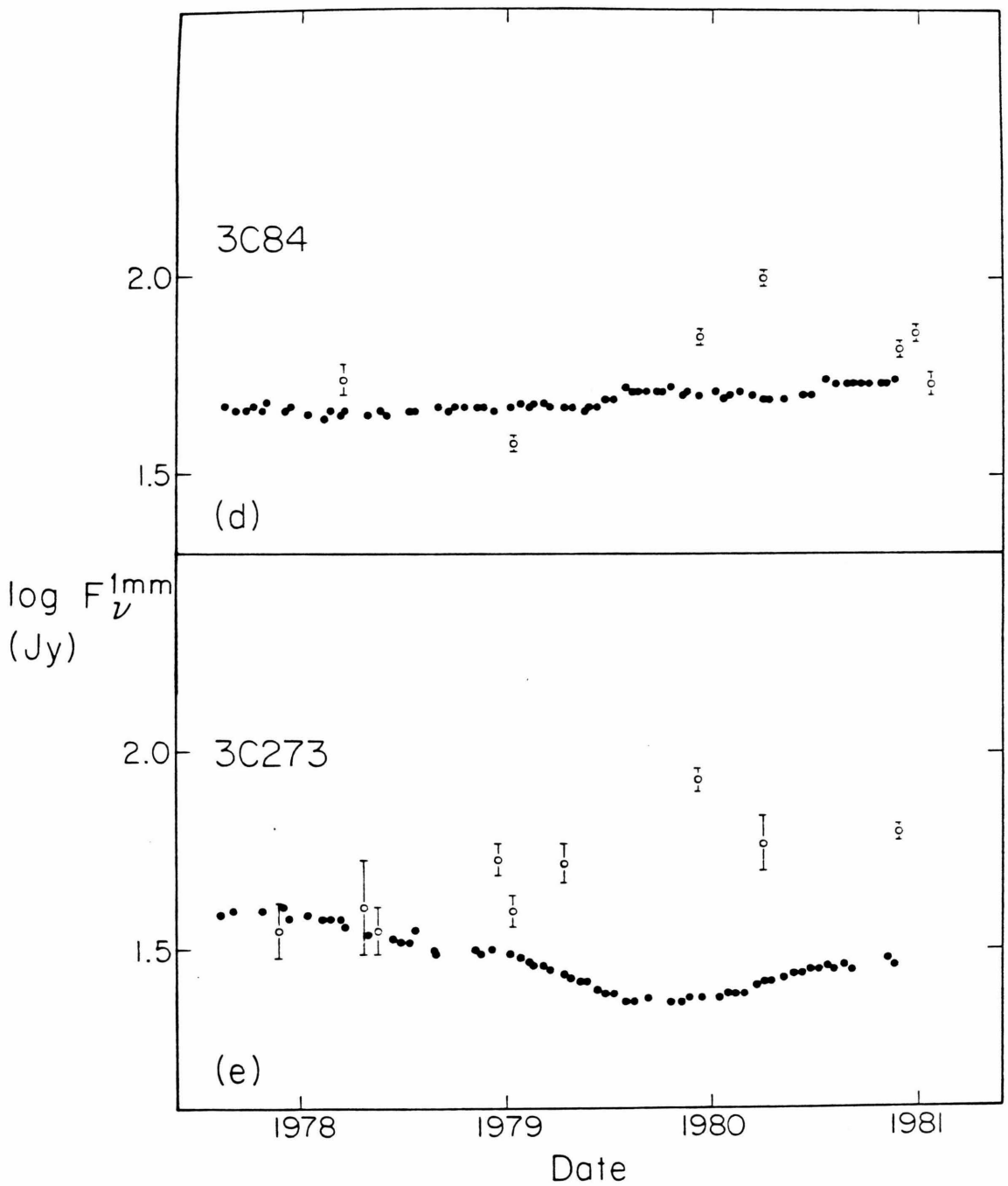

Figure 2 (cont.)

PAPER III: ONE MILLIMETER CONTINUUM OBSERVATIONS OF HIGH REDSHIFT QUASARS

ABSTRACT

Upper limits to the one-millimeter continuum flux densities of the high redshift quasars B2 1225+31, Ton 490, and PHL 957 are presented. The upper limit to the power observed from these quasars at 1mm is, on average, 1/2 the observed power in the continuum at Lα. These observations are used to constrain the temperature of a hypothetical dust shell which reddens the quasar line and continuum emission by an extinction optical depth sufficient to account for the anomalously low Lα/Hα emission line ratio observed in each of these quasars. For the quasars studied, dust shell temperatures between 25 K and 50 to 95 K are prohibited by the present data. A dust shell at a temperature within this span reradiating all the power absorbed from the quasar ultraviolet continuum would produce a one-millimeter flux density greater than the measured upper limit. The average radius of the model dust shell cannot be between 70 kpc and 1 Mpc.

I. INTRODUCTION

For quasars the presence or absence of dust is, at present, an open question. Evidence for the existence of dust in Seyfert galaxies has been seen in their infrared energy distributions by, among others, Rieke 1978, Telesco *et al.* 1980, and Rieke and Lebofsky 1981. With respect to quasars, this question has arisen most recently because of the discrepancy between the observed flux ratios of ultraviolet, optical, and infrared hydrogen emission lines and the theoretical predictions of recombination models of ionized regions (e.g., Soifer *et al.* 1981; Peutter *et al.* 1981). Reddening by dust has been proposed as an explanation for the anomalously low ultraviolet/optical line ratios of H I, He II, and O I (Netzer and Davidson 1979; Shuder and MacAlpine 1979; London 1979). On the other hand, models of the high density regions producing the broad emission lines which take into account the effects of radiative transfer and collisional processes on the energy level populations may be able to reproduce the observed line ratios for at least hydrogen without recourse to dust (Krolik and McKee 1978; Canfield and Puetter 1980; Kwan and Krolik 1981). If dust is reddening the emission from quasars it could be found on a variety of distance scales. Conceivable dust locations include the broad emission line clouds, a galaxy in which the quasar is imbedded, or the tenuous medium filling a cluster of galaxies possibly surrounding the quasar (see, for example, Davidson and Netzer 1979).

In this paper we present one millimeter wavelength observations which bear on the question of dust in three optically bright, high redshift quasars; each quasar has a measured Lα/Hα emission line ratio in disagreement by an order of magnitude with pure recombination theory. For each quasar a hypothetical dust shell is described in which all of the power removed from the intrinsic UV continuum by a an amount of dust needed to explain the reddening of the emission

lines is thermally reradiated at infrared through submillimeter rest wavelengths. It is shown that the present data, when analyzed within the context of this model, provide a constraint on the dust temperature and hence the location of the dust shell with respect to the quasar continuum source.

II. OBSERVATIONS

All of the one millimeter wavelength observations were made at the prime focus of the 5 meter Hale Telescope on Palomar Mountain. Except for the observations made in December 1979 the detector used was a composite germanium bolometer (Hauser and Notarys 1975) cooled by liquid ^{4}He to a temperature of ~1.2K. The broadband spectral response of the system was between wavelengths of 600 μm and 1.5 mm. The value of the short wavelength limit stated is representative; the actual limit during a given observing session was determined by a combination of the filtering produced by cooled fluorogold (Muehlner and Weiss 1973) and the amount of water vapor present in the atmosphere on that day (Elias *et al.* 1978). The long wavelength cutoff was due largely to diffraction by the 5 meter telescope aperture. The half-power beam diameter- as defined by the entrance aperture of a lead-molded Winston light cone (Winston 1970; Harper *et al.* 1976)- was 55 arcseconds. For observations made in December 1979 the composite germanium bolometer used was cooled to ~0.3K with liquid ^{3}He as the cryogen (Roellig 1980). In this system, a cold KRS5 filter provided the short wavelength cutoff of 750 μm and a fused silica lens was employed as field optics.

The observing procedure, data reduction process, and the method for determining the extinction in the system bandpass due to atmospheric water vapor and oxygen lines are all described in Elias *et al.* (1978). Flux density calibration at the nominal wavelength of one millimeter was accomplished using the measured brightness temperatures of Jupiter, Saturn and Mars (Werner *et al.*

1978).

III. RESULTS

None of the three quasars chosen for the one millimeter observations were detected. Column 7 of Table 1 gives the measured three sigma upper limits to the 1mm flux density from the quasars. Because of the broad bandwidth of the system response, an index for the assumed power law flux density spectrum through the band had to be chosen to obtain the one millimeter flux density (Elias *et al.* 1978). For the upper limits presented here, the index α ($F_\nu \propto \nu^\alpha$) was taken to be 3.0 consistent with the model for the dust emission described below. If α is changed from 3.0 to 0.0 there is a 45% increase in the 1mm flux density upper limit for PHL 957 presented in Table 1: for Ton 490 the increase is ~5%, while for B2 1225+31 it is 33%. The calibration uncertainty in the one-millimeter results is 20%. The submillimeter rest wavelength corresponding to an observed wavelength of 1mm is also shown in Table 1.

The observed energy distributions of the sample quasars are presented in Figure 1 as a function of the rest frequency $\nu_0=(1+z)\nu$ where z is the redshift shown in Table 1. In Table 2 the continuum power density per logarithmic frequency interval (νF_ν) for the sample quasars is shown both at a wavelength of one millimeter and at the wavelength of Lα. The data of both Figure 1 and Table 2 indicate that the upper limit to the power observed from the quasars at 1mm is, on average, 1/2 the observed power in the continuum at Lα.

IV. DISCUSSION

As an explanation for the observed emission line ratios, it has been suggested that dust associated with quasars reddens both the line and continuum emission (Netzer and Davidson 1979; Shuder and MacAlpine 1979). The one-millimeter data cannot exclude the presence of such dust in the quasars studied, but as will be shown below, it can restrict the dust temperature, or

equivalently, the distance of dust grains from the ultraviolet radiation source of the quasar.

As a working hypothesis, dust grains will be assumed to be uniformly distributed in a shell which isotropically surrounds the regions producing the line and continuum emission; the dust reddens both regions by the same amount. The isotropy of the dust shell is a reasonable supposition since the anomalous hydrogen emission line ratios are a common occurrence in large samples of quasars (Baldwin 1977;Soifer *et al.* 1981). This model differs from the situation in which the dust is within each of the gas clouds responsible for the broad line emission (London 1979) in that the small covering factor of these clouds (Oke 1974;Baldwin *et al.* 1976) precludes such dust from significantly reddening the continuum emission.

The hypothetical dust shell - assumed to be at the single temperature T_D - will reemit the absorbed energy as modified blackbody thermal radiation. Specifically, the observed one millimeter flux density, F_{1mm}, from a dust shell associated with a quasar of redshift z is given by

$$F_{1mm} = \frac{2h\nu_0^3}{c^2(1+z)^3} \frac{\tau\Omega}{e^{h\nu_0/kT_D}-1} \qquad (1)$$

where ν_0 is the rest frame frequency corresponding to an observed wavelength of one millimeter, τ is the dust absorption optical depth at ν_0, and Ω is the solid angle the dust shell subtends as seen from Earth. The factor of $1/(1+z)^3$ in this expression reflects the change in the rate of photon emission ($1/(1+z)$) and the change in the solid angle of the dust shell ($1/(1+z)^2$) in transforming the flux density from the rest frame of the quasar to the observer's frame. Dividing F_{1mm}, as given by equation (1), by the integral of the flux density over all frequencies gives

$$T_D^5\left[e^{h\nu_0/kT_D}-1\right] = \frac{2h\nu_0^4(1+z)}{c^2\sigma'}\ \frac{F_D}{F_{1mm}} \qquad (2)$$

where F_D is the total flux radiated by the dust shell and $\sigma'=1.44\times10^{3}\mathrm{Wm^{-2}K^{-5}s^{-1}}$ is the analog of the Stefan-Boltzmann constant. In deriving equation (2) it has been assumed that the dust emissivity in the far-infrared through submillimeter rest wavelength range goes as λ_0^{-1}. Evidence which favors such a wavelength dependence for dust in the Galaxy is seen in the Galactic center (Gatley 1977), in molecular clouds (e.g., Evans *et al.* 1981), and in the far-infrared flux distribution observed from the carbon star IRC+10216 (Campbell *et al.* 1976).

The measured upper limit to F_{1mm} can be used in equation (2) to provide a lower limit to the dust temperature once the total flux emitted by the grains, F_D, is determined. If the shell is heated solely by the quasar ultraviolet radiation source, F_D can be estimated from the observed emission from this source since energy conservation requires that F_D equals the flux absorbed by the dust. In calculating the heating flux, the reddening of the observed ultraviolet continuum is an important consideration. It will be assumed that the grains exhibit an extinction curve identical to that observed by Code *et al.* (1976) for Galactic dust but with the 2175 Å absorption feature arbitrarily subtracted out. It is likely that any dust grains present in quasars consist of substances not possessing this resonance; its absence in the spectra of a large sample of quasars was noted by McKee and Petrosian (1974) and Baldwin (1977). The amount of reddening the continuum is subject to can be determined from the observed hydrogen emission lines. The dust optical depth (τ_{UV}) at Lα obtained by assuming that the discrepancy between the observed Lα/Hα line ratio (shown in Table 1) and its "intrinsic" case B value of 12 (Pengelly and Seaton 1962; Brocklehurst 1972) is due to reddening by this shell is given in Table 3. In estimating the total UV flux absorbed by the grains, photons with rest wavelengths between 300Å and

6000Å were taken to effectively heat the dust (Netzer and Davidson 1979).

Substitution into equation (2) of the value for F_D evaluated in this manner and the upper limit to F_{1mm} provided by the present observations gives the limit to the dust temperature which is shown in Table 3 as T_2. If the reemitted flux is all included in the beam of the telescope, any dust shell must be warmer than this limit. It should be noted that this temperature bound depends solely on the ratio of one-millimeter flux density upper limit to dereddened ultraviolet flux and is independent of the choice of cosmological model.

Published observational data at extreme ultraviolet rest wavelengths for the high redshift quasars studied are lacking. It therefore was arbitrarily assumed that the measured ultraviolet continua of Ton 490 and PHL 957 could be directly extrapolated to a rest wavelength of 300Å (3 Ry), a procedure which is consistent with the observed X-ray flux from these objects (Figure 1). In the case of B2 1225+31, IUE observations (Snijders *et al.* 1981 and references therein) show no detectable emission between rest wavelengths of 400Å and 800Å, the radiation presumably being absorbed by an intervening system at z= 1.795. The flux density at extreme ultraviolet rest wavelengths was obtained by interpolating between the observed data at 800Å and the X-ray data (Tananbaum *et al.* 1979; Zamorani *et al.* 1980); directly extending the observed UV continuum to 300Å results in a 20% increase in the calculated heating flux in this case. In dereddening these extrapolated continua it was assumed that the dust extinction optical depth is constant for $\lambda_0 < 1100$Å (Shuder and MacAlpine 1979); for constituents of Galactic dust, this supposition finds support in both theoretical calculations (Greenberg 1968) and laboratory measurements (Huffman 1976).

Figure 2(a) illustrates the results of applying the analysis described here to B2 1225+31. Comparison of the observed and dereddened ultraviolet energy

distributions shows that once reddening is taken into account the hypothetical flux heating the dust grains is an order of magnitude larger than the observed ultraviolet flux. The dashed curve is the energy distribution of the thermal emission expected from the hypothetical dust shell with a temperature equal to the calculated lower limit T_2. The dust shell at this temperature radiates as much power as it absorbs from the dereddened ultraviolet continuum while producing a one-millimeter flux density equal to the observed upper limit. For dust temperatures larger than T_2 the the expected emission from a shell radiating the same energy is consistent with the one millimeter upper limit.

The present observations do not rule out every temperature less than T_2 for the hypothetical dust shell. At low enough dust temperatures the solid angle of the dust shell, Ω, will exceed the solid angle of the 55 arcsecond telescope beam (Ω_B) used for the present observations; in this case, the observations do not limit the total 1mm flux density the *entire* dust shell emits and equation (2) is no longer applicable. For this situation, as expected, the 1mm flux density observed from the dust shell will be given by equation (1) with $\Omega=\Omega_B$ since only the central 55 arcseconds of the dust shell contributes to the one millimeter flux density. Thus, if the emitting shell of dust is larger than the telescope beam the measured upper limit to F_{1mm} provides an *upper* limit to the dust temperature; this limit is presented in Table 3 as T_1. The observed interstellar extinction curve in the wavelength range 1100Å to 20μm (Johnson 1968; Code *et al.* 1976; Becklin *et al.* 1978) with a λ_0^{-1} extension for longer wavelengths has been used in calculating τ from τ_{IR}. For Galactic dust in the molecular clouds M17 and NGC 7129 the value of the far-infrared optical depth calculated from the visual extinction in this manner is in agreement with the measured value (Bechis *et al.* 1978; Gatley *et al.* 1979). The total column density of dust in the section of the shell subtended by the telescope beam has been used in determining τ. For

B2 1225+31 the expected emission from the central arc-minute of the dust shell at temperature T_1 is also shown in Figure 2(a).

We thus conclude that the hypothetical dust shell must be at a temperature outside of the range from T_1 to T_2 in order to be in accord with the limit to its thermal emission set by the present data. The most stringent result is for B2 1225+31 for which dust temperatures within a 73 degree span are excluded. Uncertainties in the observed Lα/Hα emission line ratio and one-millimeter flux density upper limits produce a 20% uncertainty in the temperatures shown in Table 3.

The dust temperature can be related to the radius of the shell by using the estimate of the luminosity source and the assumed grain absorption properties. In the case of B2 1225+31, for example, no dust shell can exist with a radius between 60 kpc and 2.2 Mpc. For the three high redshift quasars studied, the average radius of the model dust shell is either less than 70 kpc or greater than 1 Mpc. The limit of 70 kpc - the size of a compact cluster of galaxies or a giant cD galaxy (e.g., Bahcall 1977)- may be the physically more relevant result. These distances take q_0=1 and H_0=50kms^{-1}Mpc^{-1}; if q_0=0 the radii will be increased by the factor 1+ (1/2)z.

Observational data exist over most of the electromagnetic spectrum for 3C273 whose energy distribution is also shown in Figure 1. In addition, its emission line spectra exhibits anomalous hydrogen line ratios (Baldwin 1977; Davidsen *et al.* 1977; Boggess *et al.* 1979). It is appropriate to find if a dust shell of the type described in this paper could be reddening the line and continuum emission from 3C273. The measured Lα/Hα ratio of 1.8 (Boggess *et al.* 1979) gives a $\tau_{\gamma\gamma}$ of 2.4 which, when combined with the observed ultraviolet continuum, results in a UV luminosity absorbed by the hypothetical grains a factor of 7 larger than the upper limit to the total infrared luminosity between wavelengths

of 1μm and 500μm. If, in addition, the luminosity due to a nonthermal power law continuum (dashed line in Figure 1) known to provide a moderately good fit to the energy distribution of 3C273 (Boggess *et al.* 1979; Ulrich 1981) is subtracted from the observed infrared luminosity, the remaining power is a factor or 25 smaller than the power absorbed by the hypothetical grains. For 3C273 then, it is difficult to see how a dust shell of *any* temperature which produces the requisite reddening, could absorb all of the ultraviolet power and still reradiate flux densities consistent with all the observed near infrared through submillimeter data.

It is reasonable to ask if there is an active extragalactic object which shows evidence for a dust shell having properties similar to those discussed here. Such an object is the nucleus of the archetypal Seyfert 2 galaxy NGC 1068 whose energy distribution is shown in Figure 2(b). The dashed curve is the energy distribution of the radiation from an isothermal dust shell of temperature 170K and a $\tau_{9\gamma}$ of 4.1. This value for $\tau_{9\gamma}$ is the amount of reddening necessary to produce agreement between the observed emission line intensities (Neugebauer *et al.* 1980 and references therein) and the predictions of standard Case B radiative recombination theory. This curve provides a good fit to the observed mid infrared flux densities and, as can be seen from the dereddened UV continuum, the dust shell radiates the required total flux. In addition, the angular diameter of the model dust shell is $\sim$ 1 arcsecond, a value in excellent agreement with the measured size of the 10 μm nuclear source (Becklin *et al.* 1973). A more sophisticated treatment of dust emission models for the infrared radiation from the nucleus of NGC 1068 (Jones *et al.* 1977) yields similar results.

Due to the small angular size of the dust shell associated with the nucleus of NGC 1068, a fraction of the light scattered by the grains will intercept the telescope beam used for the measurements; this is in contrast to observations of

radiation traversing interstellar dust clouds in which most of the scattered photons are undetected (Jones 1973; Netzer and Davidsen 1979; Neugebauer *et al.* 1980). If the equations derived by Code (1973) are used to take this effect into account in dereddening the observed UV continuum from the nucleus of NGC 1068, the ensuing value for the flux heating the grains is only 20% lower than the result obtained above using the standard interstellar extinction curve. For this calculation it was assumed that the wavelength dependence of the scattering properties of the grains present in the nucleus of NGC 1068 is the same as that exhibited by Galactic-type dust. The variation of the albedo in the ultraviolet wavelength range was taken from OAO-2 measurements of the diffuse Galactic light reported by Lillie and Witt (1976). The wavelength dependence of the mean value of the cosine of the scattering angle was taken from the calculations of White (1979) who used the mixture of grain sizes and composition determined by Mathis *et al.* (1977) to give the best fit to the observed Galactic extinction curve.

A crucial assumption of the specific model presented in this paper is that the dust grains in the shell are all at the same temperature. An alternative geometry would be a dust cloud in which there are grains at a range of radii from the central UV continuum source resulting in a distribution of grain temperatures. Qualitatively, it can be seen that a dust cloud would reradiate the power absorbed from the UV continuum over the entire span of infrared wavelengths. Rieke and Lebofsky (1981) argue that the observed radiation from the type 1 Seyfert galaxy NGC 4151 between wavelengths of 2 and 100 μm can be attributed to thermal emission from a dust cloud containing grains at temperatures between 1500 and 70 K. It would, in principle, be possible to construct a similar dust cloud model for the sample high redshift quasars in which the expected 1mm flux density is consistent with the observed upper limits. Due to the lack of observational data between rest wavelengths of 300μm and 3μm for

these quasars, a detailed calculation of the energy distribution of the thermal emission from such a dust cloud is not warranted at the present time.

V. SUMMARY AND CONCLUSIONS

This paper presents a method in which infrared observations can begin to constrain the temperature and location of dust in quasars. One-millimeter wavelength observations of three high redshift quasars with measured $L\alpha/H\alpha$ emission line ratios considerably lower than the calculations of standard recombination theory have been reported. The upper limit to the power emitted by these quasars at an observed wavelength of 1mm is typically half the power in the continuum at $L\alpha$. If it is assumed that an isothermal shell of dust is reddening the line and continuum emission from these quasars, analysis of the observed 1mm upper limit constrains the physical properties of the dust. Temperatures between 25 K and 50 to 95 K (depending on the object) are ruled out for the dust shell since at temperatures within this range a dust shell emitting the requisite total luminosity would produce a 1mm flux density greater than the measured upper limit. It is found that the average dust shell radius cannot be between 70 kpc and 1 Mpc.

ACKNOWLEDGEMENTS

We are grateful to T. Roellig and J. Houck for assistance with the observations and to K. Sellgren for helpful discussions. This work was supported by NASA research grants.

TABLE 1

ONE MILLIMETER OBSERVATIONS OF HIGH REDSHIFT QUASARS

Object	Coordinates	Date of Observation	Redshift z^a	1mm Rest Wavelength (μm)	$L\alpha/H\alpha^b$	Upper Limit to 1mm Flux Density[c] (Jy)
PHL 957	0101+13	18 Feb 79	2.69	271	$1.8\pm^{1.0}_{0.5}$	0.6
Ton 490	1011+25	08 Dec 79	1.63	380	0.8 ± 0.3	0.8
B2 1225+31	1225+31	23 Nov 80	2.19	313	0.8 ± 0.2	0.7

[a] Values from Hewitt and Burbridge (1980).

[b] Values from Soifer *et al.* (1981).

[c] The upper limits are three times the statistical uncertainty. Calibration uncertainty is 20%.

TABLE 2

POWER DENSITIES PER LOGARITHMIC FREQUENCY INTERVAL

Object	$(\nu F_\nu)_{1mm}$ $(10^{-15}\mathrm{Wm}^{-2})$	$(\nu F_\nu)^{a}_{UV}$ $(10^{-15}\mathrm{Wm}^{-2})$	$\frac{(\nu F\nu)_{1mm}}{(\nu F_\nu)_{UV}}$
PHL 957	< 1.8	5.0±0.3	< 0.36
Ton 490	< 2.4	3.3±0.2	< 0.73
B2 1225+31	< 2.4	12.0±0.6	< 0.18

[a] The continuum flux density at Lα was used.

TABLE 3

DUST MODEL PARAMETERS

Object	τ_{UV}	T_1 (K)	T_2 (K)
PHL 957	2.4	27	57
Ton 490	3.5	21	50
B2 1225+31	3.5	22	95

REFERENCES

Bahcall, N.A., 1977, *Ann. Rev. Astr. Ap.*, **15**, 505.

Baldwin, J.A., Smith, H.E., Burbridge, E.M., Hazard, C., Mudoch, H.S., and Jauncy, D.L. 1976, *Ap. J. (Letters)*, **206**, L83.

Baldwin, J.A. 1977, *M. N. R. A. S.*, **178**, 67p.

Bechis, K.P., Harvey, P.M., Campbell, M.F., and Hoffmann, W.F. 1978, *Ap. J.*, **226**, 439.

Becklin, E.E., Matthews, K., Neugebauer, G., and Wynn-Williams, C.G. 1973, *Ap. J. (Letters)*, **186**, L69.

Becklin, E.E., Matthews, K., Neugebauer, G., Willner, S.P. 1978, *Ap. J.*, **220**, 831.

Bogagess, A., Daltabuit, E., Torres-Peimbert, S., Estabrook, F.B., Wahlquist, H.D., Lane, A.L., Green, R., Oke, J.B., Schmidt, M., Zimmerman, B., Morton, D.C., and Roeder, R.C. 1979, *Ap. J. (Letters)*, **230**, L131.

Brocklehurst, M. 1972, *M. N. R. A. S.*, **157**, 211.

Campbell, M.F., Elias, J.H., Gezari, D.Y., Harvey, P.M., Hoffmann, W.F., Hudson, H.S., Neugebauer, G., Soifer, B.T., Werner, M.W., and Westbrook, W.E. 1976, *Ap. J.*, **208**, 396.

Canfield, R.C. and Peutter, R.C. 1980, *Ap. J.*, **236**, 17.

Code, A.D. 1973, in *I.A.U. Symposium #52- Interstellar Dust and Related Topics*, ed. J.M. Greenberg and H.C. Van de Hulst (Dordrecht: D. Reidel Publishing Co.), p.505.

Code, A.D., Davis, J., Bless, R.C., and Hanbury-Brown, R. 1976, *Ap. J.*, **203**, 417.

Davidsen, A.F., Hartig, G.F., and Fastie, W.G. 1977, *Nature*, **269**, 203.

Davidson, K. and Netzer, H. 1979, *Rev. Mod. Phys.*, **51**, 715.

Elias, J.H., Ennis, D.J., Gezari, D.Y., Hauser, M.G., Houck, J.R., Lo, K.Y., Matthews, K., Nadeau, D., Neugebauer, G., Werner, M.W., and Westbrook, W.E. 1978, *Ap. J.*, **220**, 25.

Evans, N.J., Becklin, E.E., Beichman, C., Gatley, I., Hildebrand, R.H., Keene, J., Slovak, M.H., Werner, M.W., and Whitcomb, S.E. in press

Fanti, C., Fanti, R., Ficarra, A., Formiggini, L., Giovannini, G., Lari, C., and Padrielli, L. 1975, *Astr. and Ap. Suppl.*, **19** , 143.

Gatley, I., Becklin, E.E., Werner, M.W., and Wynn-Williams, C.G. 1977, *Ap. J.*, **216**, 277.

Gatley, I., Becklin, E.E., Sellgren, K., and Werner, M.W. 1979, *Ap. J.*, **233**, 575.

Greenberg, J.M. 1968, in *Nebulae and Interstellar Matter*, ed. B.M. Middlehurst and L.H. Aller (Chicago: University of Chicago Press), p. 221.

Harper, D.A., Hildebrand, R.H., Stiening R., and Winston, R. 1976, *Appl. Opt.*, **15**, 53.

Hauser, M.G., and Notarys, H.A. 1975, *Bull. A.A.S.*, **7**, 409.

Hewitt, A., and Burbridge, G. 1980, *Ap. J. Suppl.*, **43**, 57.

Hildebrand, R.H., Whitcomb, S.E., Winston, R., Steining, R.F., Harper, D.A., and Moseley, S.H. 1977, *Ap. J.*, **216**, 698.

Huffman, D.R. 1976, in *Solid State Astrophysics*, ed. N. C. Wickramasinghe and D.J. Morgan (Boston:Reidel), p. 191.

Johnson, H.L. 1968, in *Nebulae and Interstellar Matter*, ed. B. M. Middlehurst and L.H. Aller (Chicago: University of Chicago Press), p. 167.

Jones, T.W. 1973, *Pub. A. S. P.*, **85**, 811.

Jones, T.W., Leung, C.M., Gould, R.J., and Stein, W.A. 1977, *Ap. J.*, **212**, 52.

Jones, T.W., Rudnick, L., Owen, F.N., Puschell, J.J., Ennis, D.J., and Werner, M.W. 1981, *Ap. J.*, **243**, 97.

Krolik, J.H., and McKee, C.F. 1978, *Ap. J. Suppl.*, **37**, 459.

Ku, W.H.-M., Helfand, D.J., and Lucy, L.B. 1980, *Nature*, **288**, 323.

Kwan, J., and Krolik, J.H. 1981, preprint.

Lillie, C.F., and Witt, A.N. 1976, *Ap. J.*, **208**, 64.

London, R. 1979, *Ap. J.*, **228**, 8.

Mathis, J.S., Rumpl, W.M., and Nordsieck, K.H. 1977, *Ap. J.*, **217**, 425.

McKee, C.F., and Petrosian, V. 1974, *Ap. J.*, **189**, 17.

Muehlner, D. and Weiss, R. 1973, *Phys. Rev. D.*, **7**, 326.

Netzer, H., and Davidson, K. 1979, *M. N. R. A. S.*, **187**, 871.

Neugebauer, G., Oke, J.B., Becklin, E.E., and Matthews, K. 1979, *Ap. J.*, **230**, 79.

Neugebauer, G., Morton, D., Oke, J.B., Becklin, E.E., Daltabuit, E., Matthews, K., Persson, S.E., Smith, A.M., Soifer, B.T., Torres-Peimbert, S., and Wynn-Williams, C.G. 1980, *Ap. J.*, **238**, 502.

Oke, J.B. 1974, *Ap. J. (Letters)*, **189**, L47.

Owen, F.N., Porcas, R.W., Mufson, S.L., and Moffett, T.J. 1978, *A. J.*, **83**, 685.

Pengelly, R.M., and Seaton, M.J. 1962, *M. N. R. A. S.*, **162**, 79.

Peutter, R.C., Smith, H.E., Willner, S.P., and Pipher, J.L. 1981, in press

Rieke, G.H., and Low, F.J. 1975, *Ap. J. (Letters)*, **199**, L13.

Rieke, G.H. 1978, *Ap. J.*, **226**, 550.

Rieke, G.H. and Lebofsky, M.J. 1981, preprint.

Roellig, T.L. 1980, Ph. D. Thesis, Cornell University

Swartz, P.R., and Waak, J.A. 1978, *A. J.*, **83**, 683.

Shuder, J.M., and MacAlpine, G.M. 1979, *Ap. J.*, **230**, 348.

Snijders, M.A.J., Pettini, M., and Boksenberg, A. 1981, *Ap. J.*, in press.

Soifer, B.T., Oke, J.B., Matthews, K., and Neugebauer, G. 1979, *Ap. J. (Letters)*, **227**, L1.

Soifer, B.T., Neugebauer, G., Oke, J.B., and Matthews, K. 1981, *Ap. J.* in press

Tananbaum, H., Avni, Y., Bradvardi, G., Elvis, M., Fabbiano, G., Feigelson, E., Giaconni, R., Henry, J.P., Pye, J.P., Soltan, A., and Zamorani, G. 1979, *Ap. J. (Letters)*, **234**, L9.

Telesco, C.M., and Harper, D.A. 1980, *Ap. J.*, **235**, 392.

Ulrich, M., 1981, in press.

Werner, M.W., Neugebauer, G., Houck, J.R., and Hauser, M.G. 1978, *Icarus*, **35**, 289.

White, R.L. 1979, *Ap. J.*, **229**, 954.

Winston, R. 1970, *J. Opt. Soc. Am.*, **60**, 245.

Zamorani, G., Henry, J.P., Maccacaro, T., Tananbaum, T., Soltan, A., Avni, Y., Liebert, J., Stocke, J., Strittmatter, P.A., Weymann, R.J., Smith, M.G., and Condon, J.J. 1980, *Ap. J.*, in press

FIGURE CAPTIONS

Figure 1- Rest frame energy distributions of three high redshift quasars and 3C273. The present data at an observed wavelength of 1mm are the open circles. The vertical axis shows the observed power density per logarithmic frequency interval. The area under a given set of data points is proportional to the total power emitted by the quasar in that part of the electromagnetic spectrum. Dot-dash lines are the extrapolation of the observed UV continuum to a rest energy of 3 R; see text. The dashed line is a power law continuum fit to the observed infrared radiation from 3C273. Data sources - 3C273: radio data, Jones *et al.* (1981); 500 μm upper limit, Hildebrand *et al.* (1977); 33, 100, 116 μm upper limits, Telesco and Harper (1979); infrared data points and visual continuum, Neugebauer *et al.* (1979); ultraviolet continuum, Boggess *et al.* (1979); X-ray data, Zamorani *et al.* (1980) PHL 957: infrared data points and visual continuum, Neugebauer *et al.* (1979), X-ray data, Ku *et al.* (1980) B2 1225+31: radio points, Fanti *et al.* (1975); 3.5 and 10 μm upper limits, Neugebauer(unpublished data); near infrared data points and optical continuum, Soifer *et al.* (1979), X-ray data, Zamorani *et al.* (1980) Ton 490: radio data, Owen *et al.* (1978); 90 GHz point, Swartz and Waak (1978); near infrared points, Neugebauer (unpublished data); visual continuum, Soifer *et al.* (1980), X-ray data, Ku *et al.* (1980).

Figure 2- (a) Observed (solid circles) and dereddened (open squares) ultraviolet continua of B2 1225+31. The extrapolation of the ultraviolet continua to a rest wavelength of 300Å are shown as dot-dash lines; see text. The dashed curves are the expected emission into a one-arcminute telescope beam from the model dust shell described in the text. Dust

shells with temperatures between T_1 and T_2 would produce one-millimeter flux densities greater than the observed upper limit (open circle). The bottom scale shows the temperature of the model dust shell whose emission would peak at the given wavelength. (b) Observed infrared and ultraviolet energy distributions of the nucleus of NGC 1068 (solid circles). The dereddened ultraviolet continuum is shown as open squares. The extrapolation of the UV continua to a rest wavelength of 300Å are shown as dash-dot lines; see text. The solid line is the energy distribution of the thermal emission from the 170 K model dust shell described in the text. Data sources- infrared points, Rieke and Low (1975); ultraviolet data, Neugebauer *et al.* (1980).

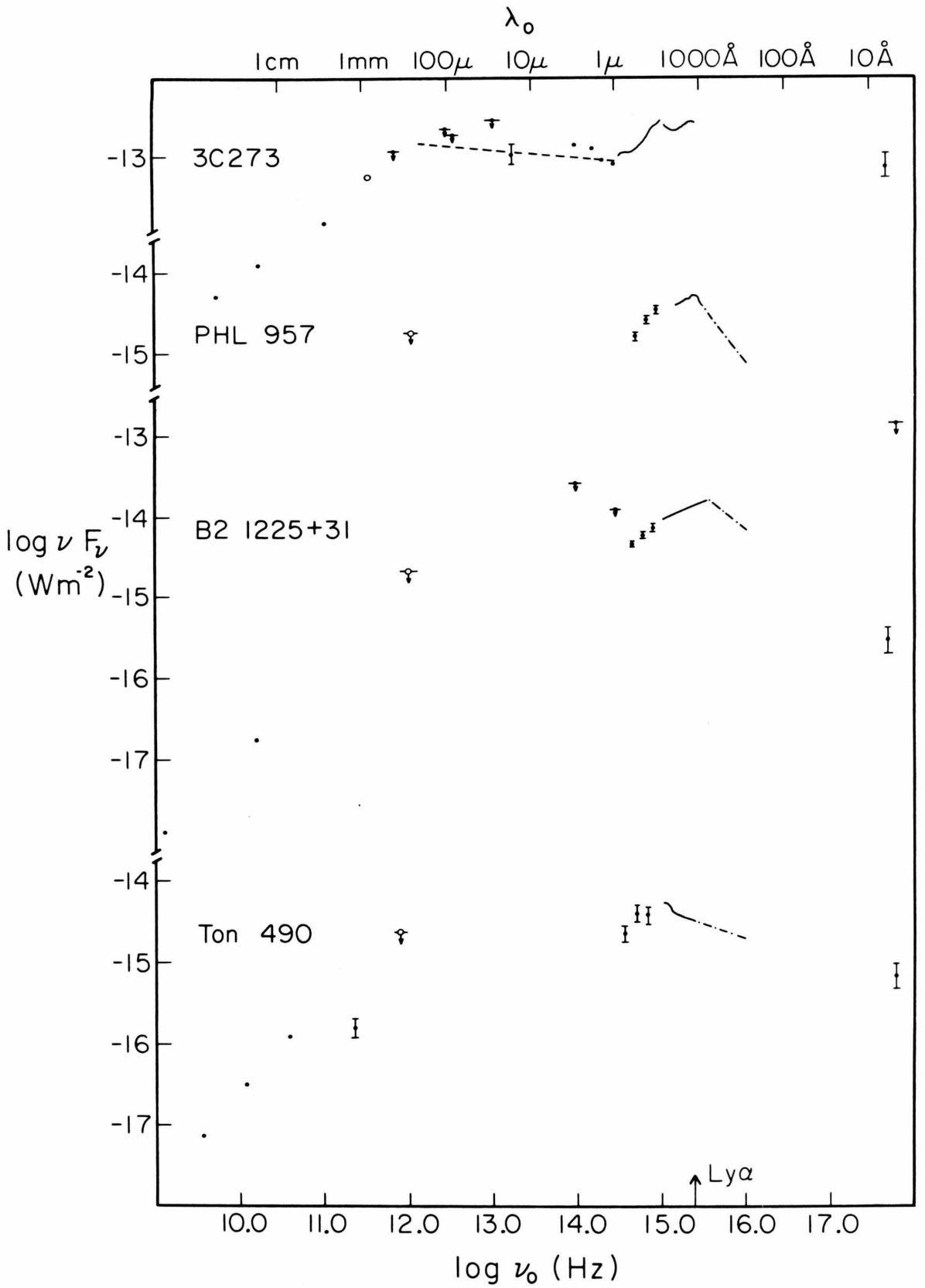
λ0
1cm
1mm
100μ
10μ
1μ
1000Å
100Å
10Å
3C273
PHL 957
B2 1225+31
Ton 490
log ν Fν
(Wm-2)
-13
-14
-15
-16
-17
Lyα
10.0
11.0
12.0
13.0
14.0
15.0
16.0
17.0
log ν0 (Hz)

Figure 1

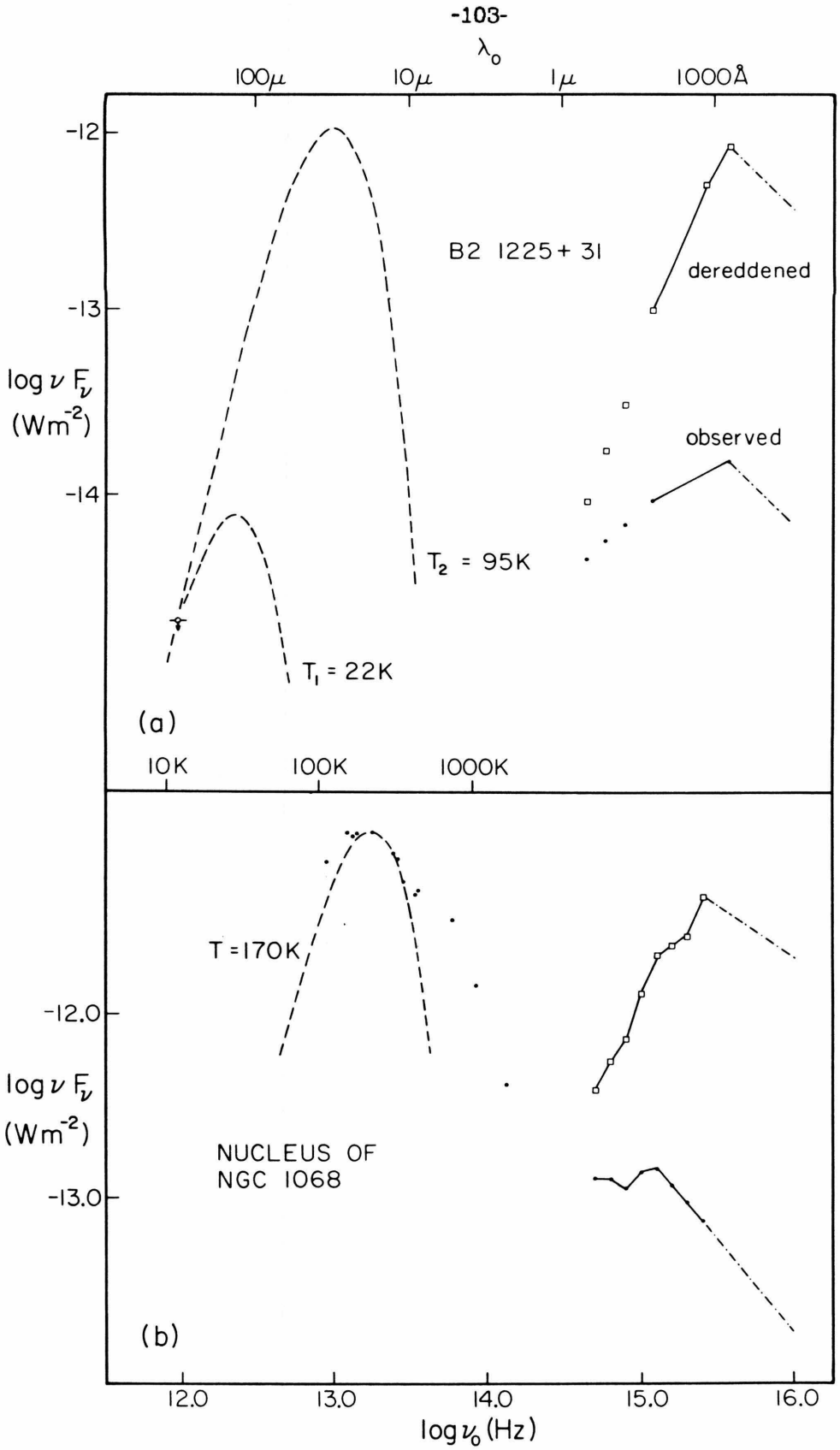
λ0
100μ
10μ
1μ
1000Å
-12
-13
-14
log ν Fν
(Wm-2)
B2 1225+31
dereddened
observed
T2 = 95K
T1 = 22K
(a)
10K
100K
1000K
T=170K
-12.0
-13.0
log ν Fν
(Wm-2)
NUCLEUS OF
NGC 1068
(b)
12.0
13.0
14.0
15.0
16.0
log ν0 (Hz)

Figure 2

CONCLUDING REMARKS

Simply stated, the major observational result of this thesis is that quasars do not exhibit evidence for excess emission at a wavelength of one millimeter. The measured 1mm flux densities for the the radio loud quasars and blazars are consistent with a direct extrapolation of their observed radio continua; the power law radio emission of these objects shows neither an increase nor a spectral steepening at a wavelength of 1mm. The quasars observed which do not have intense radio emission- the radio quiet quasars and high redshift quasars- were not detected at one millimeter; the 1 Jy sensitivity level of the present observations provides a significant limit to the 1mm emission from these objects.

This basic result is interpreted in a different manner for each type of quasar observed. For radio quiet quasars, the lack of 1mm emission can be seen as evidence against synchrotron self-absorption or free-free absorption processes suppressing the radio emission. In terms of a Comptonization model for the infrared emission of radio quiet quasars, the limit to the observed 1mm emission implies that the seed photons must have frequencies above 300 GHz (λ = 1mm). For the high redshift quasars with measured Lα/Hα emission line ratio lower than standard recombination theory predictions, the lack of 1mm flux indicates that significant emission from dust within a certain temperature range is not present. For radio loud quasars, compact synchrotron components emitting primarily at 1mm and thereby producing a 1mm flux density in excess of that expected from the radio continuum cannot be present. In addition, models of radio loud quasars in which synchrotron losses dominate at a wavelength of 1mm or in which the electrons have a relativistic Maxwellian distribution are not viable since the required spectral steepening is not observed. Finally, for blazars, the fact that the observed radio continuum remains flat to a wavelength as

short as 1mm is consistent with a model in which a synchrotron continuum is responsible for ***both*** the infrared and radio emission and has a turnover frequency in the far-infrared region of the electromagnetic spectrum. Evidence which favors a single synchrotron source producing the entire radio through optical blazar energy distribution is the observed correlation of the 1mm flux density with extrapolations of both the infrared and radio continua.

The conclusions cited above are based on an analysis of the observed energy distributions of quasars which incorporates the new results at a wavelength of 1mm; these conclusions are reinforced by the observed nature of the 1mm flux variability. For example, the result that 1mm emission outbursts of blazars are simultaneously seen at radio and infrared wavelengths is supportive of the single synchrotron source model. A specific blazar model in which the synchrotron source is a relativistic jet viewed nearly along its axis has a number of appealing features. Not only does the beamed synchrotron continuum produced by a relativistic jet have the broken power law form exhibited by the radio through infrared data, but, relativistic shocks naturally occurring in the jet flow can account for the observed correlation of the 1mm and 2cm intensity variations.

The 1mm observations presented in this thesis represent a first step toward filling in the gap in our observational knowledge of the energy distributions of quasars between infrared and radio wavelengths. Future observations of radio loud quasars, radio quiet quasars, and blazars at submillimeter, far infrared, and mid infrared wavelengths as well as 1mm observations of higher sensitivity would be quite useful. Such observations could test and extend the theoretical models for the infrared and radio emission of quasars discussed in this thesis.

APPENDIX

I. INTRODUCTION

In this appendix the radiation detector and field optics used for the thesis observations are discussed. The composite germanium bolometer and lead light cone described are the end result of a program aimed at improving the sensitivity of the 1mm observing system to radiation from astronomical sources. A measure of the sensitivity of a given combination of filters, optics and detector is the optical noise equivalent power, *NEP*, defined as the signal power incident on the entrance aperture of the optical system which produces an output signal voltage equal to the rms noise. The goal of the research described here was to develop a detection system with low *NEP*. The optical noise equivalent power can be expressed as follows

$$NEP = \frac{N}{\varepsilon S} \tag{1}$$

where N is the measured rms noise of the detector, S is the responsivity, i.e., the change in voltage across the bolometer per unit absorbed power, and ε is the transmission efficiency of the filters and field optics used. From equation (1) it can be seen that the minimum *NEP* can be achieved with a low-noise high-responsivity bolometer combined with high transmission optics. Correspondingly, the optimization program was concentrated in two areas: bolometer experimentation discussed in Section III, and, as described in Section IV, the development of an optically efficient light cone for coupling radiation to the bolometer.

II. DESCRIPTION OF DETECTOR OPERATION

Figure 1 is the schematic assembly diagram of the filter, field optics, and detector used in the present 1mm observing system. The major components shown are the detector - a germanium composite bolometer, a lead light cone, and a fluorogold disk (Muehlner and Weiss 1973) used for spectral filtering. In

operation, radiation from an astronomical source is focussed by the telescope and photometer mirrors (see Elias *et al.* 1978 for a description of the photometer) onto the fluorogold disk situated at the entrance aperture of the light cone. The radiation is then efficiently funneled by the light cone into a copper cavity in which the detector is placed. Finally, the transmitted radiation heats the bolometer whose temperature and electrical resistance change in proportion to the amount of absorbed power. By biasing the detector with a constant current, resistance fluctuations can be measured as voltage flucuations. All of the components shown in Figure 1 are inside a cryogenic dewar (Infrared Laboratories Model HD-3) and are cooled by their thermal contact with the dewar work surface. Measurements with a commercial thermometer show that the work surface is maintained at a typical temperature of 1.8K using pumped liquid helium-4.

The measured spectral response of the 1mm observing system has been discussed in Elias *et al.* (1978) and is presented in Figure 2. Briefly, the wavelength dependence shown is due to the filtering produced by the cooled fluorogold disk, a black polyethylene sheet at a temperature of 77K, a room temperature teflon window, and diffraction at the apertures in the optical train. The purpose of the spectral filtering is to define the wavelength passband desired for the observations at an effective wavelength of 1mm. More importantly, from the standpoint of bolometer performance, the presence of the filters significantly reduces the background power incident on the bolometer. Using the spectral response of Figure 2, the known throughput of the optical system ($A\Omega=1.4\times10^{-2}\mathrm{cm}^2\mathrm{sterad}$), and assuming the background is a 300K blackbody, the incident background power was calculated to be 35 nW; this result agrees favorably with the background power estimated through a comparison of load curves taken when the bolometer was under normal conditions (Figure 1) and when the bolometer only viewed the dewar work surface (see, e.g., Zwerdling *et al.* 1968). Typically, this

background power is considerably less than the Joule heating produced in the bolometer during operation (see section IIIc).

III. BOLOMETER EXPERIMENTATION

The bolometer optimization consisted of systematically varying the physical properties of the composite bolometer components in order to minimize the *NEP*. This experimentation involved the testing of a large number of bolometers; in total, 116 tests of 34 different bolometers were performed. By testing several bolometers, each having the same physical parameter (and no other) changed trends in detector performance could be ascertained and verified.

a) Composite Bolometer Description

In Figure 3, a cutaway scale diagram of the composite bolometer is presented. The crucial component of the bolometer is the gallium-doped germanium chip (A) which acts as the temperature sensing element (Low 1961). Due to commercial doping procedures, the cylindrical boule from which the germanium chips are cut, possesses both axial and radial gradients in resistivity. Thus, the resistance of the Ge:Ga chip was varied by changing both its dimensions and its original location in the boule. It was found that an operating resistance of the Ge chip on the order of a few MΩ provided the most satisfactory performance, minimizing the noise contribution from the combined bolometer/ preamplifier system (Nishioka *et al.* 1978).

In a composite bolometer the radiation is not absorbed primarily by the Ge chip but by a dielectric substrate (B) with a thin metallic film (C) deposited on one side (Clarke *et al.* 1977; Nishioka 1976). Due to its high index of refraction (n= 4.1; Draine 1974), the germanium will reflect a significant fraction (37%) of the millimeter radiation incident upon it. In addition, Ge has the low absorption coefficient of $\sim$ 20 cm^{-1} (Zwerdling and Therauilt 1972) which for a typical Ge chip thickness of 0.1 mm implies that only 18% of the non-reflected radiation is

absorbed in a single traversal of the chip. On the other hand, a metal-coated dielectric substrate can absorb 50% of the radiation incident upon it when the surface resistance of the metal film has the resonance value, i.e., the value for which the absorption is frequency independent (Hoffer 1975; Clarke *et al.* 1977).

For the bolometer used in the present observing system the absorbing substrate was 0.010 in. thick sapphire with a ~1000 Å thick bismuth film (Hauser and Notarys 1975). The use of sapphire with its relatively low heat capacity per unit volume ($c_{Ge} / c_{sapphire} \sim 10$) resulted in small time constants for the composite bolometers (Section IIIc). Square sapphire substrates of three different areas were tested: 4 x 4 mm^2, 2 x 2 mm^2, and 1.25 x 1.25 mm^2. It was found that when the detector was placed in the integrating cavity (see below) the absorption efficiency of the bolometer did not critically depend upon substrate area; thus, small area substrate were preferred for heat capacitance reasons. Primarily, bismuth films having the resonant surface resistivity of 170 Ω per square were used (taking n=3 for sapphire), although, films with other values of the surface resistivity were tested.

For optimum detector performance, all of the power absorbed by the sapphire substrate must be transferred to the Ge:Ga chip. The quality of this heat exchange is determined by the thermal conductivity of the epoxy used to join the sapphire and germanium. Three different compounds were tested: Apiezon N Grease, Thermalcote thermal joint compound, and Stycast 2850 GT epoxy. The Stycast epoxy was preferred for two reasons: 1) according to manufacturer's specifications it has the highest thermal conductivity per unit length, g, of the three compounds, and 2) on average, the measured system transmission efficiency was higher for bolometers composited with Stycast epoxy than with the other compounds.

Through tests with a laboratory radiation source it has been shown that compositing the Ge:Ga chip significantly improves the absorption properties of the bolometer. The radiation source used is an aperture covering a dewar of liquid nitrogen; the 77K blackbody radiation from the nitrogen is modulated by a blackened room temperature chopper blade. A quantity of interest for a given bolometer is the effective strength of this source, P_e, given by the ratio of the observed signal from the bolometer produced by the source to the bolometer responsivity. P_e is a measure of both the transmission of the filters and optics and of how effectively the bolometer absorbs radiation. In Table 1, the values of P_e obtained for bolometers tested before and after compositing are shown; for a given bolometer the filters and optics used were identical in both tests. The average increase in P_e obtained through compositing is a factor of $\sim$ 3.

The lead wires (D) attached to the Ge:Ga chip serve a double function: first, they provide electrical contact with the germanium thermistor, and second, they determine the thermal conductance, G, between the bolometer and the dewar work surface. The value of G has been varied by changes in both the type of metal alloy the wires were composed of and the wire cross-sectional area. The two types of lead wires tested were .0015 in. diameter brass and .001 in. diameter karma- a nickel alloy of low thermal conductivity; each lead wire had a length of 0.5 cm. By using the measured load curve of a bolometer, G can be determined (see below); it was found that $G_{brass} / G_{karma} \sim 8$ a value consistent with the thermal conductivities per unit length of the two alloys (AIP handbook). It is known from bolometer theory (Draine 1974, Zwerdling *et al.* 1968) that both the time constant τ and responsivity S are inversely proportional to G_e the effective thermal conductivity which is given by

$$G_e = G - I^2 R\gamma(1-2\delta) \qquad (2)$$

where $\gamma = d\ln R / dT$ and the remaining symbols are defined in Table 4. The higher values of τ and S measured for bolometers having karma instead of brass lead wires were in agreement with the expected values using equation (2).

b) Bolometer Construction

The first step in the construction of a composite bolometer is the preparation of the germanium thermistor. A wire saw is used to cut the Ge chip from the proper location in the boule; it is then etched to the desired dimensions with the acid CP4 (5:3:3 Nitric acid:Acetic acid:Hydrofluoric acid). The lead wires are connected to the chip with low-melting point indium solder; the soldering is performed with a copper heat strip. The amount of indium solder is kept small to minimize the heat capacitance of the entire bolometer. The bismuth coated sapphire substrate is attached to the Ge chip with the thermal epoxy.

The composited Ge chip is next loaded into the copper substrate (E) which , in operation is bolted to the work surface. The lead wires are soldered to indium pads (F) on the copper substrate; one pad is electrically grounded, the other is insulated with a shim of sapphire (H). Conducting epoxy (Eccobond 56C) provides good thermal contact between the indium pads and the Cu substrate. Mechanical support for the composite bolometer is provided by a quartz fiber (not shown in Figure 3) which anchors the sapphire to the Cu substrate.

The Cu substrate is designed so that the bolometer will be situated in a cylindrical integrating cavity (J). The purpose of the integrating cavity is to increase the absorption efficiency of the bolometer by allowing non-absorbed photons many passes through the bolometer. In accord with empirically determined guidelines (Harper *et al.* 1976), the diameter of the cavity (0.100 in.) was designed to be approximately twice the width of the sapphire substrate and the bolometer depth in the cavity is $\sim$ 0.4 of the cavity depth. Narrow (0.010 in.) slots- cut in the cavity walls to allow the lead wires access to the indium solder

pads- do not significantly decrease the reflecting area of the cavity.

c) Bolometer Testing and Performance

The procedure for testing a bolometer consisted of: 1) determining its voltage versus current characteristics, i.e., its load curve, 2) measuring the dependence of the bolometer response on the modulation frequency of the input radiation, and 3) measuring the bolometer rms voltage noise in a 1 Hz bandwidth at frequencies of 10 and 20 Hz. In Table 2, the physical, measured , and calculated parameters of the bolometer M-13 are summarized; the test data for this bolometer are plotted in Figure 4. This specific bolometer was used in the present 1mm observing system because of its high quality.

The operating point (V,I) on the measured load curve shown in Figure 4a is determined by maximizing the signal from the laboratory radiation source. As is well known (Jones 1953), the zero frequency responsivity at the operating point can be calculated from the slope of the load curve using the following relationship

$$S = \frac{V_{in}}{2VI} \tag{3}$$

where V_{in} is shown in Figure 4a. The time constant of the bolometer can be determined from the dependence of the signal S_R produced by the laboratory radiation source on ω, the modulation frequency of the input radiation. Based on the theory of bolometer operation (Draine 1974), it is expected that S_R be given by

$$S_R = P_e S(\omega) = \frac{P_e S}{\sqrt{1+\omega^2\tau^2}} \tag{4}$$

where P_e is the effective source strength defined above. The frequency response data shown in Figure 4b are well fit by the solid line given by equation (4) with

τ=5.6 ms and P_e = 33 pW. The transmission efficiency ε can be estimated by dividing P_e by the power emitted by the laboratory source into the filter bandpass of the system (Figure 2); using a procedure analogous to that described in Section II for calculating the background power loading the detector an emitted power of 240 pW is obtained. With the DC responsivity, time constant, bolometer noise, and transmission efficiency all known, the *NEP* is determined from equation (1).

In order to compare this measured *NEP* with that expected from the theoretical noise sources associated with bolometers it is necessary to measure the thermal conductance G and the form of the dependence of R on the bolometer temperature T; a technique is now described for determining both. In agreement with theoretical understanding (e.g., Miller and Abrahams 1960), laboratory measurements (Nishioka 1976; Drew and Sievers 1969) have shown that the resistance of doped germanium follows the simple functional form

$$R = R_0 \exp \frac{\Delta}{T} \tag{5}$$

If Joule heating is the dominant input power to the bolometer then the steady state bolometer temperature is constrained by the equation of energy conservation

$$G(T - T_s) = I^2 R \equiv P_J \tag{6}$$

where T_s is the known work surface temperature. Combining equations (5) and (6) gives the following expression

$$P_J = \frac{\Delta}{T_s} \left[\frac{P_J}{\ln R_s / R} \right] - G T_s \tag{7}$$

where R_s is the bolometer resistance at zero bias current which can be read off

the load curve (see Figure 4a). Figure 4c is a plot of P_J versus $P_J / (\ln R_s / R)$ for M-13; the points shown are evaluated from the load curve. The data are fit to the straight line given by equation (7) ; the slope and intercept of this line correspond to Δ = 6.7K and G = 120 nW/K respectively, both values in good agreement with results obtained for bolometers constructed of similar materials (Nishioka *et al.* 1978).

Four major sources of noise in bolometers are: 1) phonon noise due to heat fluctuations between the bolometer and the work surface (Robinson 1973), 2) noise due to fluctuations in the number of background photons incident upon the bolometer (Lewis 1947; Fellgett 1949), 3) the Johnson noise of the germanium chip, and, 4) the Johnson noise of the load resistor. The estimated contributions of each of these sources to the measured *NEP* of bolometer M-13 are listed in Table 2; the formulae used for the calculations are also shown. As expected, the quadrature sum of the individual *NEP*s is less than the actual *NEP* of the bolometer due to the phenomenon of excess current noise arising , in all probability, in both the doped Ge chip itself and the lead wire contacts to that chip (Nishioka 1976). Empirical studies (Robinson 1973) of excess current noise indicate the following dependence on bolometer parameters

$$NEP_{ex} = K_{ex} \frac{IR}{\sqrt{\omega S(\omega)\varepsilon}} \tag{8}$$

where K_{ex} is a constant of proportionality $\cong 4.2\times10^{-7}$ for this specific bolometer; this value of K_{ex} is on the order of the values published for composite germanium bolometers (Zwerdling *et al.* 1968;Nishioka *et al.* 1978).

IV. LIGHT CONE DEVELOPMENT

In order to properly employ the low- noise high- responsivity bolometer described above, a means must be found to efficiently couple it to radiation. In a previous system used for 1mm observations (Elias *et al.* 1978) a potassium

bromide field lens refocussed light from the telescope onto a germanium bolometer. A field lens arrangement has the major disadvantage that the transmission efficiency can be low due to the reflection and absorption losses of the lens. At a wavelength of 1mm the index of refraction of KBr is 2.25 which corresponds a nominal reflection coefficient in vaccuo of 30%. An antireflection coating (see, e.g. Jenkins and White 1957) of 0.004 in. thick clear polyethylene ($n \sim 1.5$) did not significantly improve the lens system transmission efficiency.

As an alternative to a lens, reflecting light cones have been used as field optics (Harper *et al.* 1976; Keene *et al.* 1978). Given that the surface area of the cone is made of highly reflective material, the transmission efficiency of a light cone optical system can be high since no lens absorption losses are present. In addition, unlike a lens, a light cone is a non-focussing optical device and is thus free from aberrations. In Figure 5 a cross sectional view of the type light cone initially developed by Hinterberger and Winston (1966) is shown. An appealing feature of the Winston light cone is its excellent angular response; all light rays within a cone of angle ϑ_T incident upon the entrance aperture (DE) are channeled by the cone onto the exit aperture (BF) while rays at angles larger than ϑ_T are reflected out. This sharp angular cutoff is accomplished by the shape of the cone surface which in the meridonal plane of Figure 5 is a segment (BD) of a parabola with vertex A, focus F at the edge of the exit aperture, and axis AF; this parabolic surface focuses parallel light at the angle ϑ_T onto the point F. The actual parabolotoriod surface of the cone is generated by rotating the curve BD around the optical axis. For astronomical observations, field optics having good angular acceptance characteristics are required in order to maximize the radiant flux received by the detector.

Because of the advantages cited above, a Winston light cone has been fabricated and used for the 1mm observations presented in this thesis. The

dimensions of the light cone constructed (see Figure 5) are determined by the optical parameters of the 5 meter Hale telescope it is designed to interface with. The size of the entrance aperture of the cone is determined by diffraction at the primary mirror; the diameter T of the cone entrance aperture equals the diameter of the Airy circle at a wavelength of 1mm. The critical angle ϑ_T can be calculated from the f-number of the light ray bundle incident upon the cone since $\sin\vartheta_T = 1/2(\text{f-number})$; for the 1mm observations, a photometer (Elias *et. al* 1978) converted the f/3.3 beam at the 5 meter prime focus to a f/4 beam entering the dewar. With T and ϑ_T determined in this manner the length of the cone, L, and the diameter of the exit aperture, t, are fixed by the following equations

$$t = T\sin\vartheta_T \qquad L = \left[\frac{\sin\vartheta_T+1}{2\tan\vartheta_T}\right]T \tag{9}$$

which follow from the equation of the cone surface.

a) Light Cone Construction

The fabrication of the light cone designed for the 1mm observations is a two stage process. First, a lathe is used to machine a steel mandril having the desired surface. In terms of the cylindrical coordinate system shown in Figure 5, the equation of the light cone surface is given by

$$\left[z\sin\vartheta_T+\rho\cos\vartheta_T+\frac{t}{2}\cos\vartheta_T\right]^2 = 2t(1+\sin\vartheta_T)\left[z\cos\vartheta_T-\rho\sin\vartheta_T+\frac{t}{2}\right] \tag{10}$$

For the machining, equation (10) was used to generate a stepwise approximation to the cone surface with the increment in ρ used was .0005 in. ($\lambda/790$). A precision of this magnitude is easily consistent with the tolerances required of the light cone surface (Harper *et al.* 1976). The final step in the construction of the mandril is to sand down the edges of the step function surface.

In the second stage the actual light cone is manufactured by molding lead around the completed mandril. Lead was chosen because its malleability facilitates the molding process. More importantly, at temperatures below 7.2K lead enters the superconducting state in which it becomes, in principle, perfectly reflecting (see, e.g., Kittel 1953). In actual operation, the lead light cone is cooled to a temperature of ~ 2K (Section II) in order to take advantage of this effect. In the first stage of the molding process, molten lead fills the cylindrical bore of the aluminum light cone holder (see Figure 1). As the heated mandril is lowered through an alignment guide into the bore hole, the molten lead is displaced into the proper shape. The entire assembly is allowed to cool and the lead resolidifies. The light cone is now completed and the mandril is removed from the holder; the mandril is undamaged by the molding process and may be used repeatedly.

c) Light Cone Performance

Use of the lead light cone in place of the KBr lens as field optics for the bolometer provided a significant increase in the transmission efficiency. The effective source strengths presented in Table 3 were obtained in tests in which the same detector first viewed the laboratory source with a KBr lens and then with the lead light cone. For both detectors used, the lead light cone provided an increase of ~ 2 in the transmission efficiency. The lead light cone was also compared with a nickel light cone constructed at the University of Chicago (Harper *et al.* 1976); the nickel cone has a thin gold layer evaporated onto its surface in order to provide a high reflection coefficient. Both light cones gave identical P_e in tests with detector MM-8; this result suggests that the cold lead is providing the expected high reflectivity.

A measure of the angular response of an optical system is the beam profile- the dependence of the signal produced by the laboratory radiation source on the

angle between it and the entrance aperture of the optics. The beam profile of the lead light cone is shown in Figure 6; the arrows in this figure mark the half-power points of an f/4 beam. As can be seen by this figure, the measured angular response of the lead light cone compares favorably with design specifications, i.e., the f/4 beam profile has a reasonably sharp angular cutoff.

V. CONCLUSIONS

The measured *NEP* presented in Table 4 is a significant improvement in the *NEP* of detection systems used for 1mm observations. This gain reflects both the success of the laboratory program to enhance bolometer performance as well as increased transmission efficiency attributed to the cooled lead light cone. The higher sensitivity of the present observing system has made possible the measurement of the 1mm flux densities from the faint extragalactic sources discussed in the body of the thesis.

The author would like to acknowledge Jim Smith for his invaluable skill in the construction of many of the bolometers tested.

TABLE 1

EFFECTS OF COMPOSITING

Bolometer	Uncomposited P_e (nW)	Composited P_e (nW)
MM-1	4	14
MM-2	6	21
MM-3	4	19
MM-6	9	22

TABLE 2
DETECTOR PARAMETERS

PHYSICAL PARAMETERS:

Ge:Ga Chip size	$1\times1\times0.2\text{mm}^3$
Diameter/type of Lead wire	.0015 in./Brass
Sapphire Substrate size	$1.25\times1.25\times0.1\text{mm}^3$
Thermal Compound	Stycast 2850 GT

MEASURED PARAMETERS:

Load Resistance	R_L	25 MΩ
Bolometer Resistance	R	4.38 MΩ
Resistance Ratio	$\delta=R/(R_L+R)$	0.15
Bias Current	I	0.11 μA
Operating point voltage	V	0.48 V
Zero-frequency Responsivity	S	3.0×10^6 V/W
Time Constant	τ	5.6 ms
Effective Source Strength	P_e	33 pW
Transmission Efficiency	ε	0.14
Noise	$N(10)$	40 nV/$\sqrt{\text{Hz}}$
	$N(20)$	35 nV/$\sqrt{\text{Hz}}$
Noise Equivalent Power	$NEP(10)$	1.0×10^{-15} W/$\sqrt{\text{Hz}}$
	$NEP(20)$	1.0×10^{-15} W/$\sqrt{\text{Hz}}$
Work surface Temperature	T_S	1.8 K
Thermal Conductance	G	120 nW/K
Energy Gap Temperature	Δ	6.7 K
Bolometer Operating Temperature	T	2.3 K

CALCULATED NOISE POWERS:

Phonon Noise	$\left[\frac{4kT^2G}{\varepsilon^2}\right]^{1/2}$	4.2×10^{-14} W/$\sqrt{\text{Hz}}$
Background Noise[a]	$\left[\frac{4(kT_b)^5A\Omega\varepsilon}{c^2h^3}\int\frac{x^4\exp x\,dx}{(\exp x-1)^2}\right]^{1/2}$	6.3×10^{-15} W/$\sqrt{\text{Hz}}$
Bolometer Johnson Noise	$\left[\frac{4kTR}{\varepsilon^2S^2(10)}\right]^{1/2}$	5.9×10^{-14} W/$\sqrt{\text{Hz}}$
Load Resistor Noise	$\left[\frac{4kT_SR_L\delta^2}{\varepsilon^2S^2(10)}\right]^{1/2}$	1.9×10^{-14}
Total calculated NEP	NEP_{cal}	7.6×10^{-14} W/$\sqrt{\text{Hz}}$
Excess Noise Power	NEP_{ex}	6.5×10^{-14} W/$\sqrt{\text{Hz}}$

[a] In this equation T_b is the temperature of the background, here taken to be 300K. The integral is over the filter response of the system (Figure 2); the dimensionless variable x equals $h\nu/kT$.

TABLE 3

LIGHT CONE TESTS

Bolometer	Field Lens P_e (nW)	Light Cone P_e (nW)
MM-8	14	24
MM-9	9	16

REFERENCES

Clarke, J., Hoffer, G.I., Richards, P.L., and Yeh, N.-H. 1977, *J. Appl. Phys.*, **48**, 4865.

Draine, B.T. 1974, M.S. Thesis, Cornell University

Drew, H.D., and Sievers, A.J. 1969, *Appl. Opt.*, **8**, 2067.

Elias, J.H., Ennis, D.J., Gezari, D.Y., Hauser, M.G., Houck, J.R., Lo K.Y., Matthews, K., Nadeau, D., Neugebauer, G., Werner, M.W., and Westbrook, W.E. 1978, *Ap. J.*, **220**, 25.

Fellgett, P.B. 1949, *J. Opt. Soc. Am.*, **39**, 970.

Harper, D.A., Hildebrand, R.H., Stiening, R., and Winston, R. 1976, *Appl. Opt.*, **15**, 53.

Hauser, M.G., and Notarys, H.A. 1975, *Bull. AAS*, **7**, 409.

Hinterberger, H., and Winston, R. 1966, *Rev. Sci. Instrum.*, **37**, 1094.

Hoffer, B.I. 1975, Ph. D. Thesis, University of California, Berkeley.

Jenkins, F.A., and White, H.E. 1957, *Fundamentals of Optics* (McGraw-Hill: New York).

Jones, R.C. 1953, *J. Opt. Soc. Am.*, **43**, 1.

Keene, J., Hildebrand, R.H., Whitcomb, S.E., and Winston, R. 1978, *Appl. Opt.*, **17**, 1107.

Lewis, W.B. 1947, *Proc. Phys. Soc. (London)*, **59**, 34.

Low, F.J. 1961, *J. Opt. Soc. Amer.*, **51**, 1300.

Miller, A., and Abrahams, E. 1960, *Phys. Rev.*, **120**, 745.

Muehlner, D., and Weiss, R. 1973, *Phys. Rev. D*, **7**, 326.

Nishioka, N.S. 1976, M.S. Thesis, University of California, Berkeley.

Nishioka, N.S., Richards, P.L., and Woody, D.P. 1978, *Appl. Opt.*, **17**, 1562.

Robinson, L.C. 1973, *Physical Principles of Far-Infrared Radiation* (Academic Press: New York).

Zwerdling, S., and Theriault, J.P. 1972, *Infrared Phys.*, **12**, 165.

Zwerdling, S., Smith, R.A., and Theriault, J.P. 1968, *Infrared Phys.*, **8**, 271.

FIGURE CAPTIONS

Figure 1- Schematic assembly diagram of the fluorogold filter, lead light cone and germanium bolometer used in the 1mm observing system.

Figure 2- Measured spectral response of the 1mm observing system. The figure is taken from the work of Elias *et al.* (1978).

Figure 3- Cutaway diagram of the composite bolometer in its substrate. The various components are labelled in the inset and described in detail in the text.

Figure 4- Test data for bolometer M-13. The figures shown are a) Load curve, b) Test signal versus modulation frequency, c) Joule heating curve; see text for explanation.

Figure 5- Cross-sectional view of light cone constructed for the 1mm observations. Parameters shown are described in the text.

Figure 6- Beam profile of the lead light cone.

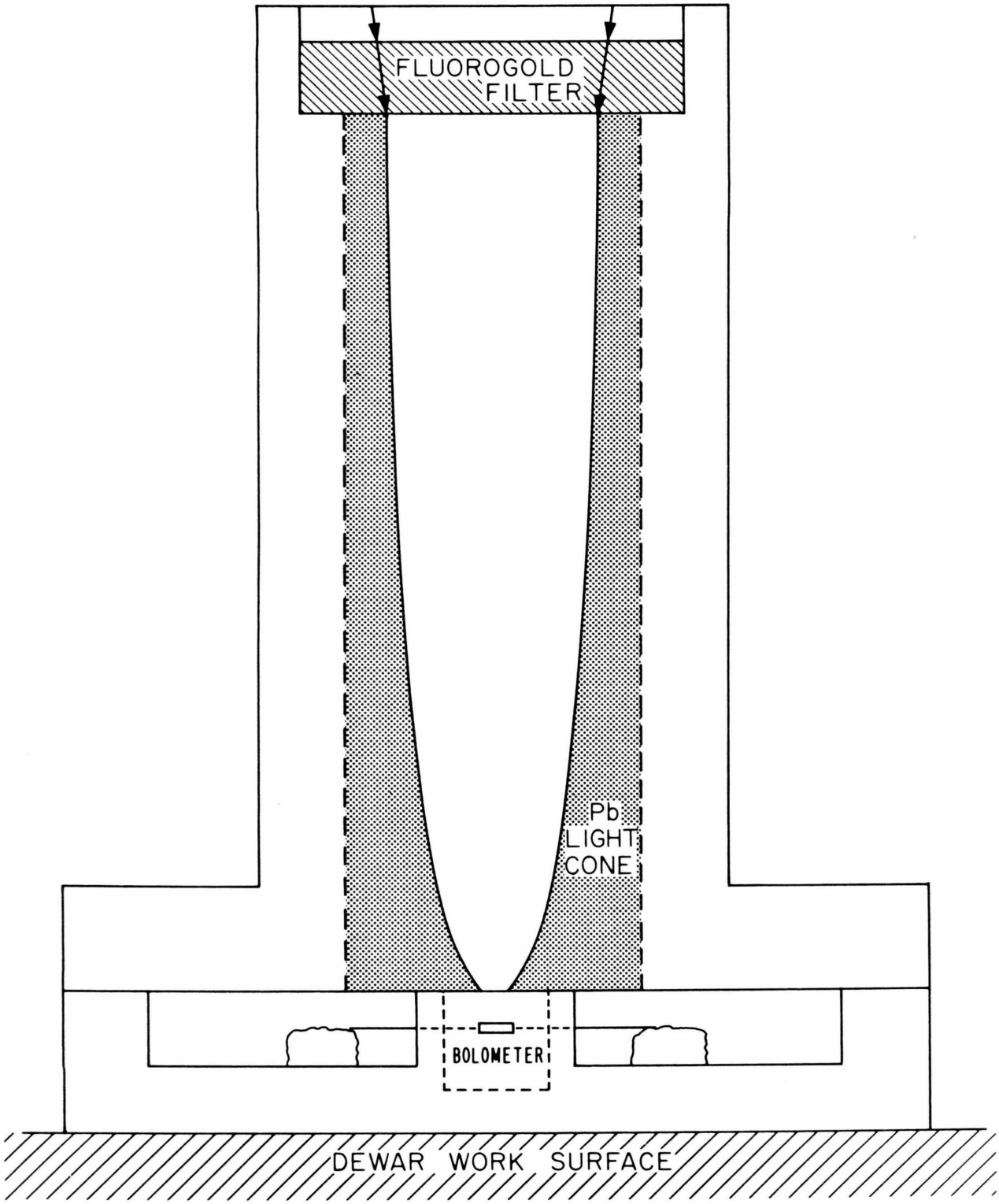
FLUOROGOLD
FILTER
Pb
LIGHT
CONE
BOLOMETER
DEWAR WORK SURFACE

Figure 1

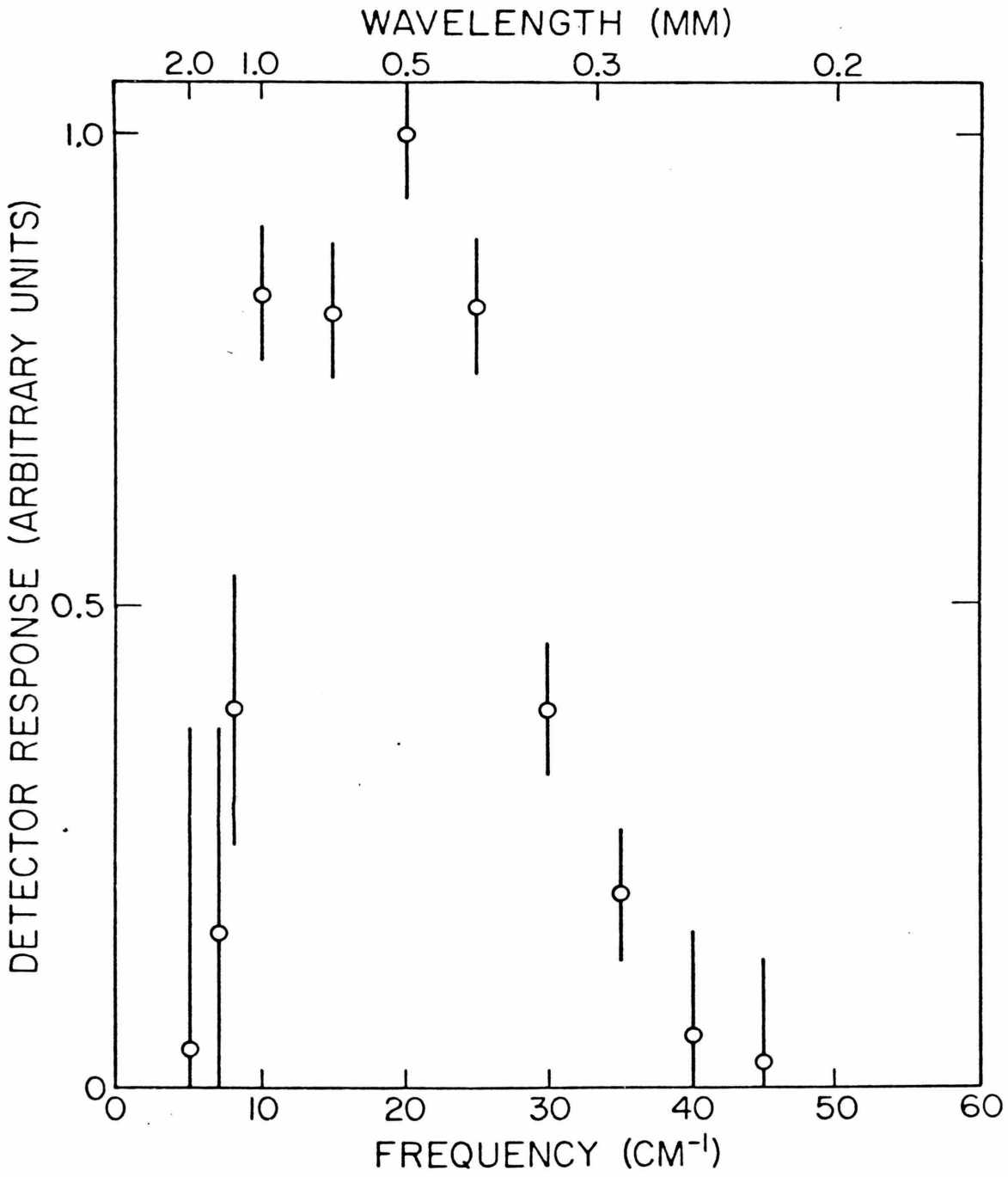
WAVELENGTH (MM)
2.0
1.0
0.5
0.3
0.2
DETECTOR RESPONSE (ARBITRARY UNITS)
1.0
0.5
0
0
10
20
30
40
50
60
FREQUENCY (CM⁻¹)

Figure 2

COMPOSITE BOLOMETER AND CAVITY SUBSTRATE

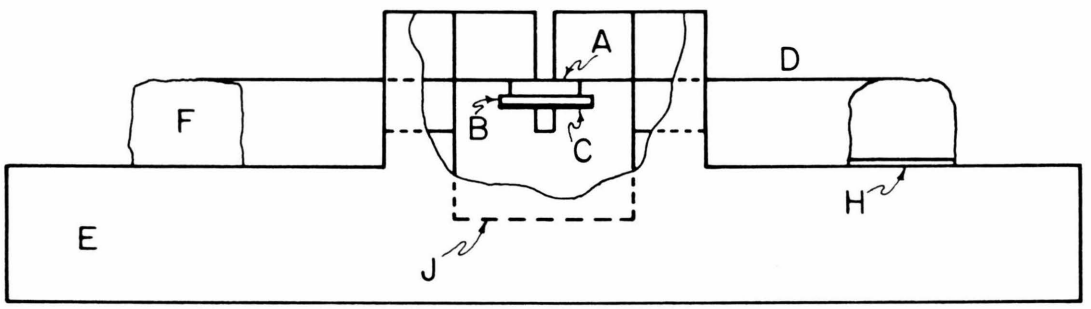

A. Ge:Ga chip

B. Sapphire substrate

C. Bismuth film

D. Brass lead wires

E. Copper substrate

F. Indium solder pads

H. Sapphire insulating shim

J. Integrating cavity

Figure 3

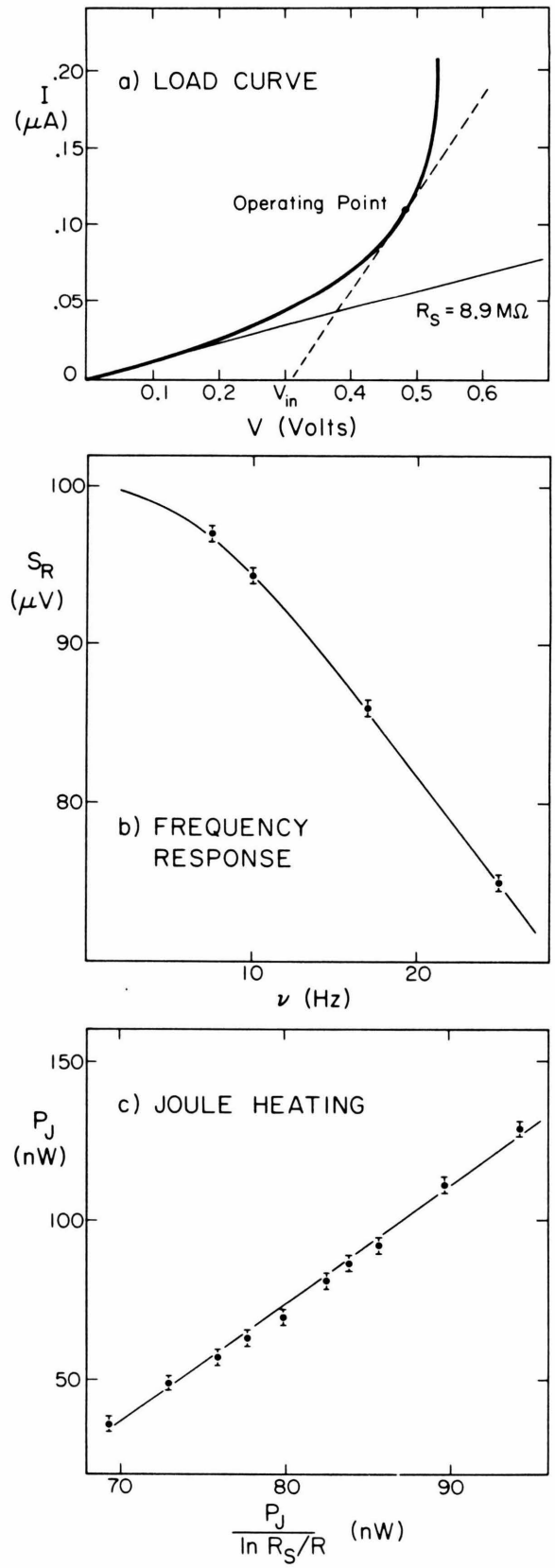
a) LOAD CURVE
I
(μA)
.20
.15
.10
.05
0
Operating Point
R_S = 8.9 MΩ
0.1
0.2
V_{in}
0.4
0.5
0.6
V (Volts)
100
90
80
S_R
(μV)
b) FREQUENCY
RESPONSE
10
20
ν (Hz)
150
100
50
P_J
(nW)
c) JOULE HEATING
70
80
90
$\frac{P_J}{\ln R_S/R}$ (nW)

Figure 4

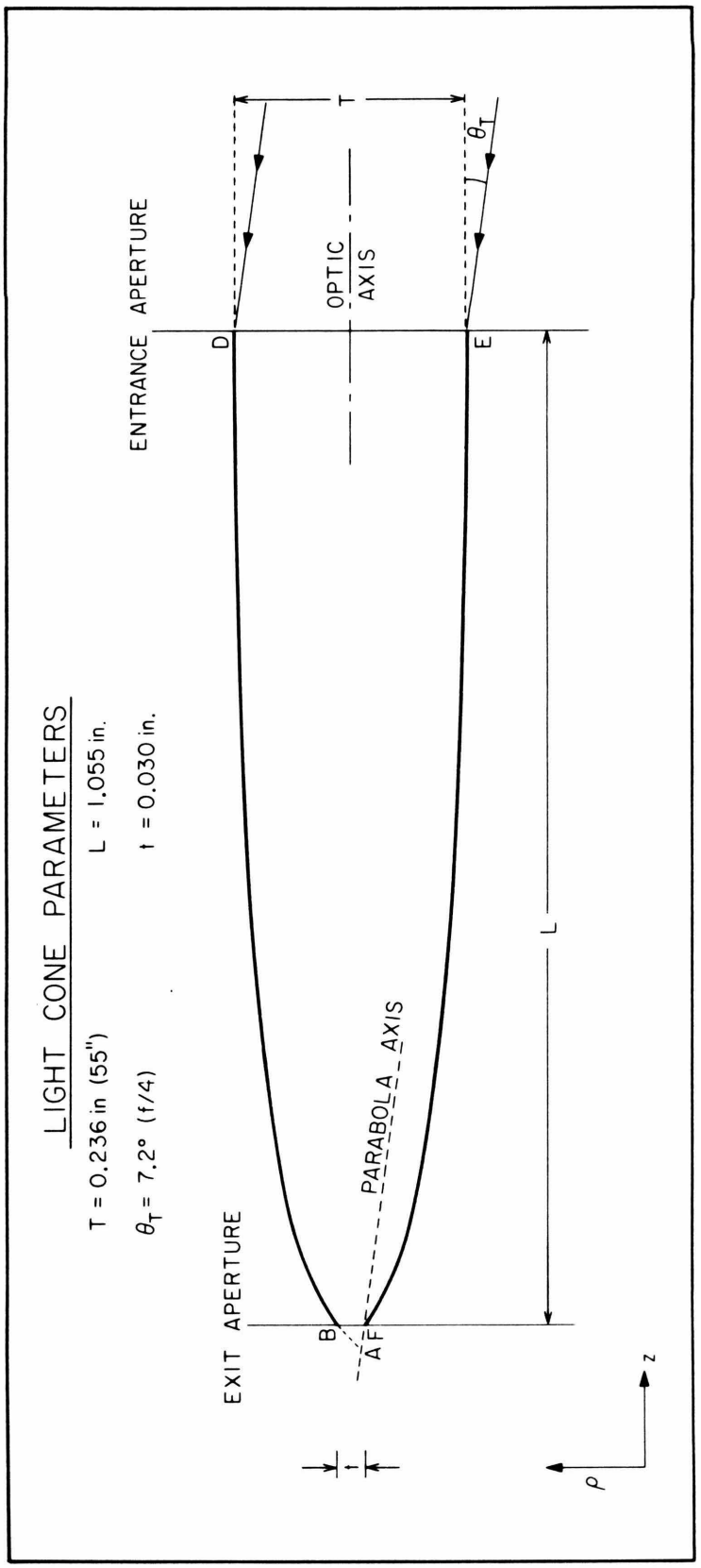
LIGHT CONE PARAMETERS
T = 0.236 in (55")
L = 1.055 in.
θ_T = 7.2° (f/4)
t = 0.030 in.
ENTRANCE APERTURE
EXIT APERTURE
OPTIC AXIS
PARABOLA AXIS
D
E
B
A F
T
θ_T
L
t
z
ρ

Figure 5

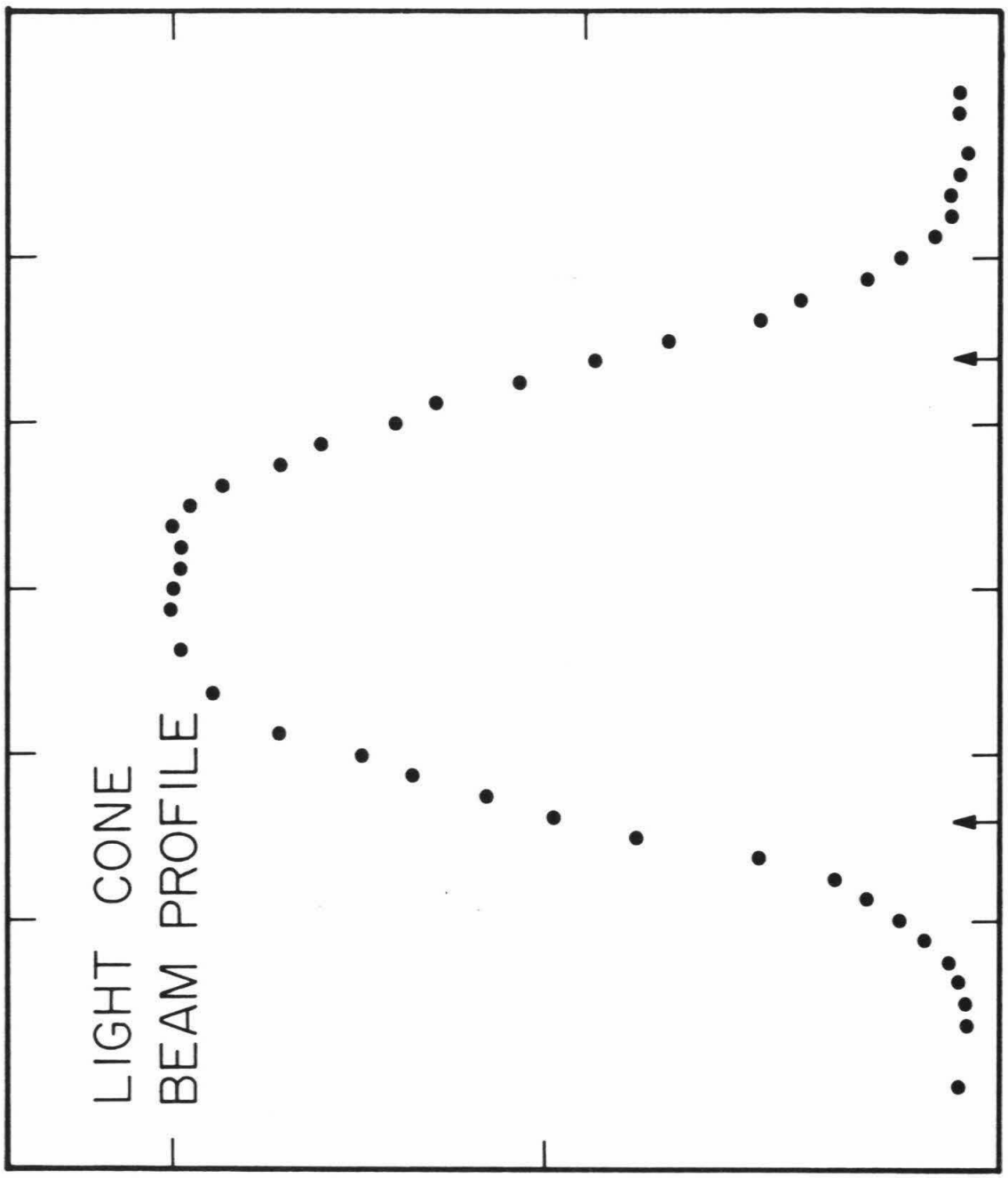
LIGHT CONE
BEAM PROFILE
Normalized
Signal
1.0
0.5
10
5
0
5
10
θ (degrees)

Figure 6